

POLITECNICO DI TORINO

Dipartimento di Ingegneria Meccanica e Aerospaziale



Corso di Laurea Magistrale in Ingegneria Meccanica LM33

MECHANICAL PERFORMANCE STUDY OF SUBMARINE POWER CABLES

Relatore

Prof. Aurelio Somà

Correlatori

Prof. Filippo Berto

Dr. Luigi Mario Viespoli

Candidato
Luigi Panza

Aprile 2020

ABSTRACT

Submarine power cable is an element used to convey electric energy underwater. Different materials with various mechanical behaviours are involved due to layered structure that such cables have. From a structural viewpoint, lead sheathing is the critical element; it has the task to protect against water infiltration the underlying insulation and conductor. Some cables, called HVDC (High Voltage Direct Current), work with powers about 600 MW and voltage about 500 kV. It means that a current of 1.2 MA must flow on the conductor and a great amount of heat is generated. Even if a part is taken away from marine environmental, however, conductor and insulation are subjected to a significant increment of temperature and the liquid inside insulation system expands against the overlying lead sheath. Hence, steel tapes are wrapped around the lead sheath in order to limit its deformation. The experience shows that when a submarine power cable has a mechanical fault, a crack on the lead sheath is always happened.

The purpose of this work is to enhance the fatigue performance of lead sheath, and therefore of the whole cable.

In order to reach this target, a preliminary, but fundamental, study of creep-fatigue models was necessary. The lead has a time-dependent mechanical behaviour because thermally phenomena are active, so creep damage, fatigue damage, or creep-fatigue damage could occur. Subsequently, a finite element model of a real submarine power cable was created to perform a qualitative study of the lead sheath's mechanical behaviour. Once realized the model, were thought design changes that didn't involve dimensional changes to not affect other aspects besides to the mechanical one. In fact, the dimensioning of cable components is led by taking into accounts electric, thermal and mechanical aspects. Therefore, it was chosen to simulate different winding angle conditions of steel tapes to investigate their effect on the stress triaxiality state into lead sheath.

Simulation results underline how the winding angle of steel tape affects the triaxiality factor of lead sheath, that's an influencing parameter for fatigue life.

The work is divided into four parts. In the first part is illustrated a presentation of the mechanical problem. The second part deals with theoretical study of main mechanical behaviour models. The third part is dedicated to the creation of the numerical model, while the last part shows the results obtained.

CONTENTS

PART I: PRESENTATION OF MECHANICAL PROBLEM

1 APPLICATIONS OF SUBMARINE POWER CABLES	1
1.1 POWER SUPPLY OF ISLANDS	1
1.2 CONNECTION OF AUTONOMOUS GRIDS	2
1.3 OFFSHORE WIND FARMS	2
1.4 SUPPLY OF MARINE PLATFORMS.....	2
1.5 OTHER APPLICATIONS.....	3
2 BRIEF DESCRIPTION OF CABLE COMPONENTS	4
2.1 CONDUCTOR.....	4
2.2 INSULATION SYSTEM.....	4
2.3 LEAD ALLOY SHEATH.....	5
2.4 POLYETHYLENE SHEATH	5
2.5 REINFORCEMENT	5
2.6 ARMOURING.....	5
2.7 OUTER SHEATH.....	5
3 MECHANICAL CONSIDERATIONS	6
3.1 TYPES OF LOAD UNDER SERVICE CONDITIONS	6
3.1.1 External water pressure	6
3.1.2 Internal pressure	7
3.1.3 Cyclic bending.....	7

PART II: THEORETICAL STUDY OF PROBLEM

4	TIME-INDEPENDENT MECHANICAL BEHAVIOUR.....	9
4.1	SUMMARIZATION OF TIME-INDEPENDENT LINEAR ELASTIC ANALYSIS.....	9
4.2	SUMMARIZATION OF TIME-INDEPENDENT INELASTIC ANALYSIS.....	10
4.2.1	Yield criteria	10
4.2.2	Plastic flow	11
4.2.3	Work hardening laws.....	12
5	TIME-DEPENDENT MECHANICAL BEHAVIOUR.....	13
5.1	BASIC DESCRIPTION OF CREEP	13
5.1.1	Phenomenology of creep	13
5.1.2	Creep curve	13
5.1.3	Main creep mechanisms	15
5.1.4	Deformation mechanism maps.....	17
5.2	Modelling of creep behaviour	17
5.2.1	Constant uniaxial stress	17
5.2.2	Variable uniaxial stress	20
5.2.3	Variable multiaxial stress.....	22
6	TIME-DEPENDENT CYCLIC MECHANICAL BEHAVIOUR	25
6.1	FATIGUE DAMAGE ASSESSMENT	25
6.2	CREEP DAMAGE ASSESSMENT	27
6.2.1	Robinson's life fraction rule	30
6.2.2	Ductility exhaustion rule	31
6.3	UNIAXIAL CREEP-FATIGUE MODELS.....	32
6.3.1	Linear Damage Summation.....	32
6.3.2	Strain Range Partitioning (SRP).....	32
6.3.3	Frequency modified fatigue	36
6.4	SRP UNDER MULTIAXIAL CONDITIONS	36
6.4.1	Preliminary stress-strain analysis	37
6.4.2	Equivalent stress and strain parameters	37
6.4.3	Rule of sign for the dominant principal direction	38
6.4.4	Partitioned equivalent strain-ranges	38
6.4.5	Fatigue life equations modified by triaxial-state effect	40

6.4.6 Interaction damage rule	43
6.5 FINAL CONSIDERATIONS.....	44

PART III: FINITE ELEMENT ANALYSIS

7 INPUT DATA AVAILABLE.....	46
7.1 DATA PROVIDED BY NEXANS.....	46
7.1.1 Geometric data and types of material.....	46
7.1.2 Plastic flow curve of PE sheath	47
7.1.3 Plastic flow curve of outer sheath.....	48
7.2 DATA PROVIDED BY PREVIOUS EXPERIMENTAL CALIBRATION	49
7.3 DATA COLLECTED BY SEARCHES ON SUBMARINE POWER CABLES LITERATURE....	50
7.4 SUMMARIZATION OF INPUT DATA AVAILABLE	51
8 SCHEMATIZATION OF CABLE.....	52
9 MATERIAL PROPERTIES	55
9.1 CONDUCTOR.....	55
9.2 INSULATION SYSTEM.....	55
9.3 LEAD SHEATH	56
9.4 PE SHEATH.....	56
9.5 REINFORCEMENT.....	57
9.5.1 Orthotropic elastic behaviour with transversely isotropic elasticity	57
9.6 FIRST ARMOUR.....	58
9.7 SECOND ARMOUR.....	59
9.8 OUTER SHEATH.....	59
9.9 CONSIDERATIONS ON MATERIAL PROPERTIES	60
10 MESHING	61
10.1 CHOICE OF THE ELEMENTS.....	61
10.2 GEOMETRIC DISCRETIZATION.....	63

10.3 APPLICATION OF THE ELEMENTS	63
11 INTERACTIONS	64
11.1 BRIEF DESCRIPTION OF SURFACE-BASED TIE CONSTRAINT	64
11.1.1 Surface-to-surface formulation	65
11.1.2 Node-to-surface formulation.....	65
11.2 IMPLEMENTATION OF SURFACE-BASED TIE CONSTRAINT	66
12 BOUNDARY CONDITIONS.....	68
12.1 CONSTRAINTS	68
12.2 LOADS.....	70
12.2.1 Static water pressure	70
12.2.2 Static thermal expansion of insulation	71
12.2.3 Cyclic bending.....	72
12.3 CONSIDERATIONS ON BOUNDARY CONDITIONS.....	74
13 DESIGN CHANGES SIMULATED	75

PART IV: RESULT ANALYSIS

14 GLOBAL ANALYSIS OF THE STRESS-STRAIN FIELD	78
14.1 DEFORMED	78
14.2 MAIN CONTOUR PLOTS	80
14.2.1 Radial stress	81
14.2.2 Circumferential stress	82
14.2.3 Longitudinal stress	83
14.2.4 Von Mises equivalent stress.....	84
14.2.5 Equivalent pressure	85
14.3 IDENTIFICATION OF THE CRITICAL POINT	86
15 TEMPORAL ANALYSIS OF THE STRESS-STRAIN FIELD.....	87
15.1 CHARACTERIZATION OF STATIC BEHAVIOUR.....	87

15.2	CHARACTERIZATION OF TIME-INDEPENDENT CYCLIC BEHAVIOUR	88
15.3	CHARACTERIZATION OF TIME-DEPENDENT CYCLIC BEHAVIOUR.....	90
16	FINAL CONSIDERATIONS.....	91
16.1	INFLUENCE OF CREEP.....	91
16.2	INFLUENCE OF THE STEEL TAPES' WINDING ANGLE.....	91
17	CONCLUSIONS	92
	REFERENCES	94

LIST OF FIGURES

Figure 1 Submarine power cables supplying Vancouver Island, Canada [1]	1
Figure 2 Offshore wind farm with 34.5 kV in-field cables [1]	2
Figure 3 Submarine power cables supplying gas platform [1]	3
Figure 4 Various oil and gas installations requiring submarine power cables [1]	3
Figure 5 Submarine Power Cable's components	4
Figure 6 Yield surface for arbitrary stress states in the space of principal stresses [3]	11
Figure 7 Illustration of strain hardening using a stress-strain curve [3].	12
Figure 8 Stages of creep at constant stress [3]	14
Figure 9 Movement of vacancies in diffusion creep [3]	15
Figure 10 Movement of vacancies along grain boundaries in diffusion creep [3]	16
Figure 11 Grain boundary sliding [3]	16
Figure 12 Idealised deformation mechanism map [3]	17
Figure 13 Strain history prediction from Time Hardening Theory [5]	21
Figure 14 Strain history prediction from Strain Hardening Theory [5]	22
Figure 15 Plastic, elastic and total strain vs. life test data [17]	26
Figure 16 Kachanov's original notion of area loss ('damage') [5]	27
Figure 17 Schematic of creep strain growth after Kachanov [5]	29
Figure 18 Strain fraction variation with life fraction for different materials [5]	30
Figure 19 Reduction of creep ductility with increasing average strain rate [5]	31
Figure 20 Examples of partitioned strain range-life relationships [4]	33
Figure 21 Effect of frequency on creep-fatigue interaction [4]	34
Figure 22 Examples of test cycles for SRP application [9]	35
Figure 23 Schematic strain cycle in terms of signed effective strain [4]	38
Figure 24 Multiaxiality versus triaxiality factor relationships [4]	41
Figure 25 Fatigue life under uniaxial and multiaxial conditions [10]	43

Figure 26	Schematic cross section of a real submarine power cable	46
Figure 27	Plastic behaviour for PE sheath	48
Figure 28	Plastic behaviour for HDPE sheath	48
Figure 29	Plastic behaviour for Lead alloy sheath	49
Figure 30	Cross section of model	53
Figure 31	Schematic picture for the evaluation of cable length	53
Figure 32	Three-dimensional view of model	54
Figure 33	Second order three-dimensional element	62
Figure 34	Mesh of model	63
Figure 35	Node to surface approach for Tie formulation [16]	66
Figure 36	Example of Tie application in Abaqus	67
Figure 37	Coupling application for the fully constrained extreme section of model	68
Figure 38	Coupling application for the axially free extreme section of model	69
Figure 39	Constraints application for the fully constrained extreme section	69
Figure 40	Constraints application for the axially free extreme section	70
Figure 41	Static water pressure load	70
Figure 42	Initial thermal field of insulation system	71
Figure 43	Final thermal field of insulation system	71
Figure 44	Rigid rotation of the fully constrained extreme section	72
Figure 45	Rigid rotation of the axially free extreme section	73
Figure 46	Temporal trend of bending load	73
Figure 47	Setting parameters for creep analysis	76
Figure 48	Setting parameters for numerical solution	77
Figure 49	Deformed after water pressure and thermal load	78
Figure 50	Deformed of cable after water pressure, thermal load and 0.25 bending cycle	79
Figure 51	Deformed of cable after water pressure, thermal load and 0.75 bending cycle	79

Figure 52 Deformed of cable at the end of simulation (1.25 bending cycle).....	80
Figure 53 Contour plot of radial stress in lead sheathing	81
Figure 54 Contour plot of circumferential stress in lead sheathing.....	82
Figure 55 Contour plot of longitudinal stress in lead sheathing.....	83
Figure 56 Contour plot of Von Mises equivalent stress in lead sheathing.....	84
Figure 57 Contour plot of equivalent pressure in lead sheathing	85
Figure 58 Critical point of cable.....	86
Figure 59 Characterization of static behaviour.....	87
Figure 60 Characterization of time-independent cyclic behaviour.....	89
Figure 61 Characterization of time-dependent cyclic behaviour.....	90
Figure 62 Comparison between viscous and stationary behaviour in terms of equivalent inelastic strain	91
Figure 63 Winding angle effect of steel tapes for stationary and viscous behaviour	92

LIST OF TABLES

Table 1 Geometric data of real submarine power cable	47
Table 2 Plastic behaviour data for PE sheath.....	47
Table 3 Plastic behaviour data for HDPE sheath	48
Table 4 Plastic behaviour data for Lead alloy sheath	49
Table 5 Available input data	51
Table 6 Geometric data of model	52
Table 7 Material properties of insulation system	56
Table 8 Material properties implemented for the Reinforcement.....	58
Table 9 Material properties implemented for the first armour	59
Table 10 Material properties implemented for the second armour	59
Table 11 Mechanical behaviour implemented for all parts of model.....	60
Table 12 Material properties implemented for all parts of model.....	60
Table 13 Features of Tie formulations in Abaqus/Standard.....	64
Table 14 Surface characteristics for Tie formulations in Abaqus/Standard	64
Table 15 Master-Slave attributions for the surfaces of model.....	66
Table 16 Triaxiality Factor for different winding angle values of steel tapes.....	93

LIST OF ABBREVIATIONS

AC	Alternating Current
CC	tensile Creep reversed by compressive Creep
CP	tensile Creep reversed by compressive Plasticity
HVDC	High Voltage Direct Current
HDPE	High Density Polyethylene
LDS	Linear Damage Summation
MF	Multiaxiality Factor
MI	Mass Impregnated
OWP	Offshore Wind Farms
PC	tensile Plasticity reversed by compressive Creep
PE	Polyethylene
PP	tensile Plasticity reversed by compressive Plasticity
SRP	Strain Range Partitioning
TF	Triaxiality Factor
WTG	Wind Turbine Generators

PART I

PRESENTATION OF MECHANICAL PROBLEM

1 APPLICATIONS OF SUBMARINE POWER CABLES

Submarine power cables are device designed for the transport of electric energy under the sea. They are used to overcome different needs as briefly shown in the following.

1.1 POWER SUPPLY OF ISLANDS

The connection between islands and the mainland often can be entrusted to the submarine power cables that replace the power generator, frequently inefficient, directly stationed on the island. Normally are used medium-voltage (≤ 52 kV) AC cables and a power transmission of 10–30 MW per cable [1].

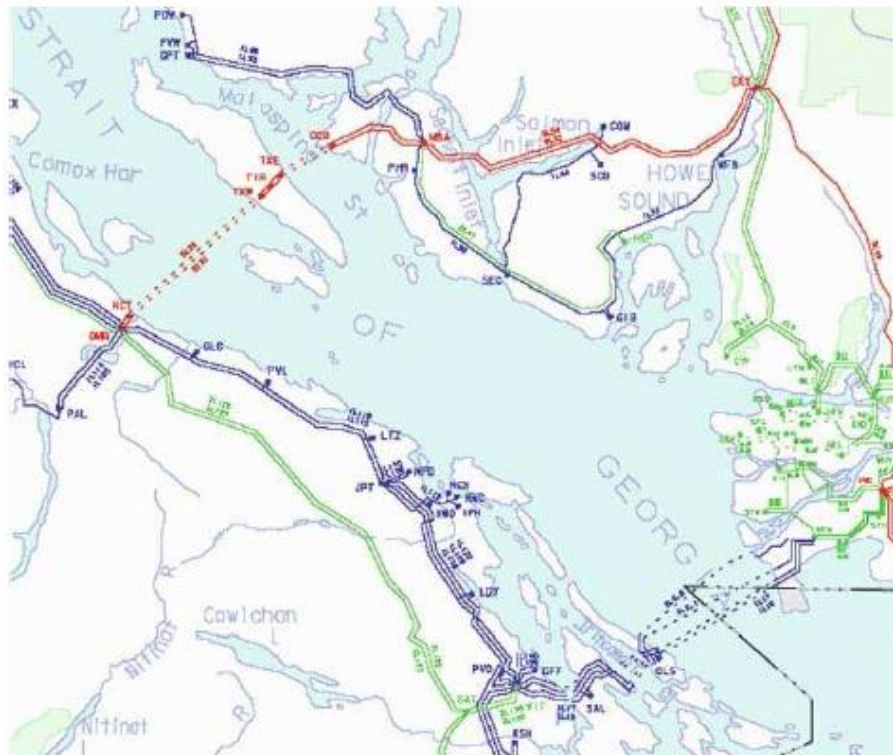


Figure 1 Submarine power cables supplying Vancouver Island, Canada [1]

1.2 CONNECTION OF AUTONOMOUS GRIDS

With the development of powerful submarine cables many grids have been interconnected, using different methods. Submarine cables connect grids of different countries. For instance: UK – France, Sweden – Germany, Denmark – Sweden, Morocco – Spain, Greece – Italy. Using HVDC (High Voltage Direct Current) techniques, regions with different frequency control can be also linked. Real examples are Store Belt in Denmark, Sweden – Germany, Norway – Netherlands [1].

1.3 OFFSHORE WIND FARMS

Offshore wind farms (OWP) have a great number of wind turbine generators (WTG). The distance between the WTGs is 300–800 m. A grid of submarine cables interconnects the WTG and bring the power to shore [1].

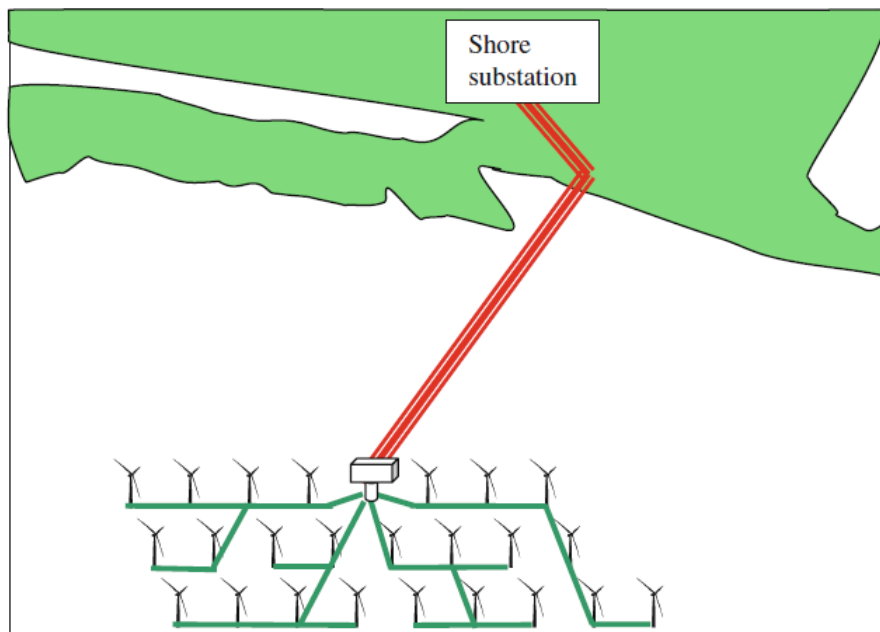


Figure 2 Offshore wind farm with 34.5 kV in-field cables [1]

1.4 SUPPLY OF MARINE PLATFORMS

Submarine power cables can supply production platforms in order to save precious space and enhance the efficiency of energy transport. In fact, the electric power for many platforms is generated from local power plants, that often work with low efficiency and take very space. For these reasons, an increasing number of platform operators invest in submarine power cables for the power supply of offshore platforms. [1]



Figure 3 Submarine power cables supplying gas platform [1]

1.5 OTHER APPLICATIONS

Hundreds of submarine power cables have been installed to transport power across rivers, channels, straits, fjords, or bays. Moreover, also in oil and gas production sector submarine power cable are used. In fact, when the installation depth become larger, more sophisticated equipment such as submersible pumps and compressors of all kind is placed on the seafloor. *Figure 4* illustrates different oil and gas installations all requiring submarine power cables.

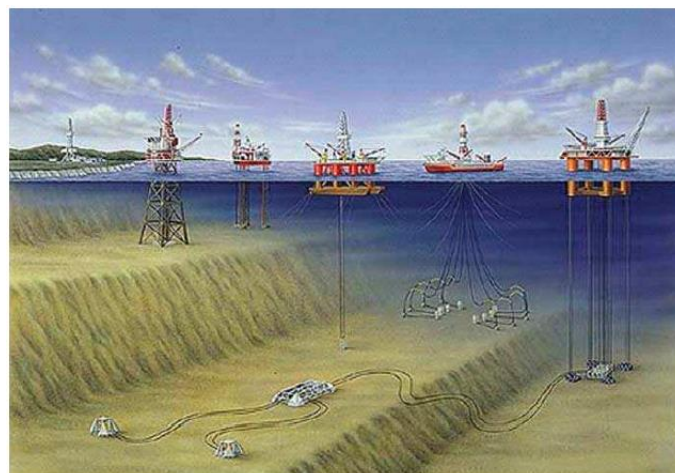


Figure 4 Various oil and gas installations requiring submarine power cables [1]

Many different types of cable exist in order to satisfy the requests involved from different applications. When the amount of electric energy and the distance become higher, HVDC MI cables (High Voltage Direct Current Mass Impregnated) are used to carry out this task. Through decades this technology has been in service for large number of power transmission links and has proven excellent reliability at a voltage up to 525 kV and a power rating exceeding 800 MW per cable [2].

2 BRIEF DESCRIPTION OF CABLE COMPONENTS

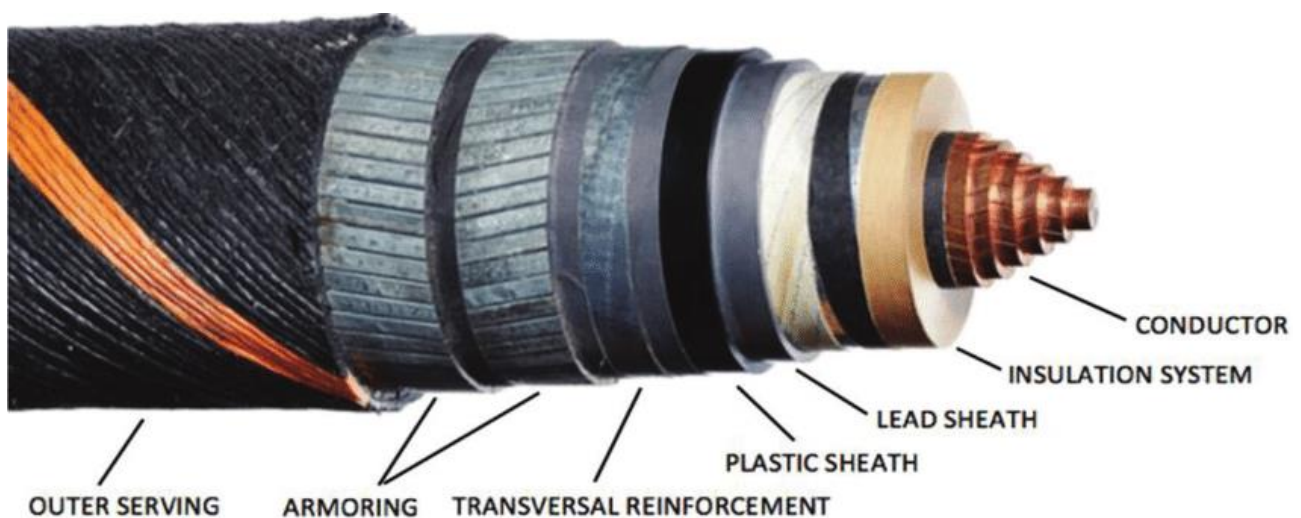


Figure 5 Submarine Power Cable's components

2.1 CONDUCTOR

The conductor is made of profile shaped wires in order to achieve a compact design with properties suitable for the electric energy carrying. Two types of materials are exploitable for submarine power cable applications: copper or aluminum. The most used is the copper, thanks to its high electric conductive properties. Aluminum has approximately two thirds of the electric conductive properties compared to copper, but the aluminum weight is three times less than the copper weight and is, hence, suited for many applications where the weight is fundamental.

2.2 INSULATION SYSTEM

The cable insulation ensures an undisturbed flow of electric current. The features required to the insulation system are compactness, robustness, resistance to temperature and aging. The insulation of a HVDC MI cable consists of Kraft paper impregnated with high viscosity oil. The oil has high viscosity even at the maximum operating temperature of the cable, so the insulation system of mass impregnated cables can be regarded as "solid".

2.3 LEAD ALLOY SHEATH

The insulation system must be protected against water ingress and therefore the most high-voltage submarine power cables have a metallic sheath. Well-produced lead sheaths are completely impermeable for water ingress and humidity diffusion. With screw extruders, submarine cables of 100 km length can be lead-covered in a single uninterrupted length at reasonable costs [1]. Long term stability, creep and extrusion properties can be improved substantially by using lead alloys.

2.4 POLYETHYLENE SHEATH

Lead and lead alloys are very soft and must be protected against mechanical damages during manufacturing, cable transport and installation. When screw-extruders are used for lead covering, a polyethylene (PE) extruder can apply a PE sheath immediately after the lead extruder, thus protecting the lead during the subsequent manufacturing. Moreover, PE sheath protects the underlying lead sheath from corrosion and abrasion.

2.5 REINFORCEMENT

Metallic tapes are applied, with a certain winding angle, as reinforcement. When the cable works, a great amount of heat is generated, and this carry to thermal expansion of the impregnation liquid inside the insulation. This causes a pressure rise on lead sheath and the primary purpose of reinforcement is to prevent expansion of lead alloy sheath.

2.6 ARMOURING

Submarine power cable armouring is built from metal wires, typically galvanized steel wires, wound around the cable with a certain winding angle. The design of armoring has a strong influence on the cable properties as bending stiffness, tensional stability, torsion balance. A good armoring design can guarantee the successful on the transport and installation operations. Thus, this is the main mechanical strength element and it ensures the integrity of cable. The armoring also acts as protection towards external mechanical influences.

2.7 OUTER SHEATH

An external sheath is still applied in order to realize another mechanical and corrosion protection to the whole structure.

3 MECHANICAL CONSIDERATIONS

Every submarine power cable must be accurately designed under three aspects: electrical, thermal and mechanical.

The main goal of thermal and electrical design is the dimensioning of conductor and insulation system in order to convey the whole amount of current in safety and reliable way, without exceed the limit temperature imposed on the cable.

Submarine power cables must be also designed to withstand all mechanical stresses during different conditions. The conditions during **manufacturing, handling, installation**, are quite predictable. In these conditions the design of the **armouring** is the crucial element.

During the installation phase, the cable is subjected to axial forces due by the weight of the hanging cable and by additional dynamic forces from the vertical movements of vessel. The effect of the helical armoring, during this phase, is to convert axial forces to torsional forces that twist the cable. When the pitch of the helical armoring is high, the steel wires run almost parallel to the cable axis, and they can bear high traction forces without create significative twisting to the cable. In this case, tensional stability and bending stiffness of the cable are very high. On the other hand, a short pitch armoring transfers much of the force to the conductor and the structural integrity of cable is not ensured. For this reason, the winding angle of the armoring is always low, and the steel wires are almost parallel to the cable axis. However, typically, the design of armoring doesn't show problems.

Without doubts, there are more difficulties for what concerns the prediction of stresses and strains during the operating conditions.

3.1 TYPES OF LOAD UNDER SERVICE CONDITIONS

From a structural viewpoint, under **service conditions**, the critical element of cable is the **lead alloy sheath**. It is used for his excellent manufacturing properties and for his complete impermeability to the water, but it not exhibits high mechanical properties. In fact, when a submarine power cable mechanically faults, always occurs a crack into lead sheath. The assessment of the lead sheath damaging is very difficult for different reasons.

Firstly, the lead alloy acts normally with homologous temperature above 0.5; it means that are active thermal activation phenomena and the **viscous behaviour** of material is important for the estimation of component duration.

Secondly, load conditions are not so easily predictable because they are very variables. With reference to a portion of cable, it's possible distinguish the following cases of load.

3.1.1 *External water pressure*

This is the most secure condition of load; it depends only by the sea depth. It produces a hydrostatic component of stress which doesn't particularly influences the inelastic behaviour of material.

3.1.2 *Internal pressure*

When the cable reaches the regime condition, the temperature of insulation system increases, and the oil inside expands against the lead alloy sheath. The expansion is limited by reinforcement and causes a significant radial load that generates irreversible deformations with a tri-axial stress state.

Moreover, the heating of the conductor, and consequently of the adjacent insulation system, depends on the electric load demand, thus the value of the radial pressure changes with the power demand. A tri-axial fatigue damage is involved.

3.1.3 *Cyclic bending*

Cyclic bending due to the tide's motion also happens. It's intuitive understand how is very difficult to predict the real amplitude of cycle since it depends from many factors. This represents another source of tri-axial fatigue damage added to the previous one.

The assessment of mechanical behaviour has to consider the **viscous behaviour** of material combined to **multi-axial fatigue models**. Multiaxial creep-fatigue interactions could occur, and this requires a carefully study of phenomena involved. It's necessary also to keep in mind that total deformation of lead alloy sheath depends by the interactions with the other components of cable. In the next section are presented some theoretical models necessary to study the problem.

PART II

THEORETICAL STUDY OF MECHANICAL BEHAVIOUR

In solid mechanics is always definable a stress tensor $[\sigma]$. Instead, the definition of a general strain model is not possible, and it depends by the context of structural application. In the context of small deformation, it's reasonable to define a strain tensor $[\varepsilon]$ in analogous way as done for the stress tensor.

Stress components must observe equilibrium equations, while strain components must satisfy compatibility equations. The relationship between stress-strain components determines the constitutive law of material, that can be time-dependent or time-independent. Cables damage evaluation requires the study of total deformation in lead alloy sheath.

The components of total deformation can be decomposed as follows:

$$\varepsilon = \varepsilon_{el} + \varepsilon_{inel} \quad (1)$$

Where:

ε_{el} is the elastic strain;

ε_{inel} is the inelastic strain.

The inelastic strain can be still divided in time-independent and time-dependent deformation:

$$\varepsilon_{inel} = \varepsilon_{pl} + \varepsilon_{cr} \quad (2)$$

ε_{pl} is the time-independent inelastic deformation, called plastic strain;

ε_{cr} is the time-dependent inelastic deformation, called creep strain.

Hence, the components of total deformation are:

$$\varepsilon = \varepsilon_{el} + \varepsilon_{pl} + \varepsilon_{cr} \quad (3)$$

Now it follows the description of some theoretical models that are most used in practical design situations in order to estimate the various types of deformation.

4 TIME-INDEPENDENT MECHANICAL BEHAVIOUR

Even if the lead sheath behaviour is affected by viscous phenomena, for a better understanding, is useful to start by reviewing some concepts of time-independent mechanical behaviour.

4.1 SUMMARIZATION OF TIME-INDEPENDENT LINEAR ELASTIC ANALYSIS

In linear elastic behaviour of material is convenient split the tensors in two parts:

$$[\sigma] = [\sigma_h] + [\sigma_d] \quad (4)$$

$$[\varepsilon] = [\varepsilon_h] + [\varepsilon_d] \quad (5)$$

Where:

$[\sigma_h] = \sigma_m[I] = \frac{I_\sigma}{3}[\sigma]$ is the hydrostatic tensor of stress;

$[\sigma_d] = [\sigma] - \sigma_m[I]$ is the deviatoric tensor of stress;

$[\varepsilon_h] = \varepsilon_m[I] = \frac{I_\varepsilon}{3}[\varepsilon]$ is the hydrostatic tensor of strain;

$[\varepsilon_d] = [\varepsilon] - \varepsilon_m[I]$ is the deviatoric tensor of strain;

σ_m and ε_m are respectively the mean stress and mean strain;

I_σ and I_ε are respectively the first invariant of stress tensor and the first invariant of strain tensor.

The hydrostatic part of stress generates hydrostatic strain, that implicates change in volume of body. Instead, the deviatoric part of stress causes change in form of body, described by the deviatoric strain. In the linear elastic regime of material there is no interaction between the two components, so the hydrostatic and deviatoric behaviour can be analysed separately.

As stress and strain tensor are symmetric, usually the six independent components of each tensor are collected in the following vectors:

$\{\sigma\}$: stress vector, representative of stress-state.

$\{\varepsilon_{el}\}$: elastic strain vector, representative of strain-state.

The relationship between these vectors is achieved with the elastic matrix $[E]$ that determine the following elastic constitutive law:

$$\{\sigma\} = [E]\{\varepsilon_{el}\} \quad (6)$$

With the hypothesis of linear elastic behaviour are necessary 21 independent material parameters in order to characterize the elastic matrix. With the introduction of isotropic hypothesis, the material independent parameter become 2 and, moreover, if the material is assumed to be isotropic, these constants are the same in all the material.

4.2 SUMMARIZATION OF TIME-INDEPENDENT INELASTIC ANALYSIS

When a component is in the plastic field, the deformation of body isn't described by the strain tensor because the value of deformation doesn't remain small.

To characterize a material in the plastic field is always used the tensile test in addition to a simplified plasticity model of reference, the Ramberg-Osgood model. This is a power mathematical model with two parameters characteristics of material. The quantities derivable from this experimental model are compared with equivalent scalar values computed in the components through the theory of plasticity. The latter is composed by three items:

- Yield criteria;
- Plastic flow;
- Work hardening laws.

4.2.1 Yield criteria

They are mathematical models based on phenomenological assumptions to determinate if a component is or not is in the plastic field. The idea is to define an equivalent stress σ_{eq} , as a function of the six stress independent components σ_{ij} , to compare with a critical value σ_{cr} obtained from the tensile test:

$$\sigma_{eq}(\sigma_{ij}) = \sigma_{cr} \quad (7)$$

If the material is isotropic, the equivalent stress can be computed in the reference system of principal stresses:

$$\sigma_{eq}(\sigma_I, \sigma_{II}, \sigma_{III}) = \sigma_{cr} \quad (8)$$

Typically, the expression is used in the implicit form:

$$\sigma_{eq}(\sigma_I, \sigma_{II}, \sigma_{III}) - \sigma_{cr} = 0 \quad (9)$$

Where $\sigma_I, \sigma_{II}, \sigma_{III}$ are the principal stresses.

Yield criteria are superficies in the space of principal stresses. Experimentally has been observed that a hydrostatic stress state doesn't influence particularly the plastic behaviour of material. The mean stress, representative of hydrostatic stress state, is invariant and therefore can be described by using the principal stresses. It follows that yield surfaces are cylinders with axis along the diagonal of the three principal directions and they are defined as a function only of the deviatoric stress as shown in *Figure 6*.

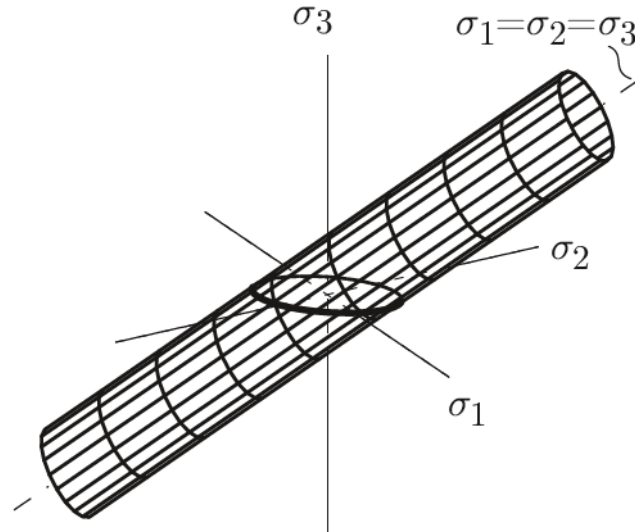


Figure 6 Yield surface for arbitrary stress states in the space of principal stresses [3]

Hence, it's possible to define yield criteria only by using the invariants of deviatoric stress and because first invariant is equal to 0, it follows:

$$f(II_{\sigma_d}, III_{\sigma_d}) - \sigma_{cr} = 0 \quad (10)$$

In particular, II_{σ_d} defines the distance from the hydrostatic axis and III_{σ_d} defines the form of the cylindric section.

Von Mises criterion states that the material starts to deform irreversibly when the deviatoric energy Φ_d (or distortion energy) reaches a critical value measured in the tensile test. Deviatoric energy is directly valuable as follows:

$$\Phi_d = \frac{1 + \nu}{E} II_{\sigma_d} \quad (11)$$

Deviatoric energy depends only from the second invariant of deviatoric stress, thus the yield surface is a cylinder with circular section and III_{σ_d} isn't influential.

$$f(II_{\sigma_d}) - \sigma_{cr} = 0 \quad (12)$$

4.2.2 Plastic flow

It's a constitutive law of material which correlates increments of plastic deformation with stress components. The calculation procedure requires to prescribe finite deformation increments and compute numerically the necessary stress components. The working point, in the space of principal stresses, never leaves the yield surface. As plastic deformation increases, the stress state increases and therefore yield surface must modify consequently.

4.2.3 Work hardening laws

In order to model the evolution of yield surface during the plastic deformation, it is necessary to edit his mathematical formulation. In particular, the equivalent stress must be compared with a variable critical value. The latter is called plastic flow stress σ_F and it depends from the components of deformation ε_{ij} , the temperature T , the strain rate $\dot{\varepsilon}$, and other parameters that consider the deformation history of material. Thus, the formulation become:

$$\sigma_{eq} = f(\sigma_{ij}) = \sigma_F(\varepsilon_{ij}, T, \dot{\varepsilon}, \dots) \quad (13)$$

Often σ_F is expressed as a function of unique scalar value, equivalent plastic strain ε_{eq}^{pl} :

$$\sigma_{eq} = f(\sigma_{ij}) = \sigma_F(\varepsilon_{eq}^{pl}) \quad (14)$$

Now it follows a schematic illustration of the work-hardening process.

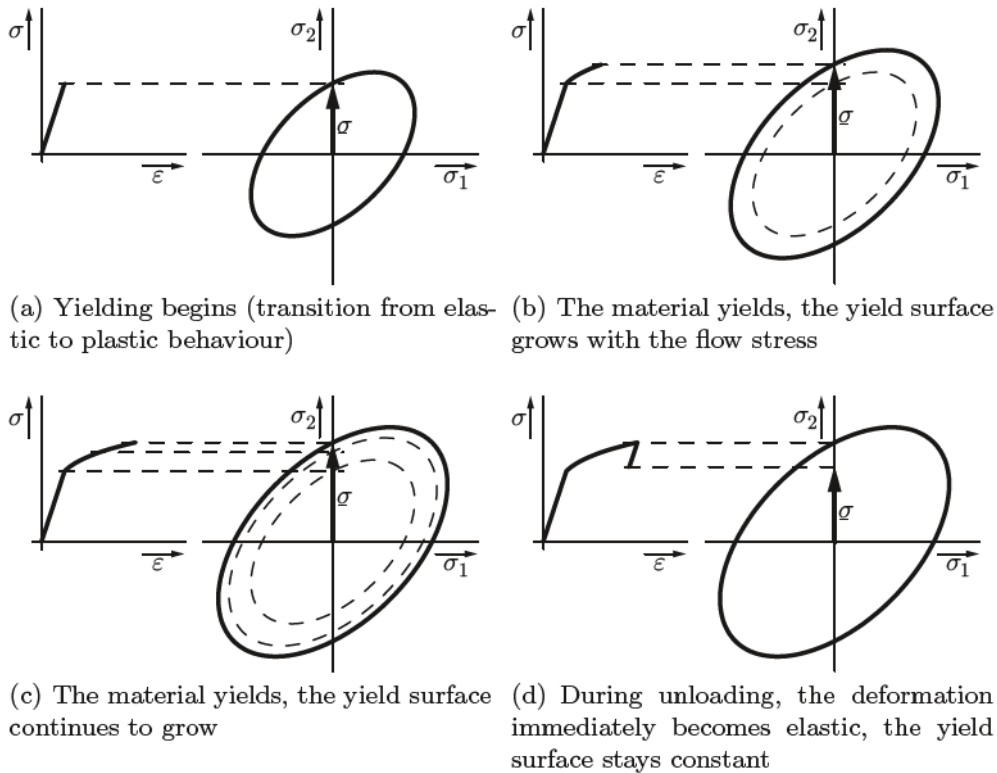


Figure 7 Illustration of strain hardening using a stress-strain curve [3].

In conclusion, the yield criteria indicate how to compute σ_{eq} and if this one is equal to the σ_F the material deforms plastically. σ_F changes during the deformation and work hardening law suggests how. To do this is necessary the whole stress state assessable by the plastic flow.

5 TIME-DEPENDENT MECHANICAL BEHAVIOUR

Creep is time dependent deformation that occurs at high temperature relative to the melting point of metallic materials [4]. The combination of stress σ , temperature T and time t determine the phenomena. Under stress, thermal energy can, over time, develop inelastic strain that causes degradation of material. The higher the temperature, the greater is thermal energy available for the atomic motion and consequent deformation.

5.1 BASIC DESCRIPTION OF CREEP

5.1.1 Phenomenology of creep

High-temperature deformation phenomena are characterized by an activation energy. For creep processes it is found that activation energy is equal to the activation energy for self-diffusion ΔH [3]. The latter is related with the energy to break atomic bonds and is a material constant. To overcome the activation energy of self-diffusion is necessary to provide thermal energy. Absolute temperature T is a direct indicator of thermal energy involved in a process, expressed as kT , where k is the Boltzmann's constant. The classical relationship for thermally activated processes is called Arrhenius equation, which models the rate of diffusion as proportional to $\exp\left(-\frac{\Delta H}{kT}\right)$.

It's important to observe that if no stress is applied, there will be no creep; that is, the material will not change its dimension with time. Application of stress reduces the atomic bond strength locally, thus reducing the apparent activation energy. At a given temperature and zero stress, atoms are in a constant stage of agitation and can jump randomly from one atomic position to another. The presence of stress alters the atomic spacing. Local tensile stress opens the spacing of atoms in the direction of stress, facilitating atomic motion in that direction because less energy is required for diffusion in this dilated state. At the same time, the Poisson contraction, perpendicular to the stress, draws the atoms close together in transverse direction, making atomic transverse movement more difficult and hence less likely to occur. With more jumps of atoms into positions aligned with tensile stress direction, the length of material will increase in that direction. This extension is creep deformation. The greater the stress, the greater amount of creep strain accumulates in given time; thus, the creep rate is greater. Similarly, at a given stress, the higher the temperature, the greater is the driving force for atomic motion [4].

5.1.2 Creep curve

Ever since the recognition of creep as a problem in the design of high-temperature components, the constant tensile stress creep test has been the most important means of providing creep data. The information gained from this test reveals, in a simplified way, how a given material will act under different combinations of loading and temperature. From this test it's possible to extract the creep curve, schematically represented in *Figure 8* [5].

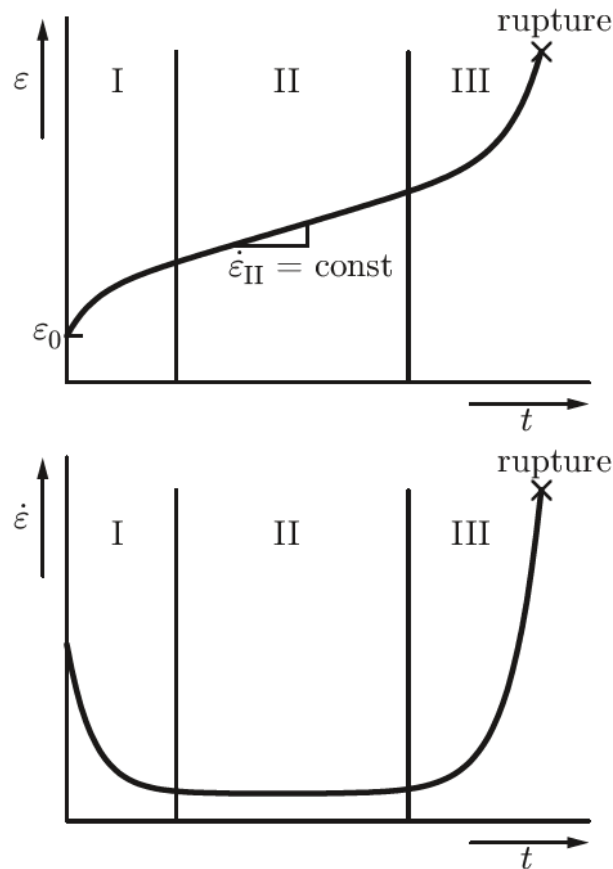


Figure 8 Stages of creep at constant stress [3]

Initially, the material reacts with a time-independent strain which consists of an elastic and a plastic part. With time, the strain increases and are distinguishable three distinct regions:

- **Primary or transient creep:**
in the first temporal phase, work-hardening mechanisms dominate creep mechanisms and therefore the strain increases, but with a decreasing strain-rate.
- **Secondary or steady-state creep:**
after enough time, creep-mechanisms balance work-hardening mechanisms and strain rate is constant. This is the typical work phase of creep.
- **Tertiary creep:**
the inelastic deformation developed by creep mechanisms have significantly degraded the material. The material has reached an internal damage such that the strain rate again increases drastically leading fracture.

The *steady-state creep strain-rate* is the control parameter in design of components.

5.1.3 Main creep mechanisms

Depending on temperature and stress, different microscopic processes are important in determining creep behaviour.

Dislocation creep

Dislocations can overpass the obstacles not with a dislocation glide mechanism, as it happens at low temperature in a time-independent inelastic deformation, but thanks to a high temperature active mechanism: *dislocation climb*. In this case, the stress applied to dislocations is not enough to put them in motion, but the temperature makes possible the movement of vacancies, and dislocations can change the slip planes by avoiding the obstacles. The vacancies current density and dislocation density determine the creep strain rate.

Diffusion creep

In this case the material deforms without dislocation movements, but the vacancies directly diffuse largely, by causing irreversible deformations. This mechanism is obviously predominant for temperatures higher than that involved in dislocation creep.

In this process, grain boundaries are sources and sinks of vacancies. The vacancies can diffuse inside the grains by activating a process called *Nabarro-Herring creep*, but the vacancies can also move directly along the grain boundaries with a process called *Coble creep*. Coble creep is most important if the grains are small. Since the activation energy of self-diffusion along the grain boundaries is smaller than in the volume, Coble creep is also dominant compared to Nabarro-Herring creep at low temperatures [3].

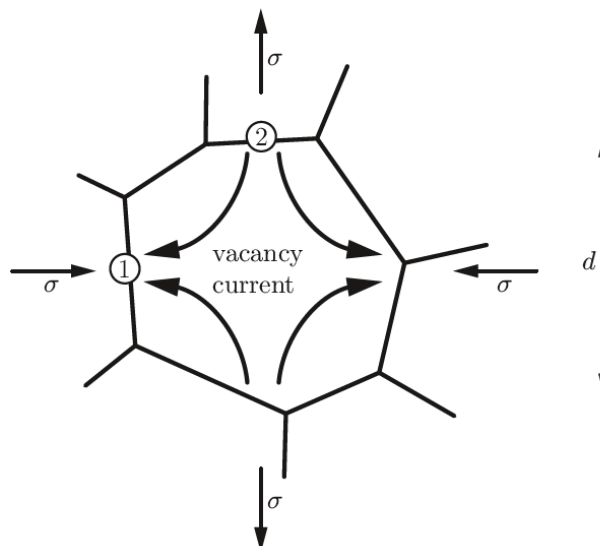


Figure 9 Movement of vacancies in diffusion creep [3]

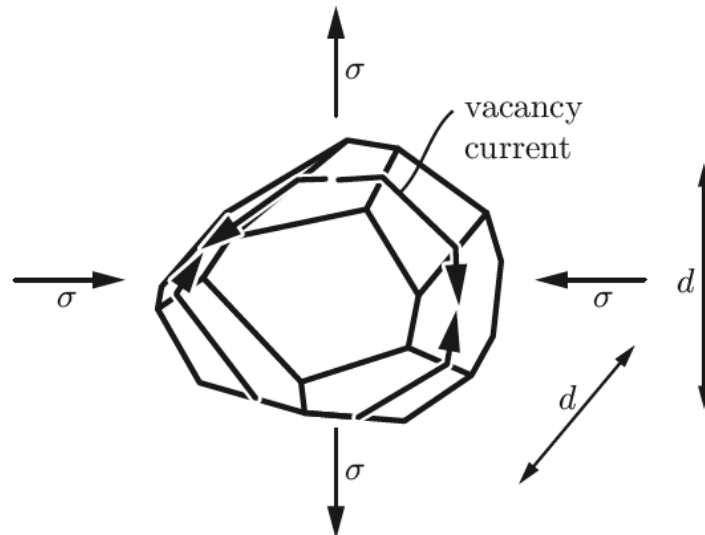


Figure 10 Movement of vacancies along grain boundaries in diffusion creep [3]

In this kind of creep mechanism, the creep strain rate depends by the vacancies current density and by the grain size.

Grain boundary sliding

In metals, grain boundary sliding contributes only slightly to the overall deformation, but it is, nevertheless, important for two reasons:

- In diffusion creep, grains change shape and grain boundary sliding ensures the necessary compatibility during deformation.
- At points where three grain boundaries are meet, movement of the grain boundaries by sliding can cause a large concentration in local stress and thus induce damage by rupture of the grain boundaries.

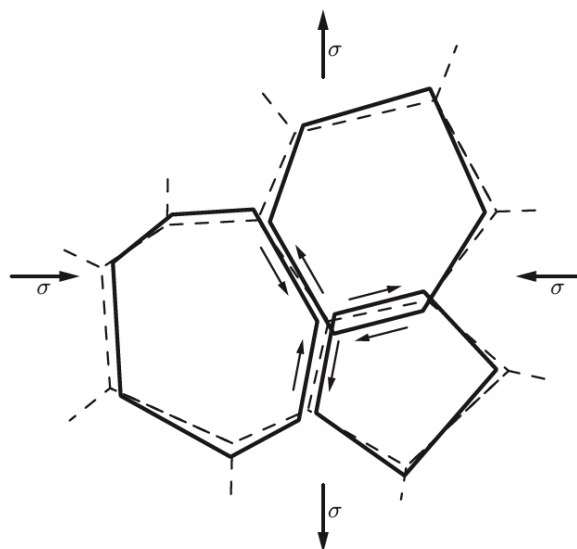


Figure 11 Grain boundary sliding [3]

5.1.4 Deformation mechanism maps

In order to help the designer of components in detection of dominant creep mechanism, deformation mechanism maps have been created. These maps show regions which specific dominant creep mechanism depending on the values of stress and temperature. It follows a schematic representation.

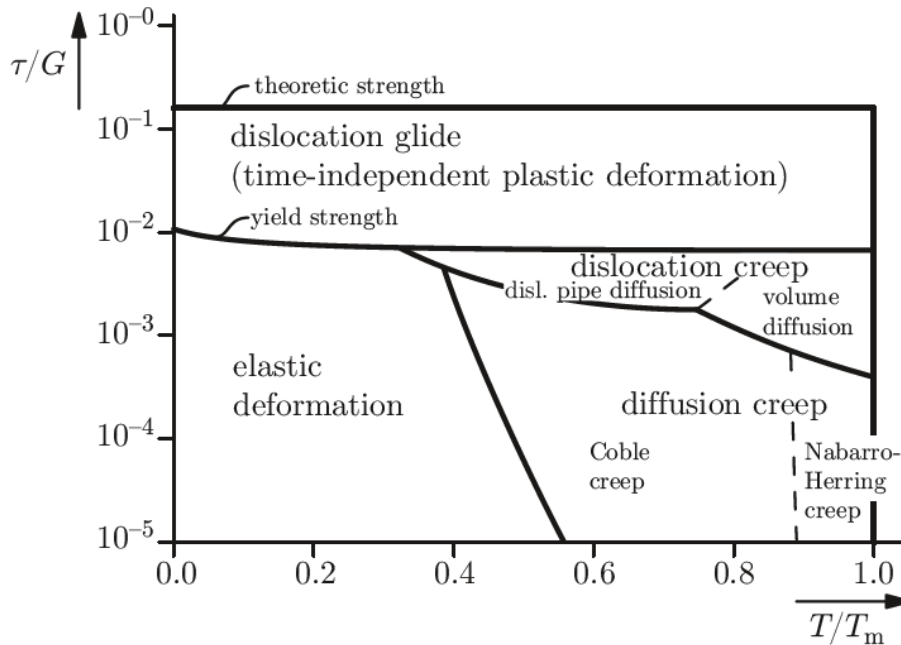


Figure 12 Idealised deformation mechanism map [3]

As can be seen, in the map are shown all the concepts previously discussed. For a specific material, the map change in function of *grain size*. Bearing in mind that material structure can change over time, deformation mechanism map must be used as instantaneous photography of the material situation.

5.2 Modelling of creep behaviour

In order to be able to predict the deformation of components in the creep range, it is necessary, firstly, to start by studying the problem under constant uniaxial stress. Subsequently, the study is expanded to more complex cases.

5.2.1 Constant uniaxial stress

As previously mentioned, creep deformations depend by the combination of stress, temperature and time.

$$\varepsilon_{cr} = f(\sigma, t, T) \quad (15)$$

Commutative law is a good first approximation for studying the problem:

$$\varepsilon_{cr} = f_1(\sigma) f_2(t) f_3(T) \quad (16)$$

The separation between stress function and temperature function is acceptable. Less acceptable is the separation of time function and often a unique time-temperature function is used.

Stress function

The most commonly used function is the *power law* attributed to Norton.

$$f_1(\sigma) = A \sigma^n \quad (17)$$

Where A and n are material constants.

The shape of this function is independent of the magnitude of load. In the secondary creep range, power law fits data best than other models, but an exponential function is more accurate at high stress. Experimental results show the loss of linearity on a bi-log chart at higher stresses. In high-stress regime a hyperbolic sine law can be used:

$$f_1(\sigma) = A [\sinh(\sigma)]^n \quad (18)$$

Time function

By choosing idealized mechanism to represent the basic material behaviour, it's often possible to derive many of these time functions. Used with care and within the context of their derivation, there are different time functions suitable [5].

One of the most important time-function is the *Garofalo equation*:

$$f_2(t) = \theta_1 (1 - e^{-\theta_2 t}) + \dot{\epsilon}_{II} t \quad (19)$$

Where:

θ_1, θ_2 are material constants;

$\dot{\epsilon}_{II}$ is the creep strain rate in the secondary creep.

The primary and the secondary part of creep curve are frequently described with this kind of law.

Temperature function

Temperature has two effects on creep strain:

- *Changing of material parameters:*
if the temperature range on service is not too large, it's possible use a mean value of such parameters.
- *Influencing on creep mechanism:*
dislocation creep or diffusion creep.

Anyway, the temperature dependence is often modelled with Arrhenius equation.

$$f_3(T) = \exp\left(\frac{-\Delta H}{kT}\right) \quad (20)$$

Bearing in mind the possible interaction between time and temperature, often is used:

$$f(t, T) = t \exp\left(\frac{-\Delta H}{kT}\right) \quad (21)$$

Main constitutive laws

A reasonable constitutive law is obtainable joining the previous considerations:

$$\varepsilon_{cr} = \left[t \exp\left(\frac{-\Delta H}{kT}\right) \right] f_1(\sigma) \quad (22)$$

More generality can be given to this law if the exponent of $f(t, T)$ can be different from 1:

$$\varepsilon_{cr} = \left[t \exp\left(\frac{-\Delta H}{kT}\right) \right]^n f_1(\sigma) \quad (23)$$

Creep constitutive laws based on creep mechanism are also available. Some are presented below as a function of secondary creep strain rate.

- *Dislocation creep law*

$$\dot{\varepsilon}_{II} = \frac{A \sigma^n}{kT} D_0 \exp\left(\frac{-\Delta H}{kT}\right) \quad (24)$$

Where D_0 is the diffusion constant of material.

The creep exponent of power law function typically takes value between 3 and 8.

- *Nabarro-Herring creep law*

$$\dot{\varepsilon}_{II} = A_{NH} \frac{\sigma \Omega}{kT} \frac{D_0}{d^2} \exp\left(\frac{-\Delta H}{kT}\right) \quad (25)$$

Where:

A_{NH} is a material constant;

Ω is the volume of a vacancy;

d is the grain size.

It's possible to observe as fine grain is not a good condition in creep regime.

- *Coble creep law*

$$\dot{\epsilon}_{II} = A_C \frac{\sigma \Omega}{kT} \frac{\delta D_{GB}}{d^3} \quad (26)$$

Where:

A_C is a material constant;

δ is the thickness of the grain boundary;

D_{GB} is the diffusion coefficient of self-diffusion along the grain boundary.

These specific equations grounded on creep mechanisms require the knowledge of material constants of complex detectability and their application is not so easy in a design context.

5.2.2 Variable uniaxial stress

Most of data available for creep behaviour of material come from constant uniaxial stress. This is an obstacle for what regards the modelling of creep behaviour under variable stress-state. Different theories have been created, but none of them is satisfactory in all the possible scenarios. It follows the presentation about two main models used in design situations.

Time-hardening formulation

Creep strain rate depends by the stress level and by changing of material structure over time.

$$\dot{\epsilon}_{cr} = \frac{d\epsilon_{cr}}{dt} = f(\sigma, t, T) \quad (27)$$

Under isothermal conditions it's possible write:

$$\frac{d\epsilon_{cr}}{dt} = f_1(\sigma) \frac{df_2(t)}{dt} f_3(T) \quad (28)$$

Changing in material structure are very common in creep phenomena, but they are mainly of softening character that cause an increasing of creep strain rate and tertiary creep. Time effects, like precipitation hardening, could predict hardening effect in primary creep, but they anyway are not able to predict correctly primary creep. Time hardening formulation could be used for materials that show only secondary and tertiary creep. However, it offers inferior results compared to other models [5].

The *Figure 13* shows schematically the strain history prediction with the time-hardening formulation.

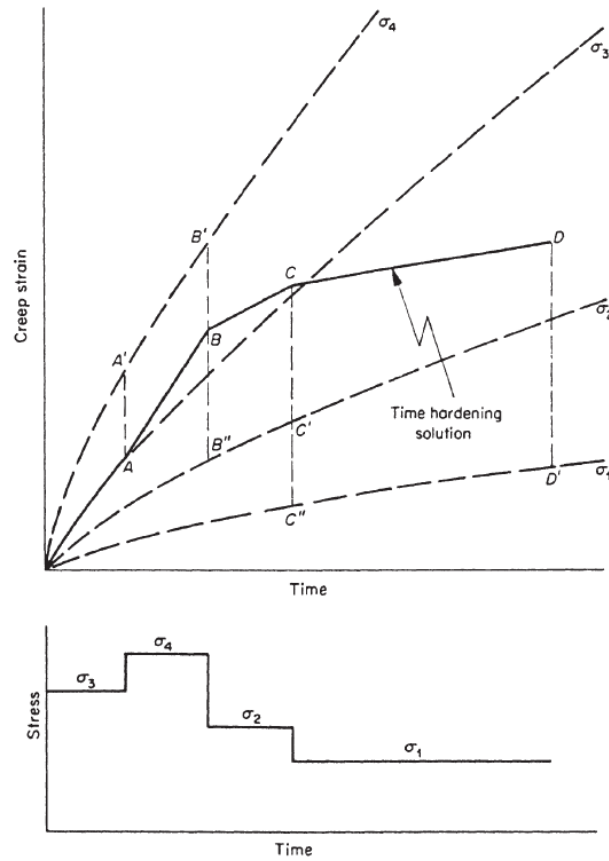


Figure 13 Strain history prediction from Time Hardening Theory [5]

Strain-hardening formulation

This model expects a hardening effect due to changing in material during deformation, i.e. for work-hardening. The formulation is explicable as:

$$\dot{\varepsilon}_{cr} = \frac{d\varepsilon_{cr}}{dt} = f(\sigma, \varepsilon_{cr}, T) = g_1(\sigma) g_2(\varepsilon_{cr}) g_3(T) \quad (29)$$

A special case is when $g_1(\sigma)$ and $g_2(\varepsilon_{cr})$ follow both a power law. Under isothermal conditions it's possible obtain:

$$\frac{d\varepsilon_{cr}}{dt} = \frac{n A^{\frac{1}{n}} \sigma^{\frac{m}{n}}}{\varepsilon_{cr}^{\frac{1-n}{n}}} \quad (30)$$

The temporal integration of this equation leads at:

$$\varepsilon_{cr} = \int_0^t \dot{\varepsilon}_{cr} dt = A \sigma^m t^n \quad (31)$$

Strain-hardening hypothesis model adequately primary creep.

When thermal softening and metallurgic changing are absent, experimental results state that strain-hardening formulation interpolate results better than other models [5].

The following picture shows how the strain-hardening formulation can be used for the prediction of stress history.

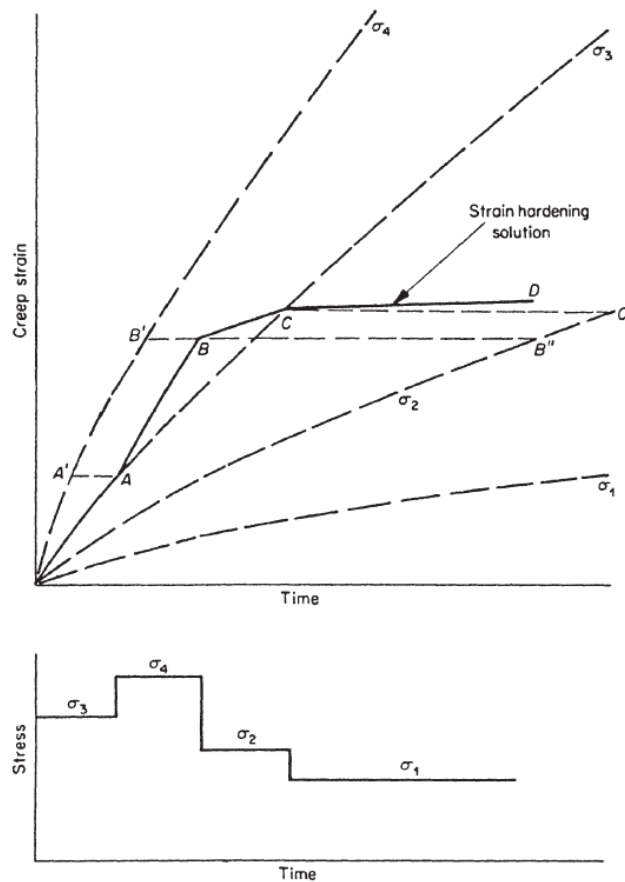


Figure 14 Strain history prediction from Strain Hardening Theory [5]

5.2.3 Variable multiaxial stress

Typically, as it has previously mentioned, experimental results are available only for constant uniaxial stress case. Modelling of multiaxial creep has done extending uniaxial models. This goal is achieved by using the concepts of plasticity theory.

In transition from uniaxial case for multiaxial case, two problems must be solved:

- 1) Find the equivalent effect of triaxial stress state.
- 2) Find a way on how the deformations are distributed along the direction of space.

For what concerns the *first problem*, in time-independent inelastic deformation the yield criteria are used to evaluate the equivalent stress. For creep problems, are used two twin quantities:

$$\text{Equivalent stress:} \quad \sigma_{eq} = \sigma_{eq}(\sigma_x, \sigma_y, \sigma_z, \tau_{xy}, \tau_{xz}, \tau_{yz}) \quad (32)$$

$$\text{Equivalent strain increment:} \quad \Delta\varepsilon_{eq} = \Delta\varepsilon_{eq}(\Delta\varepsilon_x, \Delta\varepsilon_y, \Delta\varepsilon_z, \Delta\gamma_{xy}, \Delta\gamma_{xz}, \Delta\gamma_{yz}) \quad (33)$$

For instance, in a power-law model it's possible write:

$$\Delta\varepsilon_{eq} = A \sigma_{eq}^m \Delta t^n \quad (34)$$

Instead, for what regards the *second problem*, hypothesis of plasticity theory are used. In particular, it's assumed the constancy of volume and the coincidence of principal directions for stress and strain.

Plastic flows allow to calculate the distribution of strain components as function of stress components. A general plastic flow rule can be obtained with the use of a scalar function, called plastic potential function.

$$\psi = \psi(\sigma_{ij}) \quad (35)$$

Increments of creep strain are evaluable with the variation of plastic potential function respect to component stress, through the application of a constant $d\lambda$:

$$d\varepsilon_{ij,cr} = \frac{\partial\psi}{\partial\sigma_{ij}} d\lambda \quad (36)$$

$d\lambda$ is a non-negative constant that can vary during the history load and is correlated with equivalent strain increments;

Ψ is correlated with stress components through the implementation of yield criteria.

In this way, it's possible to build a multiaxial creep model. It follows the illustration of some multiaxial creep models.

Power-law time-hardening multiaxial formulation

The power-law creep model is attractive for its simplicity. However, it is limited in its range of application. The time-hardening version of the power-law creep model is most suitable when the stress state remains essentially constant. The strain-hardening version of power-law creep should be used when the stress state varies during an analysis [6].

The power-law time-hardening formulation in multiaxial stress state is defined as:

$$\dot{\varepsilon}_{eq,cr} = A \sigma_{eq,d}^n t^m \quad (37)$$

Where:

$\dot{\varepsilon}_{eq,cr}$ is the equivalent creep strain rate;

$\sigma_{eq,d}$ is the equivalent deviatoric stress;

A, m, n are the material parameters of the power-law model.

Power-law strain-hardening multiaxial formulation

Instead, the power-law strain-hardening formulation for multiaxial stress case is:

$$\dot{\varepsilon}_{eq,cr} = \left\{ A \sigma_{eq,d}^n [(m+1) \varepsilon_{eq,cr}]^m \right\}^{\frac{1}{m+1}} \quad (38)$$

Where $\varepsilon_{eq,cr}$ is the equivalent creep strain.

It should be always recalled, that for either versions of the power law, the stresses should be relatively low in magnitude.

Hyperbolic-sine multiaxial model

In regions of high stress, such as around a crack tip, creep strain rates frequently show an exponential dependence of stress. The hyperbolic-sine creep law has exponential dependence on the stress [6] as shown below:

$$\dot{\varepsilon}_{eq,cr} = A \left[\sinh(B \sigma_{eq,d}) \right]^n \exp\left(-\frac{\Delta H}{kT}\right) \quad (39)$$

Where A, B and n are material constants.

6 TIME-DEPENDENT CYCLIC MECHANICAL BEHAVIOUR

The cyclic behaviour of a thermally active material is very complex because in addition to the amplitude of cycle, the duration of cycle can create damage on material due to the development of creep deformation. In these situations, the material is damaged by fatigue mechanisms and creep mechanisms.

When one mechanism is dominant on the other, only this one can be included in the study of material behaviour. Instead, when damage mechanisms are on the same magnitude, both must be included in the study and, moreover, also the interaction between them, called creep-fatigue interaction, could damage the material.

A discriminating role is played by the frequency of load. If the frequency is high, viscous phenomena don't have the time to develop, and the damage of material will be caused mainly by fatigue phenomena. If the frequency is low, viscous phenomena can damage the material much more than the fatigue mechanisms do. In intermediate frequency values, the damaging of two mechanisms are comparable. Obviously, the frequency values that distinguish one case from the other depend from specific material, temperature and loading conditions.

Creep-fatigue interaction phenomena should not be confused with thermo-mechanical fatigue. The latter appears when there are large variations on temperature that involve strains of the same magnitude of strains mechanically imposed. Instead, in creep-fatigue interaction, the temperature is constant or slightly variable in order to the strains induced by the temperature difference are negligible if compared with mechanical strains.

Before to study some creep-fatigue models, is shown a summarization about fatigue damage and creep damage separately.

6.1 FATIGUE DAMAGE ASSESSMENT

The composition of fatigue damage has done typically with Palmgren-Miner's rule. Every level of load contributes to the material damage through the ratio between number of cycles executed N_i at the i -th loading level and the relative maximum number of cycle executable $N_{f,i}$. All the ratios are then cumulated.

$$D_f = \sum_{i=1}^n \left(\frac{N_i}{N_{f,i}} \right) \quad (40)$$

n is the number of load levels.

The maximum number of cycles for each load level is computable through the **universal slope equation**, derivable from the sum of Basquin equation and Coffin-Manson equation as summarized in the following.

Total strain amplitude $\frac{\Delta\varepsilon}{2}$ can be decomposed, considering negligible the viscous behaviour, in elastic part $\frac{\Delta\varepsilon_{el}}{2}$ and plastic part $\frac{\Delta\varepsilon_{pl}}{2}$:

$$\frac{\Delta\varepsilon}{2} = \frac{\Delta\varepsilon_{el}}{2} + \frac{\Delta\varepsilon_{pl}}{2} \quad (41)$$

Elastic part is described by the **Basquin equation**:

$$\frac{\Delta\varepsilon_{el}}{2} = B N_f^b \quad (42)$$

While the plastic part is described by **Coffin-Manson equation**:

$$\frac{\Delta\varepsilon_{pl}}{2} = C N_f^c \quad (43)$$

Where E is the elastic modulus, and B, C, b, c are material parameters.

Hence, the total strain-life equation, called **universal slope equation**, is:

$$\frac{\Delta\varepsilon}{2} = B N_f^b + C N_f^c \quad (44)$$

A plot of this equation is shown in *Figure 15*.

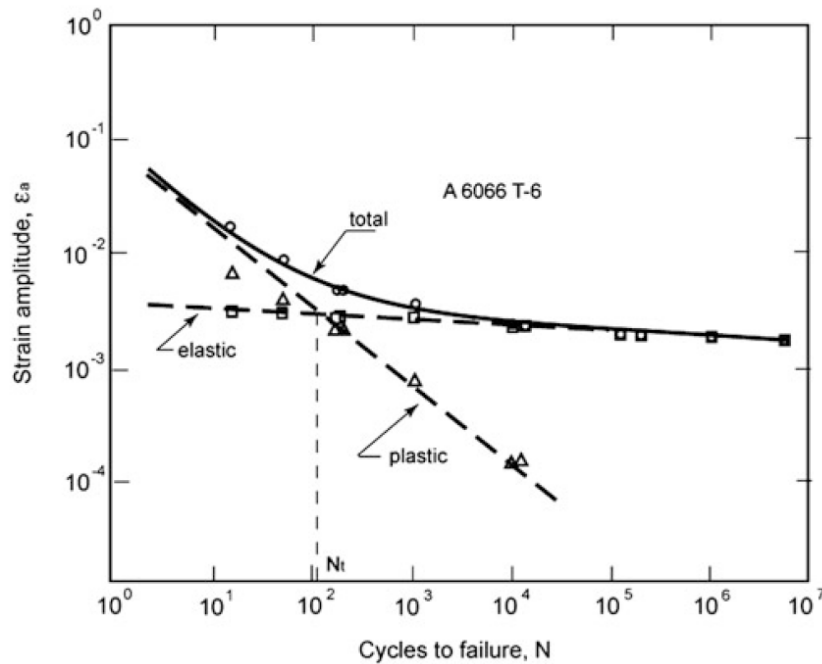


Figure 15 Plastic, elastic and total strain vs. life test data [17]

The application of Palmgren-Miner's rule is very simple to use and therefore is the most used damage fatigue criterion for engineering purpose.

However, this kind of method is not able to describe the effect of load application sequence.

6.2 CREEP DAMAGE ASSESSMENT

Material damage is a very complex interaction among many physical actions. A constitutive model of material behaviour is normally represented by a basic equation, relating creep strain rate to measurable parameters such as stress, strain, time and temperature. In addition, in order to model the process of damage accumulation, one or more so-called internal variables $\omega_1, \omega_2, \text{etc.}$ are included. The control of this internal variables can be associated with the damage control.

$$\frac{d\varepsilon_{cr}}{dt} = f(\sigma, \varepsilon_{cr}, t, T, \omega_1, \omega_2, \text{etc.}) \quad (45)$$

In addition to this equation, is also necessary to include other equations, describing the way which ω_1 , etc. evolve with time, i.e.:

$$\frac{d\omega_1}{dt} = f_1(\sigma, \varepsilon_{cr}, t, T, \omega_1, \omega_2, \text{etc.}) \quad (46)$$

Any of the variables, external or internal, can be used as a damage counter or parameter.

The practical difficulty encountered in the application of these models is the impossibility of deducing experimentally the damage parameters separately.

One model of damage stands out as unique, the **Kachanov-Rabotnov theory**. The model contains only one damage parameter, and yet it shows enough flexibility to characterize a wide range of observed material response. The reason is its relative robustness [5].

Kachanov assumed that the damage of material can be represented by a parameter called “continuity”, that’s the ratio between effective section of material A and initial section A_0 .

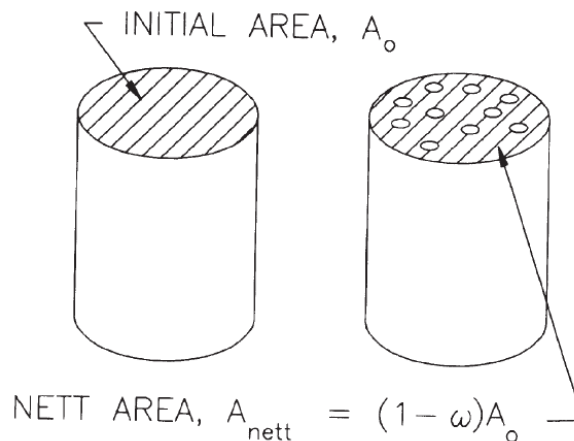


Figure 16 Kachanov's original notion of area loss ('damage') [5]

At initial time the stress is σ_0 ; as the damage increases, the internal stress increases at:

$$\sigma = \sigma_0 \frac{A_0}{A} \quad (47)$$

Subsequently, thanks to Rabotnov, “continuity” parameter was replaced by the damage parameter ω , defined as:

$$\omega = \left(1 - \frac{A}{A_0}\right) \quad (48)$$

Such parameter was implemented inside the *power-law creep equation*, obtaining:

$$\frac{d\varepsilon_{cr}}{dt} = \frac{A \sigma_0^m}{(1 - \omega)^p} = \frac{\dot{\varepsilon}_0}{(1 - \omega)^p} \quad (49)$$

Where p and m are material constants.

For $t = 0$, the model coincides with power-law model; as time increases, the damage parameter ω increases and, therefore, the creep strain rate rises.

It's necessary include a second function which describe how damage parameter vary over time. *Rabotnov* assumed the following expression:

$$\frac{d\omega}{dt} = \frac{B \sigma_0^h}{(1 - \omega)^r} \quad (50)$$

Where h and r are material constants.

The solution of the above equations is:

$$\varepsilon_{cr} = \lambda \dot{\varepsilon}_0 t_R \left[1 - \left(1 - \frac{t}{t_R}\right)^{\frac{1}{\lambda}}\right] = \lambda \varepsilon^* \left[1 - \left(1 - \frac{t}{t_R}\right)^{\frac{1}{\lambda}}\right] \quad (51)$$

or:

$$\frac{\varepsilon_{cr}}{\varepsilon_R} = \left[1 - \left(1 - \frac{t}{t_R}\right)^{\frac{1}{\lambda}}\right] \quad (52)$$

$\frac{\varepsilon_{cr}}{\varepsilon_R}$ is called **creep strain fraction**;

$\frac{t}{t_R}$ is called **life fraction**;

t_R is the **time-to-rupture**, given by:

$$t_R = \frac{1}{B (1 + r) \sigma_0^h} \quad (53)$$

And ε_R is **rupture strain**:

$$\varepsilon_R = \lambda \varepsilon^* \quad (54)$$

Where

$$\varepsilon^* = \dot{\varepsilon}_0 t_R \quad (55)$$

And

$$\lambda = \frac{1+r}{1+r-p} \quad (56)$$

It follows a schematic plot of the creep curve represented by this model.

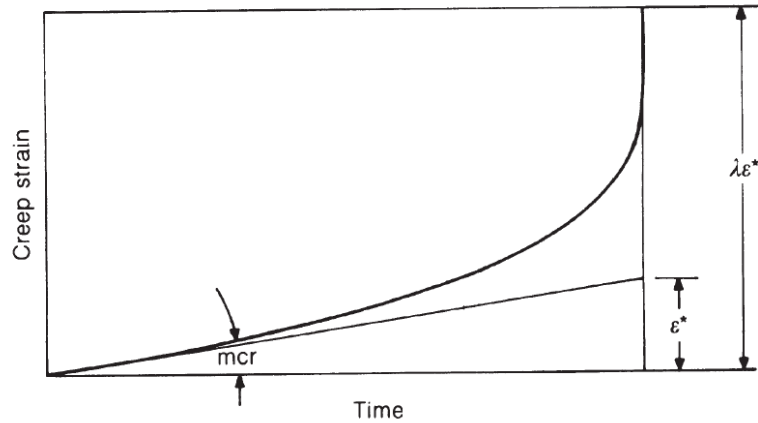


Figure 17 Schematic of creep strain growth after Kachanov [5]

This creep damage model shows some interesting features:

- It describes quite good **tertiary creep** starting from a minimum initial creep strain rate that remains constant until 25% of life-time. This consideration coming from the following equation valid for low life fraction:

$$\varepsilon_{cr} \approx \varepsilon^* \frac{t}{t_R} \left[1 + \frac{1}{2} \left(\frac{\lambda - 1}{\lambda} \right) \frac{t}{t_R} + \dots \right] \quad (57)$$

In the following charts is recognizable that the effect of λ , for different materials, is negligible in the region until 0,25 of life fraction.

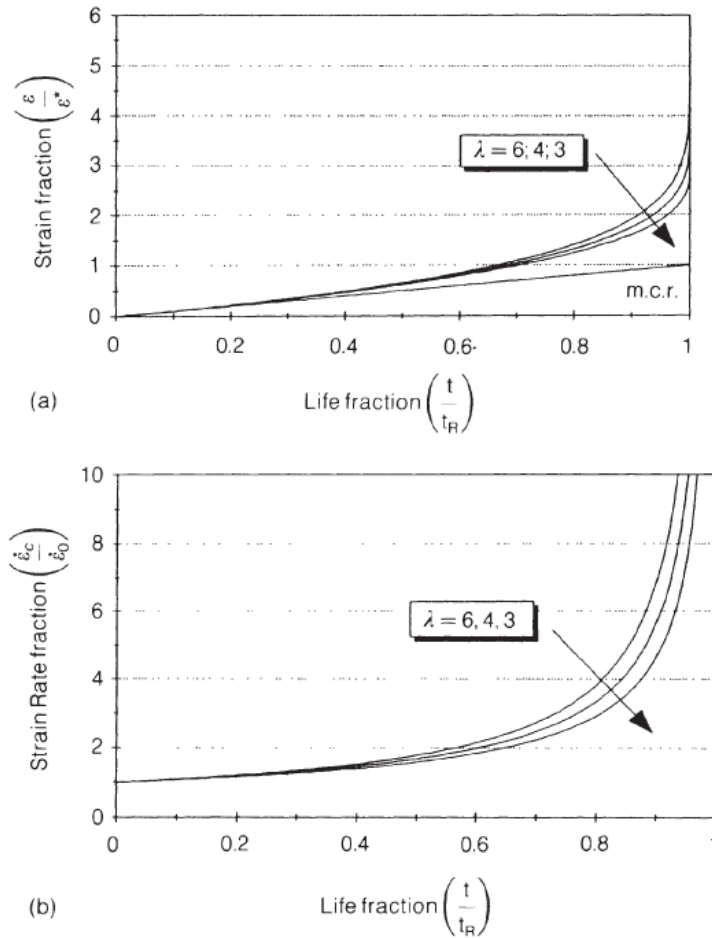


Figure 18 Strain fraction variation with life fraction for different materials [5]

- Through this model it's possible build **master curve** for creep strain growth for any **class of material**. The shape of this curve is governed by quantities which can be easily measured within the usual limits of scatter.
- The interchangeability between **creep strain fractions** and **life fractions** in this model offers two alternative possibilities in developing cumulative criteria for **damage evaluation** under variable load as below shown.

6.2.1 Robinson's life fraction rule

The criterion assumes that creep damage is accumulated by the summation of life fraction at the different stress levels.

$$D_c = \sum_{i=1}^n \left(\frac{t_i}{t_{R,i}} \right) \quad (58)$$

6.2.2 Ductility exhaustion rule

In cases of creep-fatigue interaction often strain-rate is used as driving-force in accumulation of creep damage. In a constant-stress creep test, the damage rate will change during the test. It will be low to start with, because the creep rate is high during primary creep, and will increase as the material establishes its minimum rate during secondary creep. Creep ductility found from a constant stress test is therefore a measure of damage produced under variable conditions [5].

$$D_c = \int \frac{\dot{\epsilon}_{cr}}{\epsilon_R(\dot{\epsilon}_{cr})} dt \quad (59)$$

A typical plot of $\epsilon_R(\dot{\epsilon}_{cr})$ is shown below.

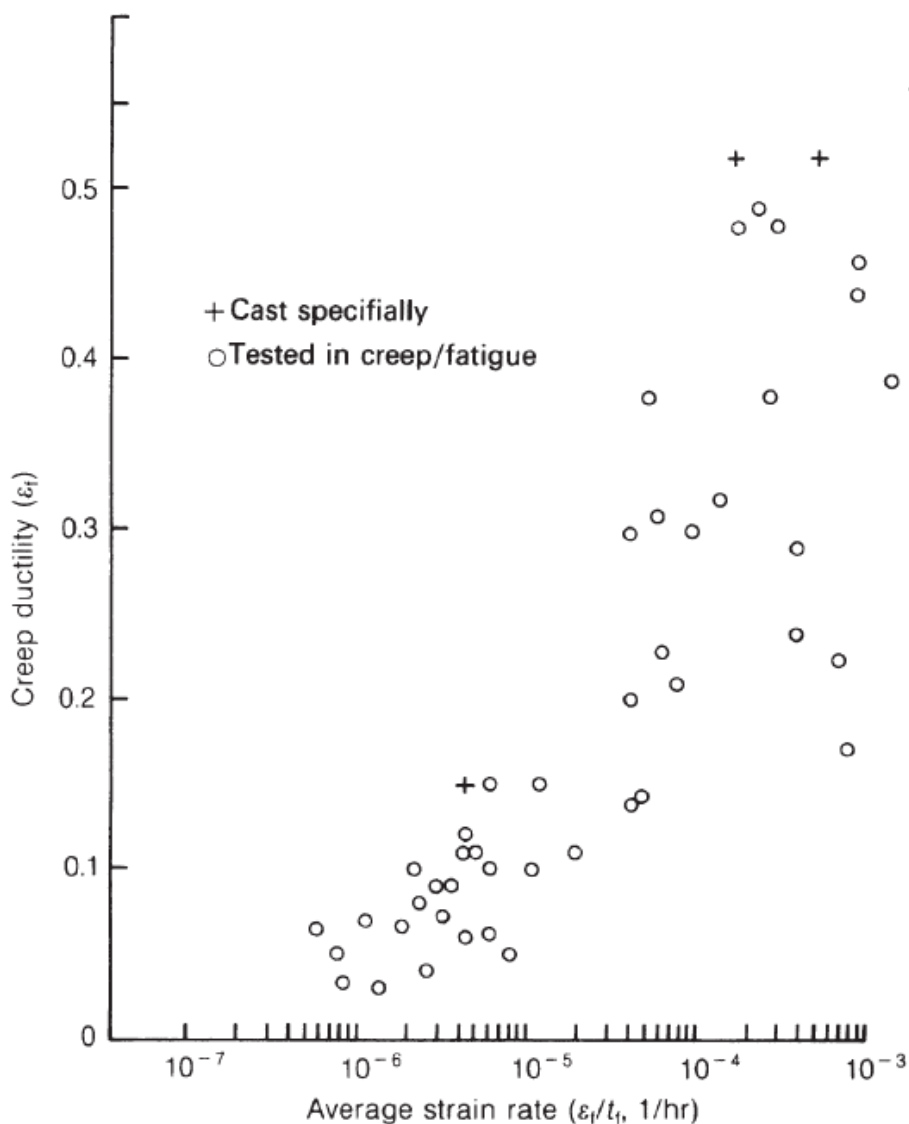


Figure 19 Reduction of creep ductility with increasing average strain rate [5]

As might be expected, the ductility increases substantially as the strain rate increases.

6.3 UNIAXIAL CREEP-FATIGUE MODELS

The separate description of creep and fatigue damage is very difficult, therefore it's not a surprise if creep-fatigue models aren't always so satisfactory in the practical design situations. Now it follows the illustration of most used methods in power and aviation community [7].

6.3.1 Linear Damage Summation

This method assumes that fatigue damage D_f and creep damage D_c are linearly cumulated; once their summation has reached unitary value, the fracture of material occurs:

$$D_f + D_c = 1 \quad (60)$$

This criterion allows to assess separately the two kind of damage.

In practice, failures have frequently been observed to occur at $D_f + D_c < 1$. It is suggested that the interaction of creep damage and fatigue damage induces additional damage, which is frequently referred to as creep-fatigue interaction damage, D_{cf} , such that failure occurs when:

$$D_f + D_c + D_{cf} = 1 \quad (61)$$

However, because of its simplicity, linear damage summation has been adopted in a high number of design codes, including the British design code for the nuclear industry and the French design code for fast-breeder reactors [7].

6.3.2 Strain Range Partitioning (SRP)

The basic premise for strain-range partitioning is that in any hysteresis loop there are combinations of just two directions of straining and two types of inelastic strain. The two directions are tension (associated with a positive inelastic strain rate), and compression (associated with a negative inelastic strain rate); the two types of inelastic strain are time dependent (creep) and time independent (plasticity).

By combining the two directions with the two types of strain, four possible kinds of strain-ranges may be used as basic building blocks for any conceivable hysteresis loop. These define how a tensile component of strain is balanced by a compressive component to close a hysteresis loop and are describe as follows:

- Tensile plasticity reversed by compressive plasticity is designated as PP strain-range and represented by $\Delta\varepsilon_{PP}$;
- Tensile creep reversed by compressive plasticity is designated as CP strain-range and represented by $\Delta\varepsilon_{CP}$;
- Tensile plasticity reversed by compressive creep is designated as PC strain-range and represented by $\Delta\varepsilon_{PC}$;

- Tensile creep reversed by compressive creep is designated as CC strain-range and represented by $\Delta\epsilon_{CC}$;

The notation for the subscripts uses the type of tensile strain first, followed by the type of compressive strain. The name strain-range partitioning was chosen because the inelastic strain-range must first be partitioned into its components. It should be noted that, in any hysteresis loop, is possible to have a maximum of only three of the four types of strain-ranges. It is not possible for the PC and CP type strain-ranges to be components of the same hysteresis loop.

The concept is that the deformation mechanism involved in reversal types may differ from each other, resulting in possible differences in life for each of the component types even if the magnitude of the strain-range is the same [8].

What has been proposed by Manson and Halford is that Coffin-Manson equation can be expanded to four relationships for dealing with thermally activated material [9].

$$\begin{aligned} \Delta\epsilon_{PP} &= C_{PP}(N_{f,PP})^{c_{PP}}; & \Delta\epsilon_{CC} &= C_{CC}(N_{f,CC})^{c_{CC}}; \\ \Delta\epsilon_{PC} &= C_{PC}(N_{f,PC})^{c_{PC}}; & \Delta\epsilon_{CP} &= C_{CP}(N_{f,CP})^{c_{CP}}; \end{aligned} \quad (62)$$

A schematic representation of the four components strain-range versus life relationships, for different materials, is shown in *Figure 20*.

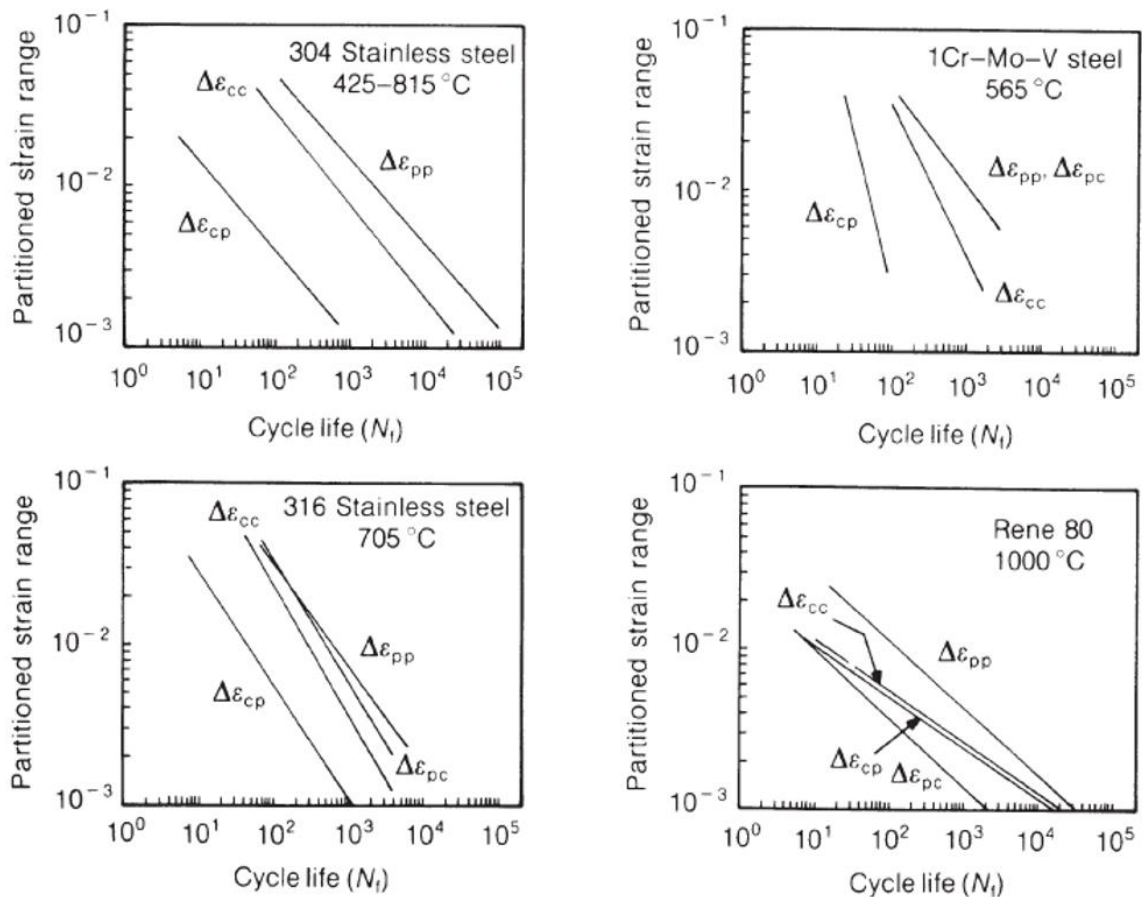


Figure 20 Examples of partitioned strain range-life relationships [4]

In order to use these relationships, is necessary produce them experimentally. Once the curves have been generated for a material, there remains the question of how to apply these curves to a more complex loading problem in order to predict life. This is accomplished in two parts:

- 1) Each hysteresis loop must be partitioned into its inelastic components. This step can be directly achieved, for instance, through a numerical stress-strain analysis.
- 2) A damage rule must be applied in order to predict the life associated with the combination of applied strain-ranges. Manson and Halford proposed the so-called Interaction Damage Rule:

$$Damage\ Cycle = \frac{1}{N_{pred}} = \frac{f_{PP}}{N_{f,PP}} + \frac{f_{CC}}{N_{f,CC}} + \frac{f_{PC}}{N_{f,PC}} \text{ or } \frac{f_{CP}}{N_{f,CP}} \quad (63)$$

Where:

$f_{ij} = \frac{\Delta\epsilon_{ij}}{\Delta\epsilon_{inel}}$ are the strain-range fractions;

$\Delta\epsilon_{inel} = \sum \Delta\epsilon_{ij}$ is the equivalent inelastic strain-range;

$N_{f,ij}$ are the cyclic lives for each SRP-type evaluated at the magnitude of $\Delta\epsilon_{inel}$.

This method of analysis for creep-fatigue interaction problems emphasizes the **effect of the frequency** on phenomena, as schematically represented below.

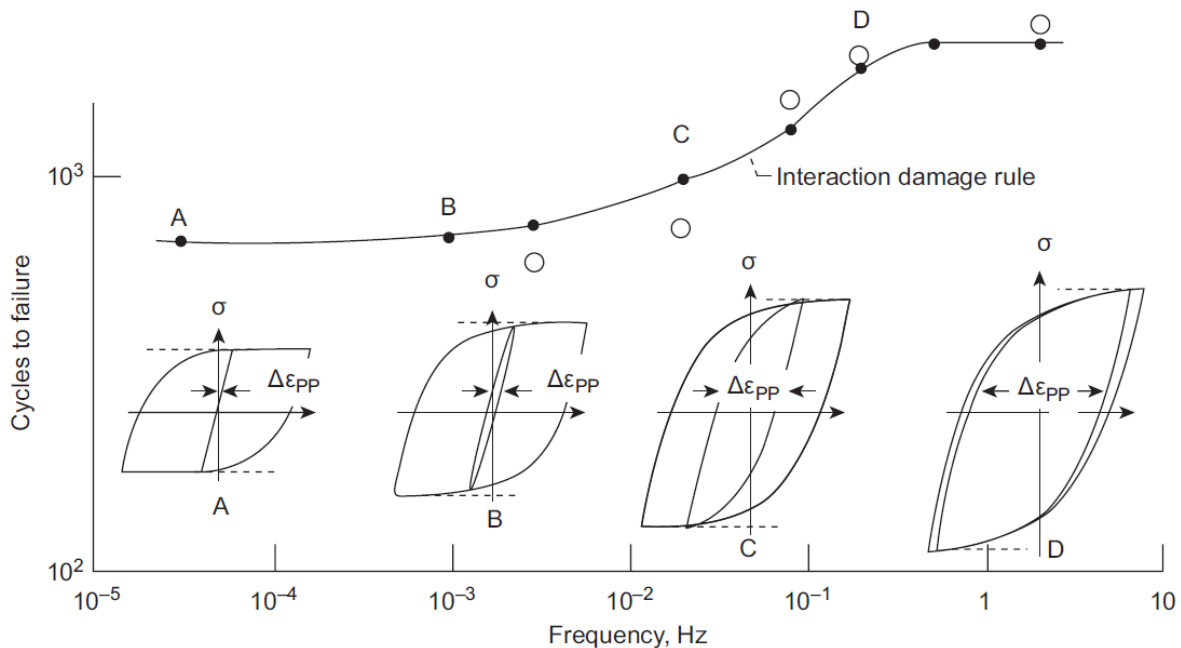


Figure 21 Effect of frequency on creep-fatigue interaction [4]

Fixed the strain amplitude, the portions of viscous or not viscous inelastic deformations depend by the frequency of load.

The primary advantage of strain-range partitioning rests on its high degree of generality. Compared to linear damage summation, the finer division into three components in the strain-range partitioning has yielded superior results. On the other hand, it demands significantly more characterisation effort using specialised test cycles [7]. The PP type hysteresis loop can be generated in a conventional manner, but the other three require some less-conventional testing procedures.

The following picture shows different types of test cycles.

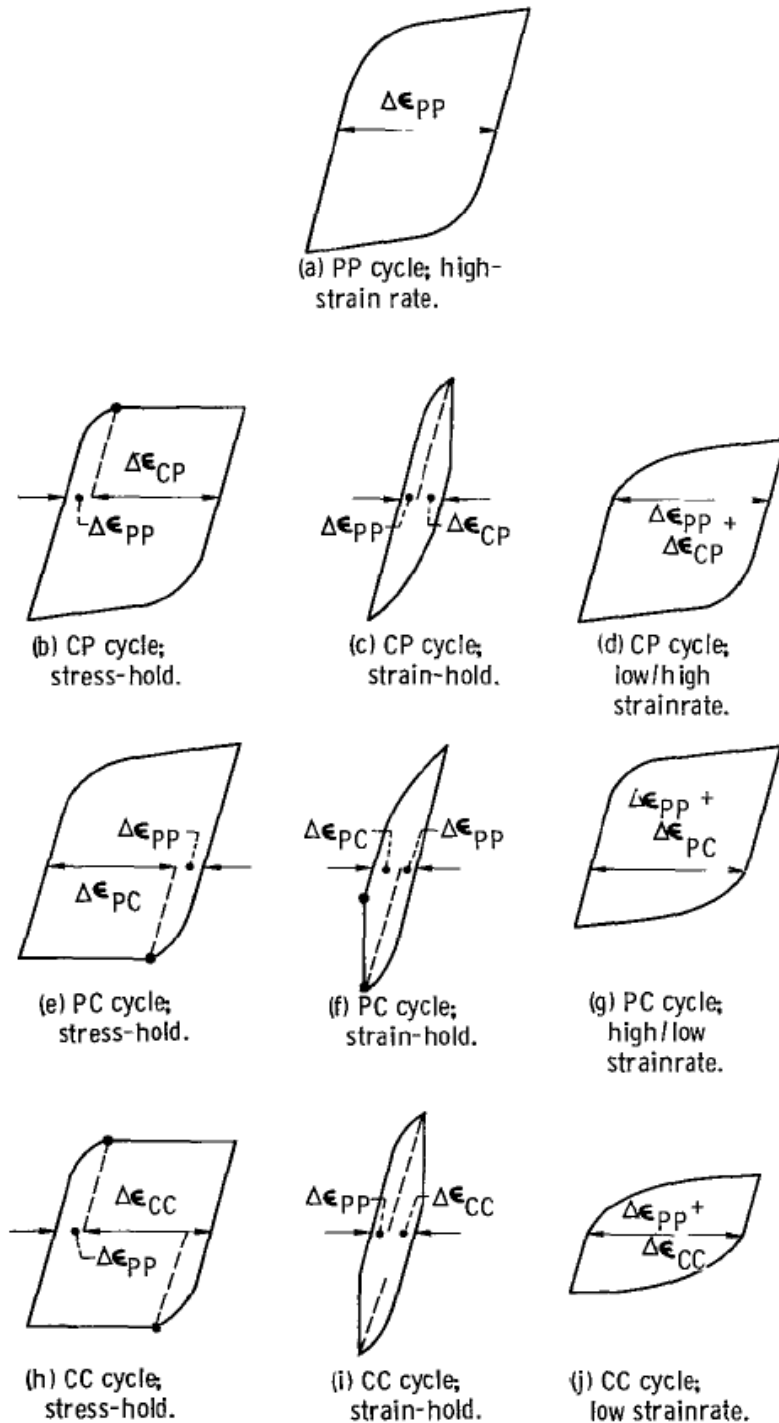


Figure 22 Examples of test cycles for SRP application [9]

6.3.3 Frequency modified fatigue

Coffin chose to modify the fatigue equation directly by using a frequency term. If the cyclic frequency is ν , then in comparison with a standard test frequency ν_0 , the relationship between plastic strain-range $\Delta\varepsilon_p$ and cycles to failure N_f is taken to be [5]:

$$\Delta\varepsilon_p = CN_f^c \left(\frac{\nu}{\nu_0}\right)^p \quad (64)$$

Where p is a small number, typically 0.1 to 0.2 [5].

The simplicity of this model has attracted great interest in the electronic-microelectronic assembly communities. However, the model has not found good agreement with practical applications [7]. It has been found that the shape of the waveform affects the degree of creep-fatigue interaction. Coffin attempted to elaborate on the frequency-modified equation, in order to account the waveform. He achieved some success, but only at the cost of increasingly complex empirical expressions.

6.4 SRP UNDER MULTIAXIAL CONDITIONS

Multiaxial stresses complicate both the physical mechanism and the analysis required to account for them in fatigue life assessment. It is commonly observed, for example, that under uniaxial loading, cracks start in a direction of maximum shear stress that is oriented at 45° to the applied loading direction and, after small growth, propagate in a direction perpendicular to the maximum applied normal stress. Thus, the ratio of the shear stress to normal stress is unity in the plane wherein the crack starts but is zero where in the crack propagates. Under multiaxial loading, however, is possible to obtain any desired value of shear to normal stress both in the crack-initiation plane and in the crack-propagation plane. Uniaxial tests may not contain all the necessary information to permit full extension to multiaxial predictions [4].

It is not surprising, hence, that many approaches have been proposed for treating multiaxial fatigue failure. Brown and Miller cited 18 criteria that had been investigated in the past and concluded that all are deficient in one respect or another [4].

A more recent assessment of large number of prominent multiaxial fatigue models was reported by Kallmeyer, Krgo, and Kurath, but no guidance was presented for creep-fatigue under multiaxial loading conditions [4].

The **strain-range partitioning** method can be easily extended to multiaxial loading if the hypothesis of **proportional loading** (stress and inelastic strains are proportional between them all times) and **Von-Mises plasticity** are used.

The extension of SRP method can be summarized into following steps:

- Preliminary stress-strain analysis;
- Equivalent stress and strain parameters;
- Rule of sign for dominant principal direction;
- Partitioning of equivalent strain-ranges;
- Use of life relationships modified by triaxial-state effect;
- Application of damage rule.

6.4.1 Preliminary stress-strain analysis

SRP method under multiaxial conditions require that the hysteresis loop for all the three principal directions can be evaluated through conventional mechanics analysis, computerized finite element analysis, or direct experimental observations. Equations appropriate for this are based on equilibrium, compatibility, plasticity theory and appropriate viscous-plastic constitutive modelling [4].

From this analysis it's possible to separate also the creep and plastic strain, in order to discriminate successively the different kinds of strain-ranges.

6.4.2 Equivalent stress and strain parameters

The idea is to use equivalent scalar parameters, representative of the triaxial state of stress and strain, in order to keep the same procedure of SRP method under uniaxial conditions.

The equivalent stress σ_{eq} and the equivalent inelastic strain $\varepsilon_{eq,inel}$ are computed by the Von-Mises model of plasticity:

$$\sigma_{eq} = \frac{1}{\sqrt{2}} [(\sigma_I - \sigma_{II})^2 + (\sigma_I - \sigma_{III})^2 + (\sigma_{II} - \sigma_{III})^2]^{\frac{1}{2}} \quad (65)$$

$$\varepsilon_{eq,inel} = \frac{\sqrt{2}}{3} [(\varepsilon_{I,inel} - \varepsilon_{II,inel})^2 + (\varepsilon_{I,inel} - \varepsilon_{III,inel})^2 + (\varepsilon_{II,inel} - \varepsilon_{III,inel})^2]^{\frac{1}{2}} \quad (66)$$

Where σ_I , σ_{II} , σ_{III} are the principal stresses and $\varepsilon_{I,inel}$, $\varepsilon_{II,inel}$, $\varepsilon_{III,inel}$ are the principal inelastic strain.

In this model it has assumed that inelastic strains are sufficiently large to make elastic strain negligible from an engineering viewpoint.

6.4.3 Rule of sign for the dominant principal direction

Rule of sign implementation is necessary to keep the cyclic character of problem since the equivalent scalar parameters are quantities always positive.

From the values of equivalent stress and equivalent strain at each point in the cycle, is possible to construct an equivalent hysteresis loop wherein, at each instant of time, the stress is equivalent stress and the strain is equivalent strain.

When one component clearly dominates the loading, the decision is unambiguous: the dominant direction is chosen based on the direction having the largest computed stress range $\Delta\sigma$.

In cases of biaxial stresses, the sign of the strain in secondary direction must be considered only if:

$$\Delta\sigma_{II} > \frac{1}{2}\Delta\sigma_I \quad (67)$$

In cases of triaxial stresses, the sign of the strain in secondary direction must be considered only if both following criteria are satisfied:

$$\Delta\sigma_{II} > \frac{1}{2}\Delta\sigma_I; \quad \Delta\sigma_{II} > \frac{1}{2}(\Delta\sigma_I + \Delta\sigma_{III}); \quad (68)$$

The treatment of secondary direction is exhaustively explained into reference [4].

6.4.4 Partitioned equivalent strain-ranges

This step requires the partitioning of equivalent strains in order to identify the different types of equivalent strain-ranges.

Once assigned the sign at equivalent strain is available the equivalent inelastic strain history as schematically shown below.

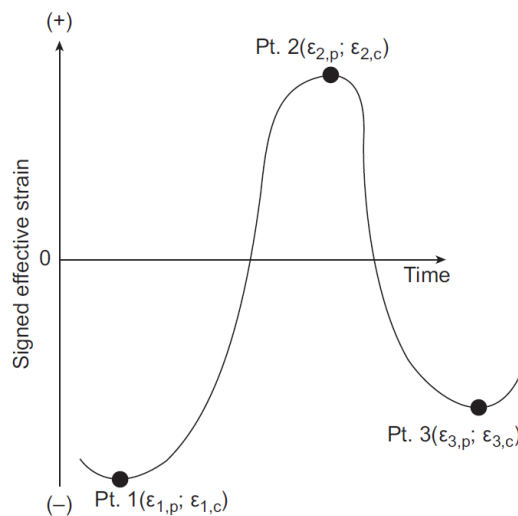


Figure 23 Schematic strain cycle in terms of signed effective strain [4]

Simple rules are followed in the assignment of equivalent strain-ranges:

- Equivalent plastic strain-range $\Delta\varepsilon_{eq,PP}$ is equal to the lesser of the equivalent plastic strain-range in the tensile direction (from minimum to maximum) or compressive direction (from maximum to minimum).
- Equivalent creep strain-range $\Delta\varepsilon_{eq,CC}$ is equal to the lesser of the equivalent creep strain-ranges in the positive or negative direction.
- If there is excess of plasticity in tension and excess creep in compression, the unbalanced equivalent strain-range $\Delta\varepsilon_{eq,PC}$ (or $\Delta\varepsilon_{eq,CP}$ if the types of strains are reversed in their directions) is equal to the lesser of these two remainders.
- Any strain that remains after the three equivalent strain ranges ($\Delta\varepsilon_{eq,PP}$, $\Delta\varepsilon_{eq,CC}$, $\Delta\varepsilon_{eq,PC}$, $\Delta\varepsilon_{eq,CP}$) have been accounted for constitute the ratchet strain δ_P or δ_C .

A general algorithm is presented below. It here refers to the *Figure 23*.

If:

- $A_2^p = \varepsilon_{2,eq,p} - \varepsilon_{1,eq,p}$: equivalent plastic strain-range for tensile half of cycle (minimum to maximum);
- $A_2^c = \varepsilon_{2,eq,c} - \varepsilon_{1,eq,c}$: equivalent creep strain-range for tensile half of cycle (minimum to maximum);
- $A_3^p = \varepsilon_{2,eq,p} - \varepsilon_{3,eq,p}$: equivalent plastic strain-range for compressive half of cycle (maximum to minimum);
- $A_3^c = \varepsilon_{2,eq,c} - \varepsilon_{3,eq,c}$: equivalent creep strain-range for compressive half of cycle (maximum to minimum);
- $A_L^p = \max(A_2^p; A_3^p)$: larger of A_2^p and A_3^p ;
- $A_S^p = \min(A_2^p; A_3^p)$: smaller of A_2^p and A_3^p ;
- $A_L^c = \max(A_2^c; A_3^c)$: larger of A_2^c and A_3^c ;
- $A_S^c = \min(A_2^c; A_3^c)$: smaller of A_2^c and A_3^c ;
- $B_2 = A_2^p + A_2^c$: equivalent inelastic tensile strain-range (point 1 to point 2);

- $B_3 = A_3^p + A_3^c$: equivalent inelastic compressive strain-range (point 2 to point 3);
- $B_S = \min(B_2; B_3)$: smaller of B_2 and B_3 , that represents the equivalent inelastic strain-range.

Then:

- $\Delta \varepsilon_{eq,PP} = A_S^p$; $\Delta \varepsilon_{eq,CC} = A_S^c$;
- $\Delta \varepsilon_{eq,PC} = B_S - A_S^p - A_S^c$; if $A_L^p = A_2^p$ and $A_S^c = A_5^c$;
- $\Delta \varepsilon_{eq,CP} = B_S - A_S^p - A_S^c$; if $A_S^p = A_2^p$ and $A_L^c = A_2^c$;
- $\delta_p = A_L^p - A_S^p - B_S + A_S^p + A_S^c = A_L^p + A_S^c - B_S$;
- $\delta_c = A_L^c - A_S^c - B_S + A_S^p + A_S^c = A_L^c + A_S^c - B_S$;

Perform the aforementioned calculations using dominant direction as the sign donor for equivalent strain. Further explanations can be found on reference [4].

6.4.5 Fatigue life equations modified by triaxial-state effect

An important influence of multiaxial states of stress is to alter the apparent ductility exhibited by engineering materials. Triaxial tensile stress reduce ductility, while compressive triaxiality can significantly increase ductility [4].

Before that life relationships (based on axial tests) are used for life predictions in multiaxial situations, recognition should be made of the significant changing in ductility and strain resistance for the presence of triaxial stress states.

The Triaxiality Factor TF is the parameter able to describe this effect. It is defined as the ratio between mean stress, representative of hydrostatic stress, and equivalent stress, representative of deviatoric stress:

$$TF = \frac{\sigma_m}{\sigma_{eq}} = \frac{\sqrt{2} (\sigma_I + \sigma_{II} + \sigma_{III})}{\sqrt{(\sigma_I - \sigma_{II})^2 + (\sigma_I - \sigma_{III})^2 + (\sigma_{II} - \sigma_{III})^2}} \quad (69)$$

Where the factor 3 at denominator lacks because in this way TF takes values of +1 for uniaxial tension, 0 for torsion, and -1 for uniaxial compression.

In order to implement an always positive numerical value in fatigue-life equation, Manson and Halford devised a new parameter, called Multiaxiality Factor MF, so defined:

$$MF = TF \quad \text{for } TF \geq 1 \quad (70)$$

$$MF = \frac{1}{(2 - TF)} \quad \text{for } TF \leq 1 \quad (71)$$

Using these definitions, MF is always a positive number, and can be used directly in the following equation, called **Equivalent strain range theory modified by MF**.

$$\Delta \varepsilon_{eq,ij} = \frac{C_{ij}}{MF} (N_{f,ij})^{c_{ij}} = C'_{ij} (N_{f,ij})^{c_{ij}} \quad (72)$$

Where the index i, j can refer to time-dependent inelastic deformation (plastic) and time-dependent inelastic deformation (creep).

As MF becomes greater than 1, ductility decreases, but as MF becomes less than 1, the ductility increases. This is illustrated in *Figure 24* where MF is plotted as a function of TF. Note that MF is plotted on a logarithmic scale, while TF is plotted on a linear scale. Superimposed on the figure is a dashed line representing the following equation, proposed by Manjoine.

$$MF = 2^{(TF-1)} \quad (73)$$

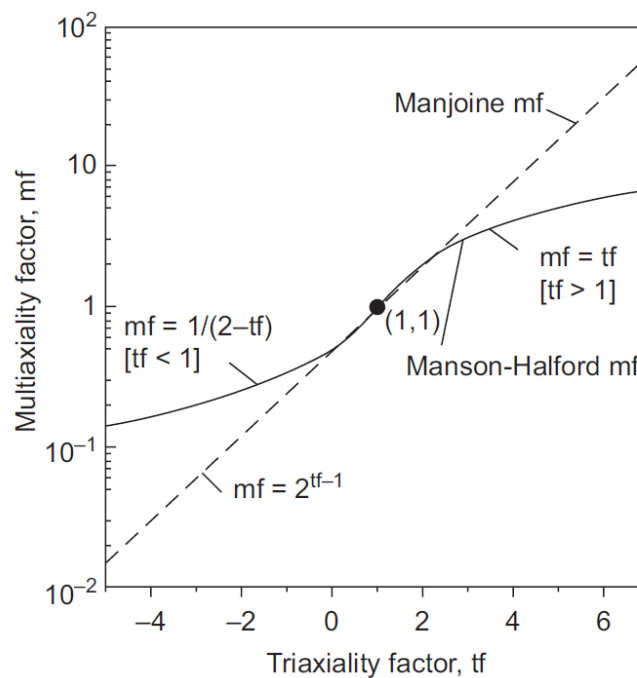


Figure 24 Multi-axiality versus tri-axiality factor relationships [4]

The same treatment of the multi-axial stress state can be done if **total strain** is considered. In this case we have the **total equivalent strain range theory modified by MF** [10].

Starting from the universal slope equation (44), valid for the uniaxial case:

$$\Delta \varepsilon = BN_f^b + CN_f^c$$

It's possible to identify as N_t the *transition life* between the elastic part and inelastic part and with $\Delta\varepsilon_t$ the relative *transition strain range*.

So:

$$\Delta\varepsilon_t = B(N_t)^b = C(N_t)^c \quad (74)$$

Solving from N_t :

$$N_t = \left(\frac{C}{B}\right)^{\frac{1}{b-c}} \quad (75)$$

And substituting in (74)

$$\Delta\varepsilon_t = C \left(\frac{C}{B}\right)^{\frac{c}{b-c}} \quad (76)$$

Now, if we consider the equivalent strain range modified by MF (72):

$$\Delta\varepsilon_{eq,pl} = \frac{C}{MF} (N_f)^c = C'(N_f)^c$$

It's reasonable to extend in the same way the concept of MF also for the total strain life equation:

$$\Delta\varepsilon_{eq} = B'(N_f)^b + C'(N_f)^c \quad (77)$$

The value of B' can be obtained by assuming that cyclic stress-strain curve remains unchanged during multiaxial loading. Then, also the transition strain range $\Delta\varepsilon_t$ remains unchanged [10]. Comparing transition strain range $\Delta\varepsilon_t$ of uniaxial case, with transition strain range $\Delta\varepsilon'_t$ of multi-axial case:

$$\Delta\varepsilon_t = C \left(\frac{C}{B}\right)^{\frac{c}{b-c}} = \Delta\varepsilon'_t = C' \left(\frac{C'}{B'}\right)^{\frac{c}{b-c}} \quad (78)$$

Substituting the expression of C' :

$$\frac{C}{MF} \left(\frac{C}{MF B'}\right)^{\frac{c}{b-c}} = C \left(\frac{C}{B}\right)^{\frac{c}{b-c}} \quad (79)$$

And solving for B' :

$$B' = B MF^{-\frac{b}{c}} \quad (80)$$

Finally, the **total equivalent strain-range theory modified by MF** assumes the following expression:

$$\Delta\varepsilon_{eq} = MF^{-b/c} B (N_f)^b + \frac{C}{MF} (N_f)^c \quad (81)$$

This is a more complex of multiaxial fatigue life relationship that can be used also for time-independent analysis.

In the following schematic figure is represented how MF can move the fatigue line. If $MF > 1$ (as in the picture) the ductility of material decreases, and the fatigue line moves down. On the other hand, when $MF < 1$, the material has able to bear a major number of cycles with the fixed total equivalent strain amplitude, and the fatigue line moves up.

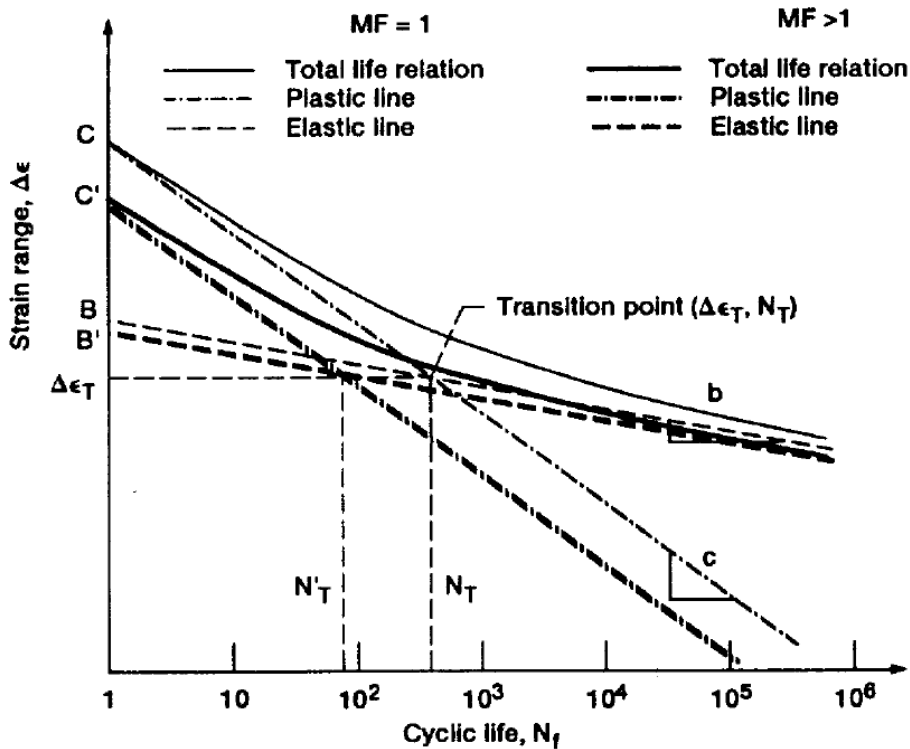


Figure 25 Fatigue life under uniaxial and multiaxial conditions [10]

6.4.6 Interaction damage rule

Finally, the expected life can be evaluated by using the Interaction Damage Rule modified to include the ratchet terms and MF.

$$Damage\ Cyle = \frac{1}{N_{pred}} = \frac{f_{PP}}{N_{f,PP}} + \frac{f_{CC}}{N_{f,CC}} + \frac{f_{PC}}{N_{f,PC}} \text{ or } \frac{f_{CP}}{N_{f,CP}} + \frac{\delta_P MF}{d_P} + \frac{\delta_C MF}{d_C} \quad (82)$$

Where d_P and d_C are respectively plastic ductility and creep ductility evaluated by uniaxial tests.

Obviously, MF affects also the fatigue life of each strain-range component as previously shown.

In [4], it's possible to find explanations on how alter the above procedure in order to use the total equivalent strain-ranges, by considering, hence, also the elastic strains, but the effects of multiaxial state of stress don't change.

6.5 FINAL CONSIDERATIONS

In the study of time-dependent cyclic behaviour stands out clearly the difficulty in the making an accurate prediction life. The material could degrade for creep damage (when the load frequency is low), for fatigue damage (when the load frequency is high), or for an interaction between the two phenomena (when the load frequency is intermediate). The frequency of load affects strongly the predominant damage mechanism, and it can also vary during the cable's service.

Anyway, each damage mechanism is influenced by the triaxiality stress state in the same way. A positive triaxiality of stress reduces the material life, while a negative triaxiality of stress increases the life of material.

Two further aspects were considered before to take the final decision:

- It's available a calibrate viscous constitutive model for the lead alloy of a real submarine power cable.
- The boundary conditions of submarine power cables are very variables and it's not practicable tests ad hoc for every possible condition of loading.

The union of these two aspects, together with results of the theoretical study executed, led to the decision to create a **finite element model for stress-strain analysis** in order to investigate the lead alloy behaviour under different operative conditions.

The next part of work shows the creation of the numerical model.

PART III

FINITE ELEMENT ANALYSIS

Purpose of the model

The theoretical study of submarine power cable's damaging, especially of lead sheath, has shown more times the necessity to know the stress and strain field to which the lead sheath is subjected.

The modelling of whole submarine power cable is a very challenging activity for what concerns the implementations of material properties, interactions between parts, types of boundary conditions.

For an accurate quantitative analysis are necessary great quantities of input data, that today, unfortunately, they are not yet available. Anyway, the team of researchers committed to the structural optimization of Nexans' submarine power cable, had experimentally obtained a viscous material calibrated model for the lead alloy sheath. This was thought to be the starting point for creation of the numerical model.

The strategy followed was to model the different components of cable in the best possible way, in according to the available data, and to model the operating conditions with hypothetical numerical values. On the base of these conditions, design changes were made in order to obtain improvements on mechanical behaviour of the lead-alloy sheath.

7 INPUT DATA AVAILABLE

Input data available can be distinguished as follows:

- data provided by the company (Nexans);
- data provided by previous experimental works;
- data collected by searches on submarine power cables literature.

7.1 DATA PROVIDED BY NEXANS

7.1.1 Geometric data and types of material

Figure 26 shows a schematic cross section of cable. Then it follows associated table of geometric data with relative type of material for each component.

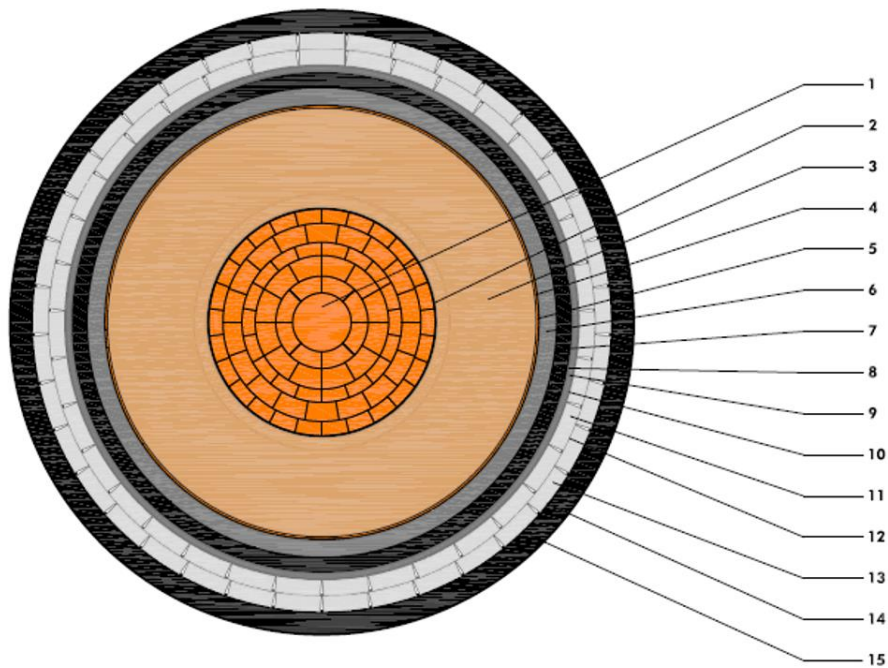


Figure 26 Schematic cross section of a real submarine power cable

7 INPUT DATA AVAILABLE

Table 1 Geometric data of real submarine power cable

NO	Description	Material	Nominal Thickness (mm)	Nominal Diameter (mm)
1	Conductor	Copper		46.3
2	Conductor screen	Carbon black paper tapes		
3	Insulation	Impregnated paper tapes	20.15	87.4
4	Insulation screen	Carbon black paper and metallized paper tapes		
5	Serving	Copper woven fabric tape		
6	Lead Sheath	E-Alloy	3.3	95.8
7	PE Sheath	PE	3.3	
8	Bedding	Semi conductive nylon tape		
9	Reinforcement	Galvanized steel	2 x 0.4	
10	Bedding	Semi conductive nylon tape		
11	Armour wires	Galvanized steel GR34	9 x 3	
12	Bedding	Plastic coated nylon tape		
13	Armour wires	Galvanized Steel GR34	9 x 3	
14	Bedding	Plastic coated polyester tape		
15	Outer sheath	HDPE	4.9	128

7.1.2 Plastic flow curve of PE sheath

The company gave the following data for the Polyethylene sheath.

- Elastic Modulus: $E = 600 \text{ MPa}$
- Poisson Modulus: $\nu = 0.46$

Table 2 Plastic behaviour data for PE sheath

σ (MPa)	2	3	4	6	7.5	9	9.5	10	10.5	11	11.5	12.5	13	13.5
ϵ_{pl}	0	0.015	0.023	0.04	0.09	0.19	0.29	0.39	0.49	0.59	0.69	0.79	0.89	0.99

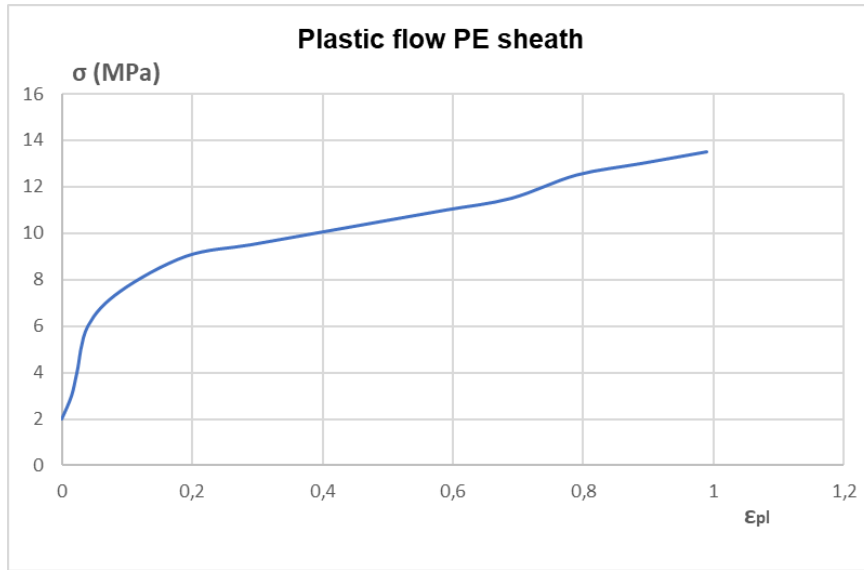


Figure 27 Plastic behaviour for PE sheath

7.1.3 Plastic flow curve of outer sheath

The company gave the following data for the outer sheath, made of HDPE.

- Elastic Modulus: $E = 780 \text{ MPa}$
- Poisson Modulus: $\nu = 0.46$

Table 3 Plastic behaviour data for HDPE sheath

σ (MPa)	10	10	10	10	10	10	10.5	11.75	14	17	20
ϵ_{pl}	0	0.2	0.5	0.8	1	1.5	1.7	2	3	4	5

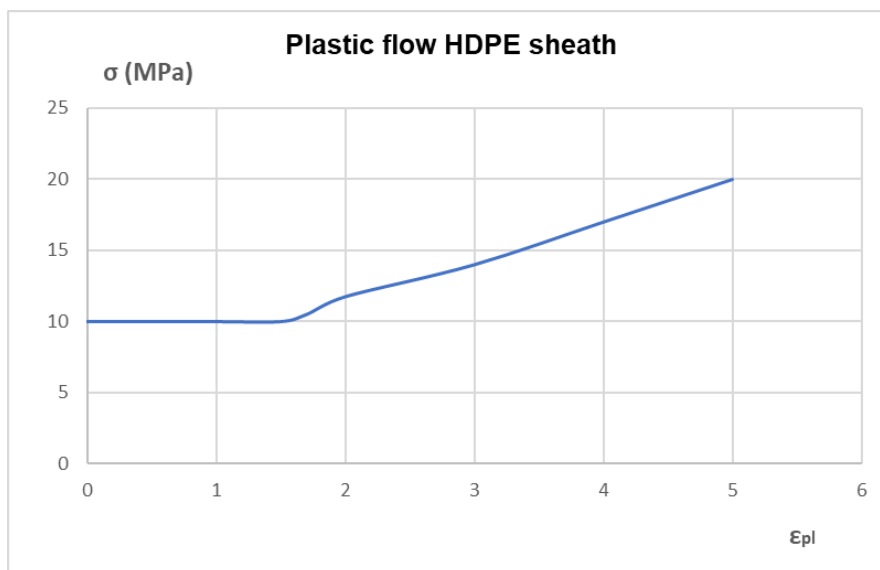


Figure 28 Plastic behaviour for HDPE sheath

7.2 DATA PROVIDED BY PREVIOUS EXPERIMENTAL CALIBRATION

As it cited previously, is available a time-dependent constitutive law obtained from previous experimental works led by Viespoli et al. [11].

The material in question is a lead alloy, called **E-Alloy**, with the following **chemical composition**: Pb: 99,3 wt%, Sb: 0,2 wt%, Sn: 0,5 wt%.

Elastic modulus and Poisson modulus are respectively: $E = 12000 \text{ MPa}$; $\nu = 0.431$.

Plastic behaviour data of the lead alloy is shown in *Table 4*.

Table 4 Plastic behaviour data for Lead alloy sheath

σ (MPa)	7.4	7.9	8.45	10.5	11.6	12.26	13.15	14.3	15.25	17.3
ϵ_{pl}	0	0.000006	0.00013	0.00044	0.0008	0.00129	0.0024	0.0052	0.0088	0.0248

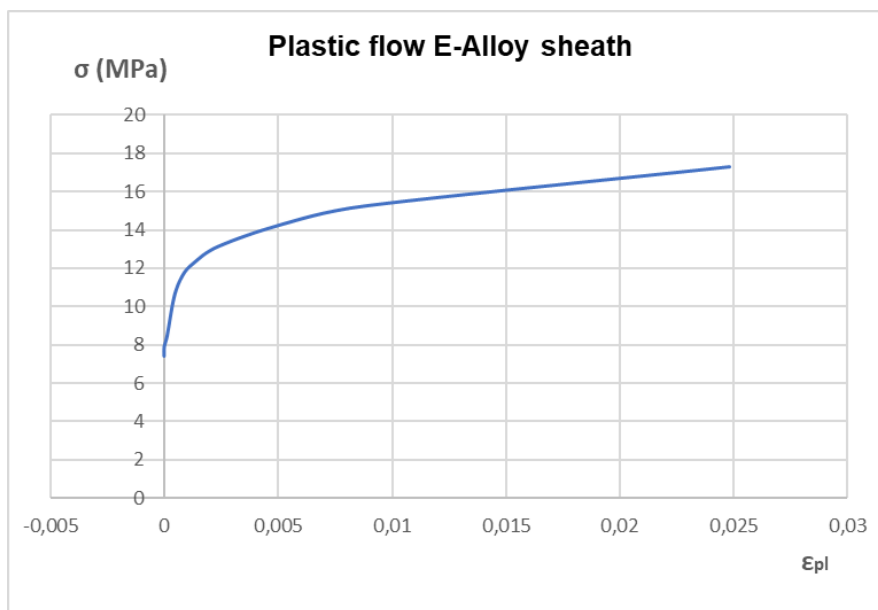


Figure 29 Plastic behaviour for Lead alloy sheath

A **power-law strain-hardening** creep model (38) was calibrated. His formulation is reported for completeness.

$$\dot{\epsilon}_{eq,cr} = \left\{ A \sigma_{eq,d}^n \left[(m+1) \epsilon_{eq,cr} \right]^m \right\}^{\frac{1}{m+1}}$$

The numerical values of material parameters obtained are:

- **A = 5,278 E-10**
- **m = -0,47**
- **n = 5,22**

The whole experimental procedure adopted is explained in [11].

7.3 DATA COLLECTED BY SEARCHES ON SUBMARINE POWER CABLES LITERATURE

With the purpose to increment the quantity of available input data, enhancing therefore the accuracy of model, it has been led a further investigation.

Fortunately, from the literature it has been possible to collect important information.

- The initial temperature of submarine ambient is about 4°C [12].
- At regime conditions, the temperature reached at the interface between insulation system and lead sheath is around 50°C [12].
- The insulation system can be considered from a mechanical point of view as a linear elastic behaviour material because the oil used has high viscosity. A typical mineral oil used is 'T2015' [12].
- From a thermal viewpoint, only the oil must be considered for modelling the thermal load. This because the oil has a thermal expansion coefficient much higher than the other components [12]. A typical value for the thermal expansion coefficient of the oil is $6.3 \cdot 10^{-4}$ (1/K) [13].
- For thermal load modelling, is necessary to consider an **impregnation level**, defined as the ratio between the oil volume and the total insulation volume. This value is useful in order to include the right volume in thermal expansion modelling. Typical values are comprised by 0.3 to 0.7, but often is used 0.4 [13].
- In first increments of temperature, the oil inside the paper expands and fill the cavities of paper without radial motion. Once it reached a limit of temperature, called **cavity free temperature**, further increments of temperature cause radial motion of the oil and the creation of internal pressure for lead sheath. A typical value of cavity free temperature is about 30°C [13]. Therefore, a reasonable thermal excursion to attribute for the thermal load modelling is about 20°C.

7.4 SUMMARIZATION OF INPUT DATA AVAILABLE

The following table reassumes the input data available for the creation of numerical model.

Table 5 Input data available

COMPONENT	INPUT DATA AVAILABLE
<i>Conductor</i>	Geometry, type of material: Copper
<i>Insulation system</i>	Geometry, type of material: Kraft paper with mineral oil
	Impregnation level $q = 0.4$
	Cavity free temperature $T_{\text{free}} = 31^{\circ}\text{C}$
	Thermal expansion coefficient $\alpha_v = 6.3\text{e-}4 \text{ } 1/^{\circ}\text{C}$
	Elastic modulus of paper $E_{\text{paper}} = 10000 \text{ MPa}$
	Usefull thermal excursion $\Delta T_{\text{useful}} = 20^{\circ}\text{C}$
<i>Lead sheath</i>	Geometry, type of material: E-Alloy
	Elastic behaviour: $E = 12000 \text{ MPa}$; $\nu = 0.431$
	Plastic behaviour: plastic table
	Creep behaviour: $A = 5.278\text{e-}10$; $m = -0.47$; $n = 5.22$
<i>PE sheath</i>	Geometry, type of material: PE
	Elastic behaviour: $E = 600 \text{ MPa}$; $\nu = 0.46$
	Plastic behaviour: plastic table
<i>Reinforcement</i>	Geometry, type of material: galvanized steel tapes
	Winding angle: 70 degrees from the cable axis
<i>Armour 1</i>	Geometry, type of material: galvanized steel wires
	Winding angle: 12.7 degrees from the cable axis
<i>Armour 2</i>	Geometry, type of material: galvanized steel wires
	Winding angle: -10.5 degrees from the cable axis
<i>Outer sheath</i>	Geometry, type of material: HDPE
	Elastic behaviour: $E = 780 \text{ MPa}$; $\nu = 0.46$
	Plastic behaviour: plastic table

8 SCHEMATIZATION OF CABLE

Starting from the real geometry of cable all the main components were included in Abaqus/CAE. Only plastic films, with the function of separation between principal parts, weren't modelled. These films are useful during coiling and uncoiling operations because allow the slipping between different parts by avoiding the rising of stress. However, under service conditions, all parts are pressed against each other and no slip is allowed. For this reason, the separation films are neglected in this analysis.

Conductor, reinforcement and armours were modelled as continue bodies.

The implemented geometry is reported in the following table. Each part modelled was labelled with a letter.

Table 6 Geometric data of model

Part	Components	Description	Material	t (mm)	Rint (mm)	Rext (mm)
A	1	Conductor	Copper			23.15
	2	Conductor screen	Carbon black paper tapes	0.4	23.15	23.55
B	3	Insulation	Impregnated paper tapes	20.15	23.55	43.7
	4	Insulation screen	Carbon black paper and metallized paper tapes			
	5	Serving	Copper woven fabric tape			44.6
C	6	Lead Sheath	E-Alloy	3.3	44.6	47.9
D	7	PE Sheath	PE	3.3	47.9	51.2
	8	Bedding	Semi conductive nylon tape			
E	9	Reinforcement	Galvanized Steel	0.8	51.2	52
	10	Bedding	Semi conductive nylon tape			
F	11	Armour wires	Galvanized Steel GR34	3	52	55
	12	Bedding	Plastic coated nylon tape			
G	13	Armour wires	Galvanized Steel GR34	3	55	58
	14	Bedding	Plastic coated polyester tape			
H	15	Outer Sheath	HDPE	6	58	64

A cross section of modelled cable is shown in *Figure 30*.

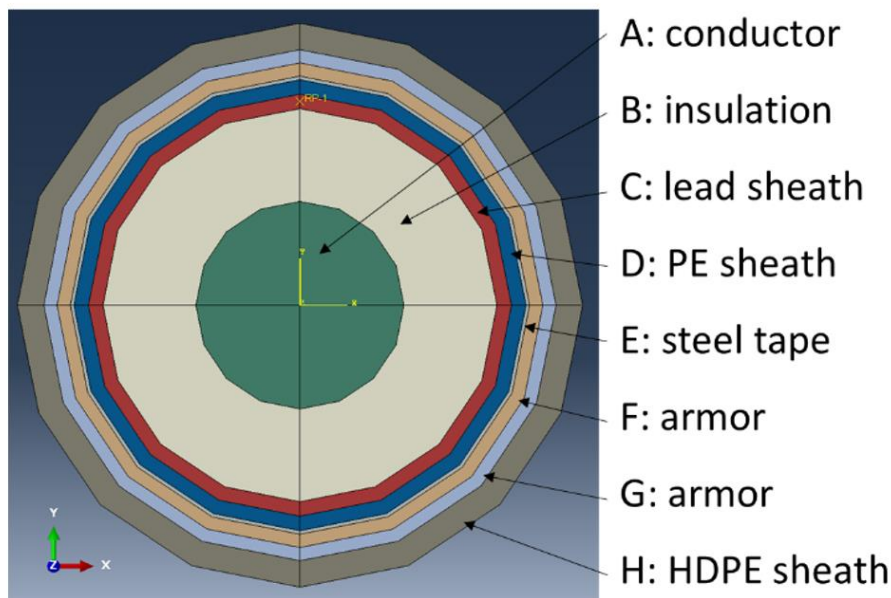


Figure 30 Cross section of model

It was decided to model a cable length necessary to consider a complete turn of the armour around the cable. The armour chosen is that with a smaller winding angle, identified here as 'Armour 2'.

Let:

r_{Arm2} the average radius of the second armour;

α_{Arm2} the winding angle of the second armour;

p_{Arm2} the axial pitch of the second armour.

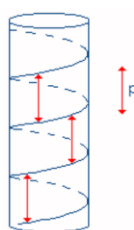


Figure 31 Schematic picture for the evaluation of cable length

With the aid of schematic *Figure 31* it's possible write the simple relation:

$$p_{Arm2}^2 + (2\pi r_{Arm2})^2 = \left(\frac{p_{Arm2}}{\cos \alpha_{Arm2}} \right)^2 \quad (83)$$

Solving for p_{Arm2} and substituting the proper values:

$$p_{Arm2} = \left[\frac{(\cos(\alpha_{Arm2}) 2\pi r_{Arm2})^2}{1 - \cos(\alpha_{Arm2})^2} \right]^{\frac{1}{2}} = 1915,41 \text{ mm} \quad (84)$$

The cable length was chosen equal to 2 meters.

A longitudinal section of the cable modelled is shown in *Figure 32*.

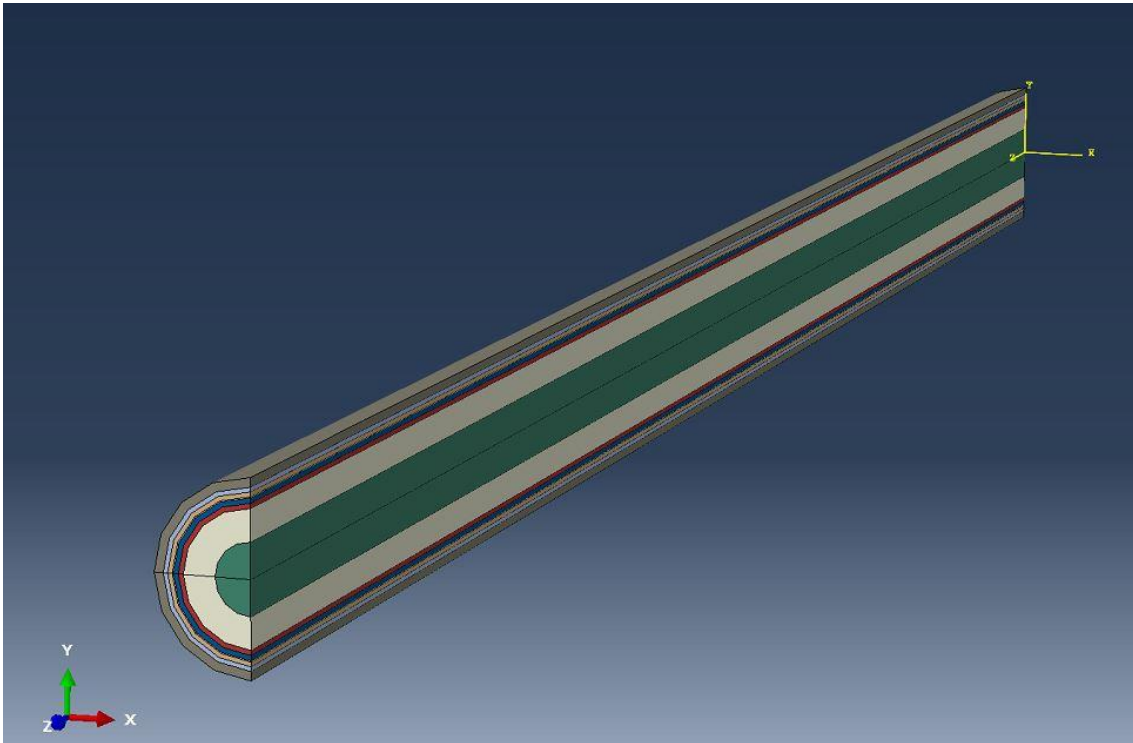


Figure 32 Three-dimensional view of model

9 MATERIAL PROPERTIES

Now it follows the description of material properties for each part included in the model.

9.1 CONDUCTOR

The conductor is made of very high pureness copper. His mechanical behaviour was modelled as isotropic linear elastic material, therefore only two parameters are necessary: elastic modulus and Poisson's coefficient. These values can be easily found on literature.

The assigned values are:

- $E = 120000 \text{ MPa}$
- $\nu = 0.34$

9.2 INSULATION SYSTEM

Mechanical behaviour of insulation system is very complex and there aren't satisfactory data for an accurate prediction. For this reason, different **approximations** were introduced:

- Insulation system was modelled as unique body with isotropic linear elastic behaviour;
- Elastic modulus of insulation system was computed by considering an equivalent elastic modulus of the various parts. The parts included are Kraft-paper impregnated with high viscosity oil and the serving made of copper woven fabric tape.
- The value of the elastic modulus for the Kraft-paper impregnated with high viscosity oil is not available. From the literature was observed that the Kraft-paper can have some GPa as value of elastic modulus, thus 10 GPa was considered in this analysis.
- Poisson's coefficient was assessed as weight average between the volumes.
- A representative value of Poisson's coefficient was assumed for what regards the Kraft-paper impregnated with high viscosity oil.

With these approximations an equivalent elastic modulus was computed by considering the following procedure.

Because the parts are subjected at the same curvature Γ during the bending load M_f , they are considered in parallel. Therefore, the equivalent bending stiffness $k_{f,eq}$ of system is the sum of singles bending stiffness $k_{f,i}$. Each bending stiffness is evaluable as the product of elastic modulus E_i and moment of bending inertia $I_{f,i}$. The latter is directly computable by the geometry of the single parts. The fundamental formulas are shown.

$$k_{f,i} = E_i I_{f,i} \quad (85)$$

$$M_f = \Gamma k_{f,eq} = \Gamma \sum (E_i I_{f,i}) = \Gamma E_{eq} I_{f,eq} \quad (86)$$

$$E_{eq} = \frac{\sum (E_i I_{f,i})}{I_{f,eq}} \quad (87)$$

The equivalent Poisson's coefficient ν_{eq} was computed with the following formula:

$$\nu_{eq} = \frac{\sum (\nu_i V_i)}{V_{eq}} \quad (88)$$

Where ν_i, V_i, V_{eq} are respectively the Poisson's coefficients, the volumes and equivalent volume of the parts included in calculus.

Table 7 Material properties of insulation system

MATERIAL	Paper Kraft		Cu	Equivalent
COMPONENT	3	4	5	B
E (MPa)	10000	/	120000	19340
R_int (mm)	23.55	/	43.7	23.55
R_ext (mm)	43.7	/	44.6	44.6
I (mm ⁴)	2.62E+06	/	2.43E+05	2.87E+06
K (Nmm ²)	2.62E+10	/	2.92E+10	5.54E+10
ν	0.45		0.34	0.44
V/L (mm ²)	1064	/	62	1127

As it cited in input data available, the **thermal expansion coefficient** is assumed equal to that of the oil, 6.3e-4 1/K.

It must be noted, as large approximations are involved in the assessment of mechanical behaviour of insulation system.

9.3 LEAD SHEATH

The lead alloy sheath is the part with well-known mechanical behaviour. Data can be found on 'input data available'.

9.4 PE SHEATH

Data for elastoplastic behaviour of PE sheath can be found on 'input data available'.

9.5 REINFORCEMENT

Reinforcement of submarine power cable is made of galvanized steel tapes. As anticipated, reinforcement was modelled as continue body and no tape was included. In order to consider the winding angle of reinforcement the mechanical behaviour was implemented as orthotropic in linear elastic field. The winding angle of reinforcement is 70 degrees.

Orthotropic elastic behaviour with transversely isotropic elasticity was chosen from the Abaqus library. This kind of behaviour must observe the following rules.

9.5.1 Orthotropic elastic behaviour with transversely isotropic elasticity

Orthotropic materials have two orthogonal symmetry planes for the elastic properties. A special subclass of orthotropy is transverse isotropy, which is characterized by a plane of isotropy at every point in the material.

Assuming the 1-2 plane to be the plane of isotropy at every point, **transverse isotropy requires:**

$$\begin{aligned}
 E_1 &= E_2 = E_p \\
 \nu_{31} &= \nu_{32} = \nu_{tp} \\
 \nu_{13} &= \nu_{23} = \nu_{pt} \\
 G_{13} &= G_{23} = G_t \\
 G_p &= \frac{E_p}{2(1 + \nu_p)}
 \end{aligned} \tag{89}$$

Where p and t stand for “in-plane” and “transverse”, respectively.

While ν_{tp} has the physical interpretation of the Poisson’s ratio characterizing the strain in the plain of isotropy resulting from stress normal to it, ν_{pt} characterizes the transverse strain in the direction normal to the plane of isotropy resulting from stress in the plane of isotropy.

In general, the quantities ν_{tp} and ν_{pt} are not equal and related by the following rule:

$$\frac{\nu_{tp}}{E_t} = \frac{\nu_{pt}}{E_p} \tag{90}$$

Following the mentioned rules, the stress-strain law has the classic form of the linear elastic material.

Material stability requires:

$$\begin{aligned}
 E_p, E_t, G_p, G_t &> 0 \\
 |v_p| &< 1 \\
 |v_{pt}| &< \left(\frac{E_p}{E_t}\right)^{\frac{1}{2}} \\
 |v_{tp}| &< \left(\frac{E_t}{E_p}\right)^{\frac{1}{2}} \\
 1 - v_p^2 - 2v_{tp}v_{pt} - 2v_p v_{tp} v_{pt} &> 0
 \end{aligned} \tag{91}$$

For the implementation, a cylindrical reference system was created where 1 is the radial direction, 2 is the tangential direction, and 3 is the winding direction.

The value of elastic modulus for the winding direction was chosen equal to 200000 MPa, typical value for the steel. Transversal values were reduced of 100 times. The reason of this reduction is to assign representative value in agree with other studies led on orthotropic materials [7]. The same reasoning was done for what concerns Poisson's coefficient.

Table 8 Material properties implemented for the Reinforcement

Orthotropic Elastic Behaviour with transversely isotropic elasticity		
Winding angle	70	°
E₁	2000	MPa
E₂	2000	MPa
E₃	200000	MPa
Nu₁₂	0.3	
Nu₁₃	0.003	
Nu₂₃	0.003	
G₁₂	770	MPa
G₁₃	770	MPa
G₂₃	770	MPa

9.6 FIRST ARMOUR

Armouring of submarine power cable is made of galvanized steel wires. As for the reinforcement, also armour wires weren't modelled, but a unique continue body was created in Abaqus/CAE. In order to consider the winding angle, orthotropic linear elastic behaviour was assigned also for the armouring. Obviously, procedure, relationships and criterion for the assignment of orthotropic properties for the armouring are identic at what seen for the reinforcement.

Table 9 Material properties implemented for the first armour

Orthotropic Elastic Behaviour with transversely isotropic elasticity		
Winding angle	12,7	°
E₁	2000	MPa
E₂	2000	MPa
E₃	200000	MPa
Nu₁₂	0.3	
Nu₁₃	0.003	
Nu₂₃	0.003	
G₁₂	770	MPa
G₁₃	770	MPa
G₂₃	770	MPa

9.7 SECOND ARMOUR

Obviously, the modelling is the same of the first armouring. The only difference is the winding angle.

Table 10 Material properties implemented for the second armour

Orthotropic Elastic Behaviour with transversely isotropic elasticity		
Winding angle	-10.5	°
E₁	2000	MPa
E₂	2000	MPa
E₃	200000	MPa
Nu₁₂	0.3	
Nu₁₃	0.003	
Nu₂₃	0.003	
G₁₂	770	MPa
G₁₃	770	MPa
G₂₃	770	MPa

9.8 OUTER SHEATH

Elastoplastic behaviour of outer sheath, made of HDPE, is also an input data available. Numerical values can be found on 'input data available'.

9.9 CONSIDERATIONS ON MATERIAL PROPERTIES

The assignment of material properties at all cable components is surely an element that introduce a large approximation in the model. Components are many and their mechanical behaviour are very complex. For an accurate quantitative analysis, should be necessary a great experimental work in order to characterize any mechanical behaviour. This, obviously, is not the goal of this work, and the approximations introduced allow, however, to reach the purpose explained in the initial part.

A summarization of mechanical behaviour implemented in the model is reported in *Table 11*. Then, for clearness, in *Table 12* follow all material properties implemented.

Table 11 Mechanical behaviour implemented for all parts of model

PART	ELASTICITY	PLASTICITY	CREEP
Conductor	linear isotropic	-	-
Insulation	linear isotropic	-	-
Lead sheath	linear isotropic	isotropic	power-law strain hardening formulation
PE sheath	linear isotropic	isotropic	-
Reinforcement	linear orthotropic: 70 degrees	-	-
First armour	linear orthotropic: 12.7 degrees	-	-
Second armour	linear orthotropic: - 10.5 degrees	-	-
HDPE sheath	linear isotropic	isotropic	-

Table 12 Material properties implemented for all parts of model

COMPONENT	MATERIAL PROPERTIES IMPLEMENTED
Conductor	Type of material: Copper
	Elastic behavior: E = 120000 MPa; $\nu=0.34$
Insulation system	Type of material: Kraft paper, oil, copper tapes
	Elastic behavior: E = 19340 MPa; $\nu=0.44$
	Thermal expansion coefficient $\alpha_v = 6.3e-4 \text{ } 1/^{\circ}\text{C}$
	Impregnation level $q = 0.4$
Lead sheath	Type of material: E-Alloy
	Elastic behaviour: E = 12000 MPa; $\nu = 0.431$
	Plastic behaviour: plastic table
	Creep behaviour: A = 5.278e-10, m = -0.47, n = 5.22
PE sheath	Type of material: PE
	Elastic behaviour: E = 600 MPa; $\nu = 0.46$
	Plastic behaviour: plastic table

Reinforcement	Type of material: galvanized steel tapes
	Winding angle: 70 degrees from the cable axis
	Orthotropic elastic behaviour: elastic table
Armour 1	Type of material: galvanized steel wires
	Winding angle: 12.7 degrees from the cable axis
	Orthotropic elastic behaviour: elastic table
Armour 2	Geometry, type of material: galvanized steel wires
	Winding angle: -10.5 degrees from the cable axis
	Orthotropic elastic behaviour: elastic table
Outer sheath	Type of material: HDPE
	Elastic behaviour: E = 780 MPa, $\nu = 0.46$
	Plastic behaviour: plastic table

10 MESHING

Once that material properties and geometries were implemented in the model, was necessary convert continuous model in a discrete model, characterized by a finite number of degrees of freedom.

10.1 CHOICE OF THE ELEMENTS

Most of the elements in Abaqus are formulated in a global cartesian coordinate system. Primary vector quantities, such as displacements $\{u\}$ and rotations $\{\Phi\}$, are defined in terms of nodal values through scalar interpolation functions. For example, the displacement vector can be interpolated as:

$$\{u\} = [N]\{u_N\} \quad (92)$$

Where $[N]$ is the matrix of the shape functions and $\{u_N\}$ is the vector of nodal displacements.

The same parametric interpolation can be used for the coordinate vector $\{x\}$:

$$\{x\} = [N]\{x_N\} \quad (93)$$

Where $\{x_N\}$ is the vector of nodal positions.

When position field and displacement field are interpolated by using the same interpolation functions, elements are called **iso-parametric elements**. They are capable to represent all rigid body modes and homogeneous deformation modes exactly. The latter is a necessary condition for convergence to the exact solution when the mesh is refined.

Because the stress-state in most parts of model, especially in the lead sheath, is expected to be three-dimensional, **three-dimensional elements** (solid elements) were chosen from the Abaqus library.

Most common solid elements can have 8 nodes, with a displacement field interpolation of the first order, or they can have 20 nodes, with a displacement field interpolation of the second order. When thin components are subjected to a **bending** load, the strain variation through the thickness must be at least linear. Therefore, the choice of the **second-order elements** become easier. Iso-parametric interpolation is defined in terms of iso-parametric element coordinates g, h, r in Abaqus. They each span the range -1 to +1 in an element. Corner nodes are numbered first, followed by the mid-side nodes. The representation of this element is shown in the following figure.

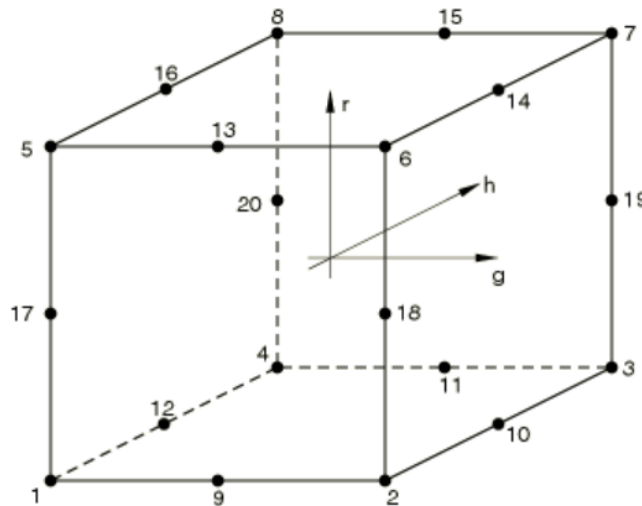


Figure 33 Second order three-dimensional element

For each of these elements is necessary compute a 60x60 stiffness matrix, by increasing a lot the computational cost. A decreasing of the computational cost can be obtained by using the reduced integration without accuracy loss.

Reduced integration usually means that an integration scheme one order less than the full scheme is used to integrate the element's internal forces and stiffness. For second-order elements, the reduced integration points have the Barlow point property: the strains are calculated from the interpolation functions with higher accuracy at these points than anywhere else in the element. Not only is this important with respect to the values available for output, it is also significant when the constitutive model is nonlinear (like it happens for the lead sheath), since the strains passed into the constitutive routines are a better representation of the actual strains [14]. As it anticipated, reduced integration computes the solution in 8 points, instead that in 27 points as it happens with the full integration. This can help to make the calculation leaner.

Finally, in cases of mechanical interactions between various parts of model, is preferred to use a minor number of quadratic elements rather than more linear elements. This statement was taken by FEM contact problems, as reported in [15]. In cases of curved geometry, the convergence is reached more rapidly if quadratic elements are used.

For all these reasons, in all the model were used **three-dimensional quadratic elements with reduced integration**.

10.2 GEOMETRIC DISCRETIZATION

Geometric discretization in Abaqus/CAE is simple. Discretization conditions were decided and then imposed through graphic interface. The conditions are reported below.

- **Longitudinal discretization:**
for all the parts, was chosen a longitudinal size of 20 mm. This value allows to have 100 elements along the axis cable, that's a right compromise between accuracy of model and computational cost.
- **Circumferential discretization:**
For A and B parts, 6 elements for $\frac{1}{4}$ of circumference was chosen. Because these parts are not of interests, the value chosen is adapt for the accuracy required. From C part to H part, 12 elements for $\frac{1}{4}$ of circumference was decided in order to have a finer mesh for lead sheath and all the other thin parts.
- **Radial discretization:**
A and B parts have 5 elements along the thickness, while all the other components have 2 elements along the thickness. These are the good values for the accuracy required.

10.3 APPLICATION OF THE ELEMENTS

Thanks to Abaqus/CAE environment, the application of elements to the discretized geometry is very easy. In following picture is shown the whole mesh of model.

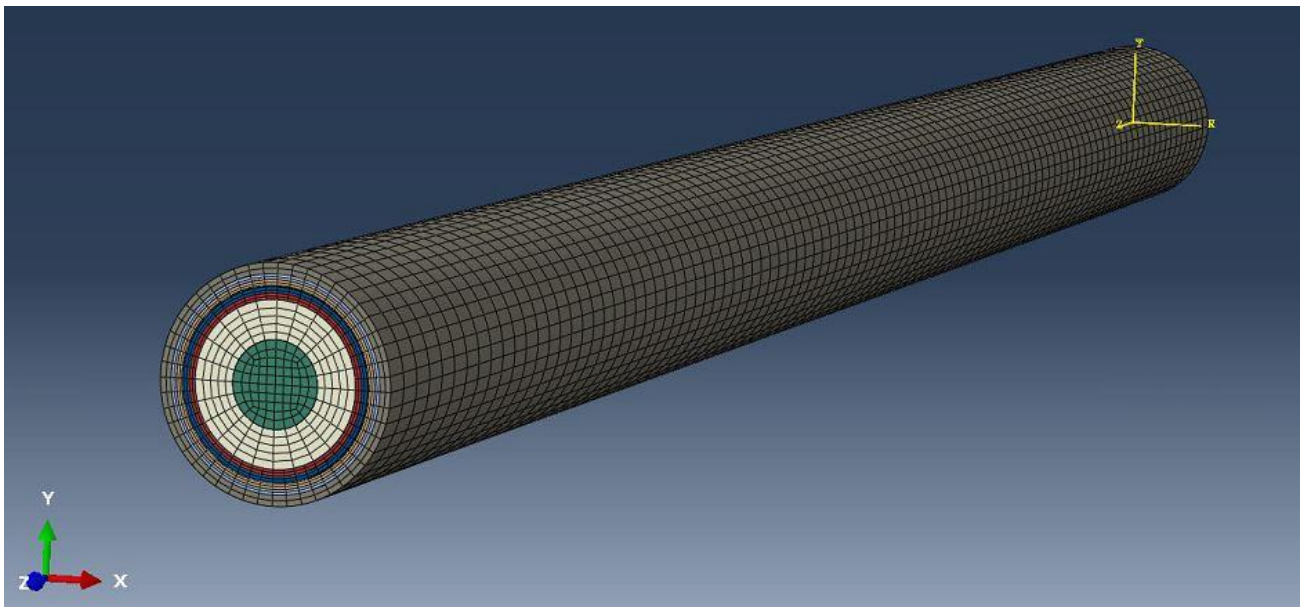


Figure 34 Mesh of model

In summary, the total number of elements in the model is 78000, while the total number of nodes is 412389. It should be noted how all the parts have the sharing nodes at the same position in order to simplify the subsequent implementation of component interactions.

11 INTERACTIONS

The model created is a multi-component finite element model, thus is necessary to choose a right method of interactions between the various parts. Surely, the more accurate way to model these interactions should be the implementation of contact problem. Anyway, contact implementation could be logic if steel tapes of reinforcement and steel wires of armour were implemented. Again, steel tapes implementation and steel wires implementation could be reasonable if available input data were more numerous and accurate. With the input data available there was no logical sense in the implementation of the above conditions.

For these reasons, the various parts must interact each other on the base of **surface-based tie constraints** implemented. Tie constraints don't allow any separation between the surfaces and this is a good assumption for what regards the operative conditions which the parts are held against each other and no slip can happen.

11.1 BRIEF DESCRIPTION OF SURFACE-BASED TIE CONSTRAINT

Surface-based tie constraint imposes at the nodes on the **slave surface** to have the same motion of the nodes on **master surface**. The choice of master and slave surfaces is decided by the user and must follow some rules. Master surface must be stiffer than the slave surface, thus, coarser mesh and surface with material less deformable are conditions suitable for the attribution of the master surface.

Mathematically, two tie formulations are available: the **surface-to-surface formulation** and the **node-to-surface formulation**. The surface-to-surface formulation generally avoids stress noise at tied interfaces. The following tables provide comparisons of characteristics for the different formulation and analysis codes.

Table 13 Features of Tie formulations in Abaqus/Standard

Tie formulation	Optimized stress accuracy	Node-based surfaces allowed	Mixture of rigid and deformable subregions allowed	Treatment of nodes/facets shared between master and slave surfaces
Surface-to-surface	Yes	Reverts to node-to-surface formulation	No	Eliminated from slave
Node-to-surface	No	Yes	No	Eliminated from slave

Table 14 Surface characteristics for Tie formulations in Abaqus/Standard

Tie formulation	Double-sided	Discontinuous	T-intersection	Edge-based
Surface-to-surface	Master: Yes Slave: Yes	Master: Yes Slave: Yes	Master: No Slave: Yes	Reverts to node-to-surface formulation if either surface is edge-based
Node-to-surface	Master: Yes Slave: Yes	Master: Yes Slave: Yes	Master: No Slave: Yes	Master: Yes Slave: Yes

The determination of which nodes must fuse together is very important because **mesh distortion** or **not tied zones** could be happened. In fact, when two surfaces are tied together, slave nodes are enforced to fuse with the master nodes and, if mesh is not accurately designed, mesh distortion problem could be born. On the other hand, if the nodes to fuse together are not correctly identified, some regions of model could remain separated.

By default, Abaqus uses a position tolerance criterion to determine the constrained nodes based on the distance between the slave nodes and the master surface. The default position tolerance for element-based master surfaces is 5% or 10% of the typical master facet diagonal length for the node-to-surface and surface-to-surface tie formulations, respectively [16].

It's simple understand how the **mesh design** and the **position tolerance criterion** are fundamental when surface-based tie constraints are used.

Once determined which slave nodes will be tied to the master surface, Abaqus forms constraints between these slave nodes and the nodes on the master surface. A key aspect in forming the constraint for each slave node is determining the **tie coefficients**. These tie coefficients are used to interpolate quantities from the master nodes to the tie point. Abaqus can use one of two approaches to generate the coefficients: the surface-to-surface approach or the node-to-surface approach.

11.1.1 Surface-to-surface formulation

Surface-to-surface formulation minimizes numerical noise for tied interfaces involving mismatches meshes. This approach enforces constraints in an average sense over a finite region, rather at discrete points as in the traditional node-to-surface formulation. Surface-to-surface formulation for surface-based tie constraints is similar at surface-to-surface contact formulation. A fundamental difference, however, is that each surface-based tie constraint involves only one slave node (and multiple master nodes), while each surface-to-surface contact constraint involves multiple slave nodes. More information are available directly on [16].

Surface-to-surface formulation guarantees more insensitivity to the choice of master and slave surface, and more accurate results.

11.1.2 Node-to-surface formulation

The traditional node-to-surface approach sets the coefficients equal to the interpolation functions at the point where the slave node projects onto the master surface. This approach is somewhat more efficient and robust for complex surfaces. In order to establish the tie coefficients with an element-based master surface for the node-to-surface method, the point on the surface closest to each slave node is calculated and used to determine the master nodes that are going to form the constraint. An illustrative example is reported in the following figure.

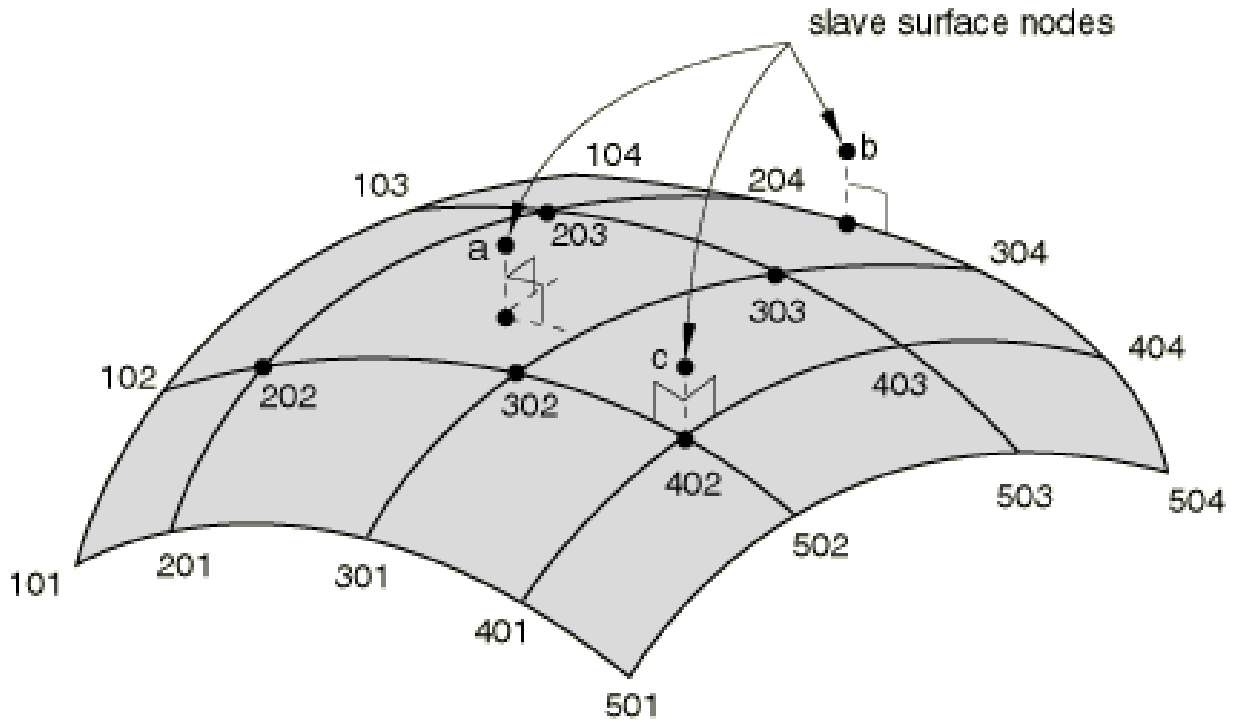


Figure 35 Node to surface approach for Tie formulation [16]

Nodes 202, 203, 302 and 303 are used to constraint node a. Nodes 204 and 304 are used to constraint node b, while node 402 is used to constraint node c.

The choice of slave and master surfaces can have significant effect on the accuracy of the solution if the node-to-surface formulation is used.

11.2 IMPLEMENTATION OF SURFACE-BASED TIE CONSTRAINT

In Abaqus, for each part, were defined all the internal and external surfaces in order to simplify the implementation of master and slave surface. On the ground of mesh size and elastic modulus of various parts, the following attributions were made.

Table 15 Master-Slave attributions for the surfaces of model

Interaction	AB	BC	CD	DE	EF	FG	GH
Master	A_ext	B_ext	C_ext	E_int	F_int	G_int	G_ext
Slave	B_int	C_int	D_int	D_ext	E_ext	F_Ext	H_int

With illustrative scope, it's reported in the Figure 36 the implementation of tie constraint between the external surface of the lead sheath and the internal surface of the PE sheath.

11.2 IMPLEMENTATION OF SURFACE-BASED TIE CONSTRAINT

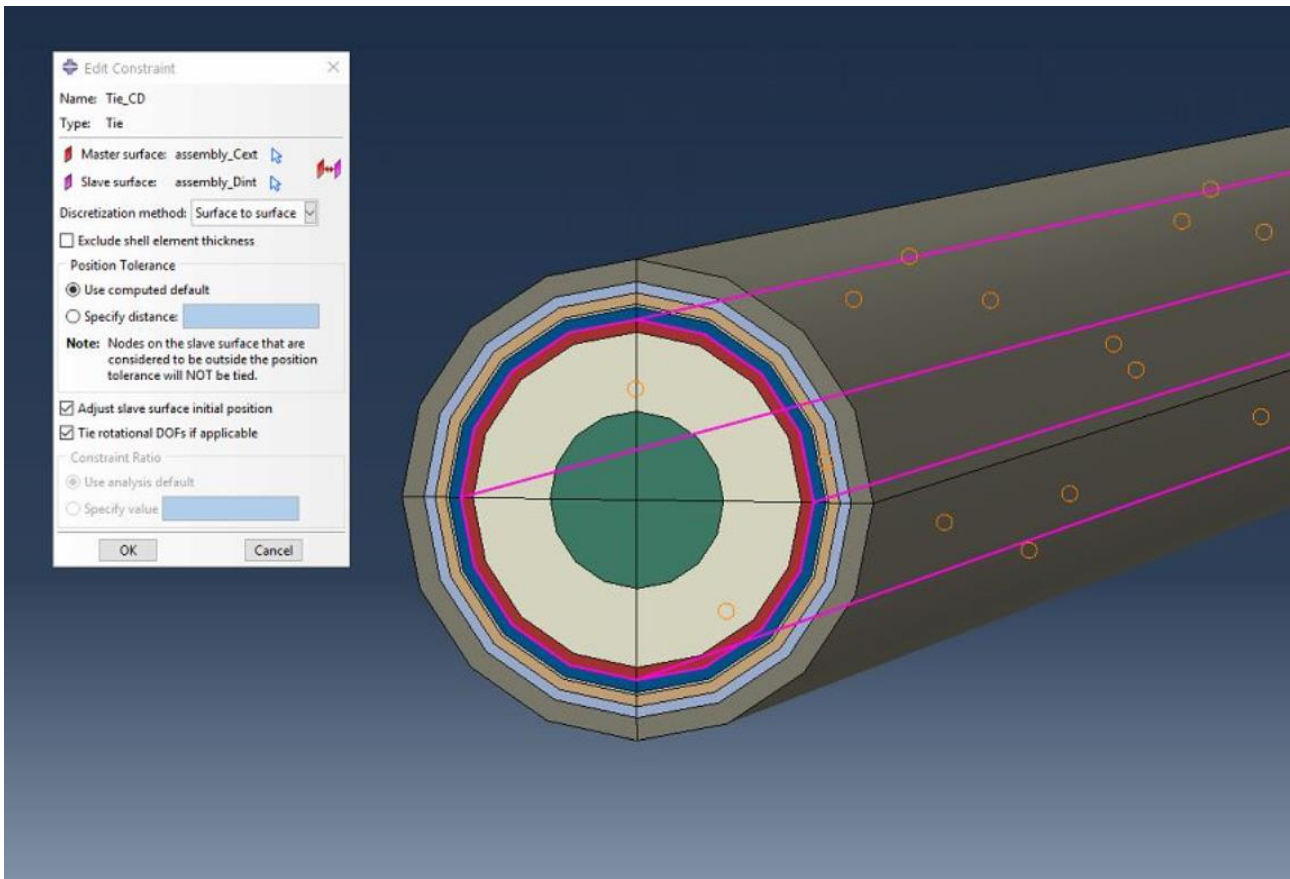


Figure 36 Example of Tie application in Abaqus

12 BOUNDARY CONDITIONS

12.1 CONSTRAINTS

The simulated cable length is 2 meters. Real submarine power cable length is about tens of kilometres. Thus, a sure assumption could be full constraining of the extreme sections. However, the cable expands for the heating during the electricity transport, and a longitudinal translation is possible when only a portion of cable is examined.

Hence, an extreme section was fully constrained, while the other extreme section can translate longitudinally.

The application of these constraints was made through the **coupling constraint command**. This choice was necessary for the subsequent implementation of the cable bending because the elements don't have the rotational degree of freedom.

In fact, **'kinematic coupling constraint'** associates the motion of a group of nodes to the rigid body motion defined by a reference node. For each extreme section, the **reference node** is the **central point** of the section, and the **group of nodes** are the remaining total nodes of the **section**.

Kinematic coupling constraint is very useful to apply load or boundary conditions to a model. His implementation, for each section, is shown in the following figures.

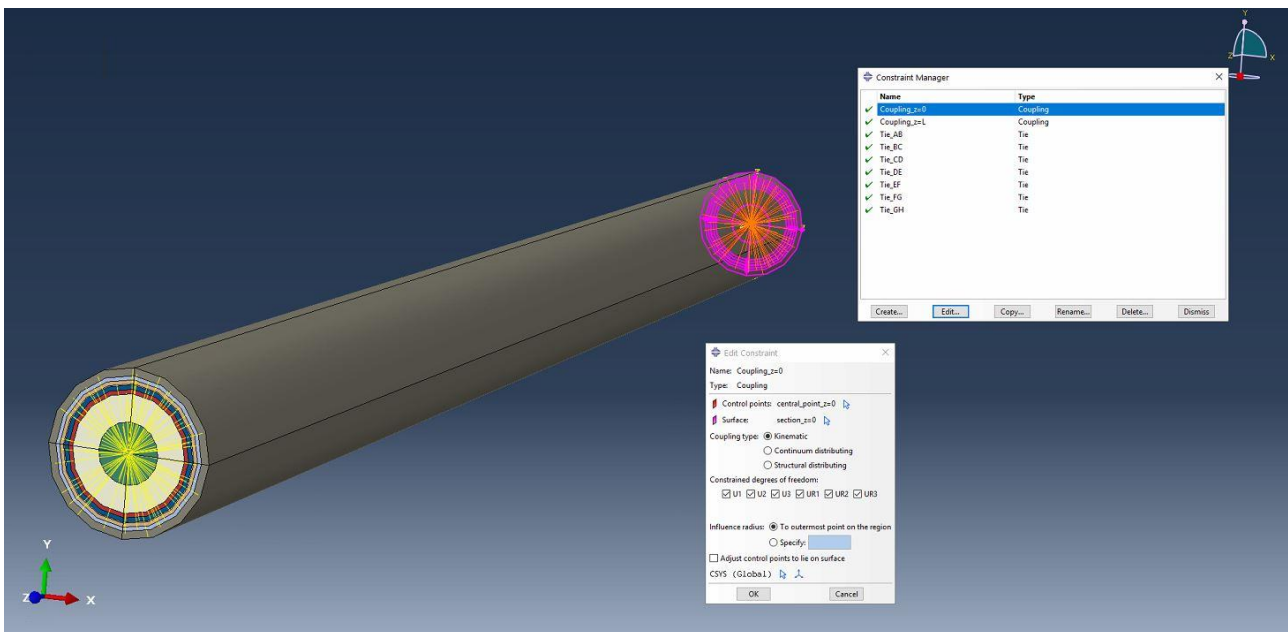


Figure 37 Coupling application for the fully constrained extreme section of model

12 BOUNDARY CONDITIONS

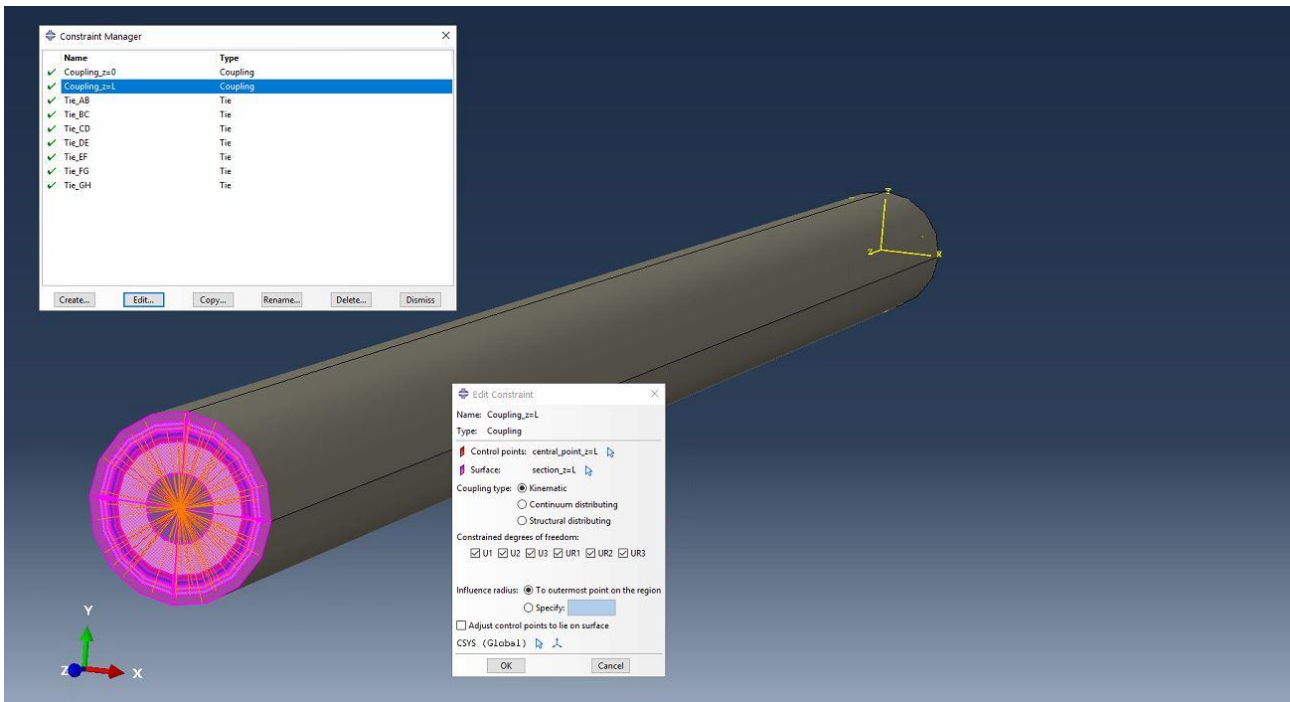


Figure 38 Coupling application for the axially free extreme section of model

With the kinematic coupling applied, is very simple constrain the sections. In fact, as shown below, is enough to apply the boundary condition only to the reference node. It must be noted that these conditions remain active also in the subsequent steps, until the application of bending.

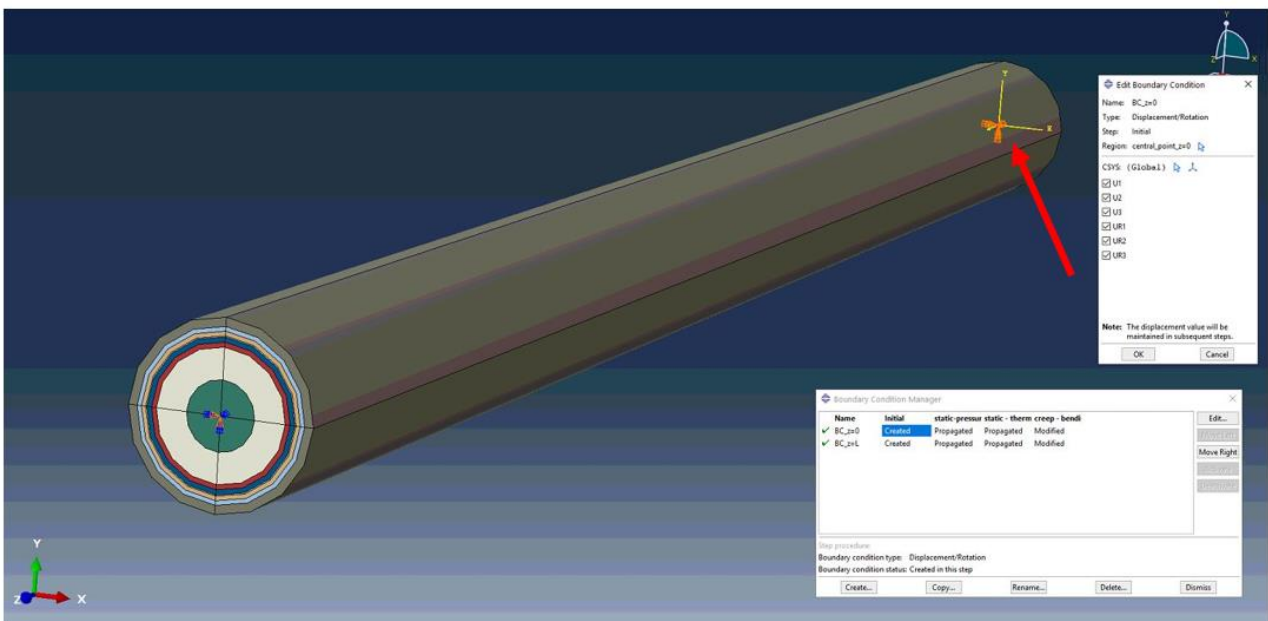


Figure 39 Constraints application for the fully constrained extreme section

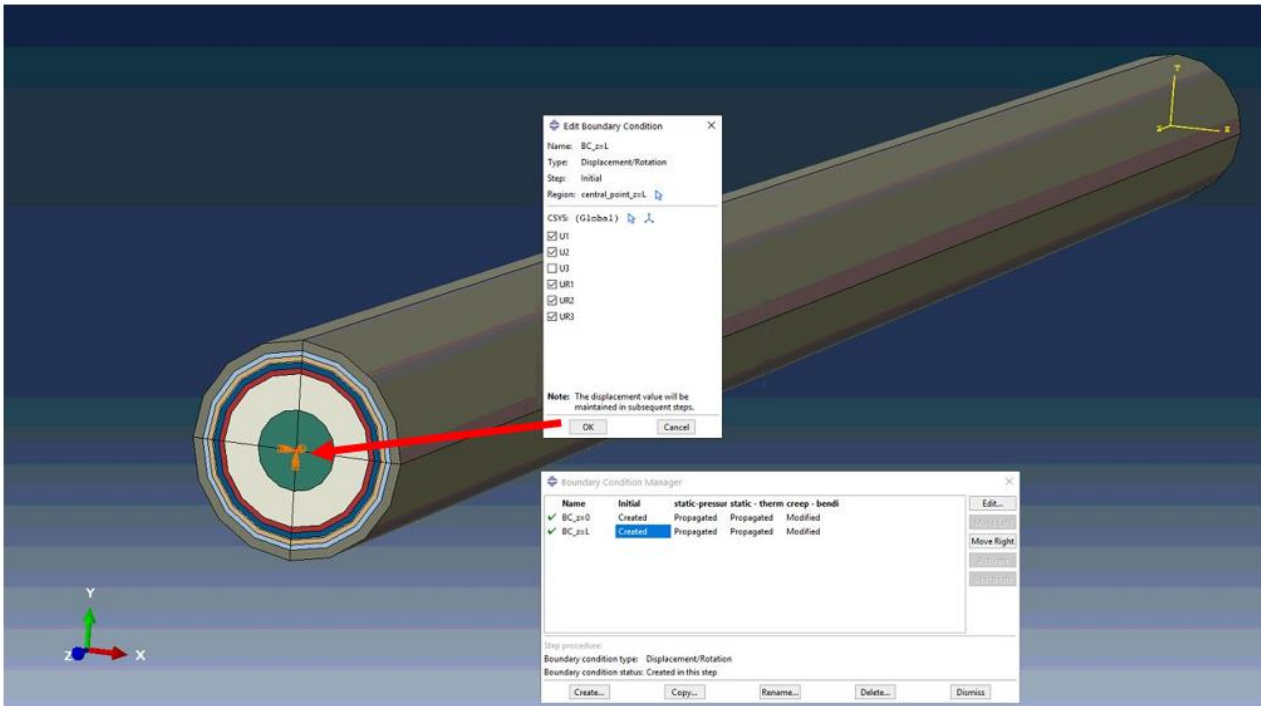


Figure 40 Constraints application for the axially free extreme section

12.2 LOADS

The types of loads implemented are reported in the following.

12.2.1 Static water pressure

As it was anticipated at the early of work, this is the most secure and easy condition of load. Static water pressure interacts with the hydrostatic behaviour of material and does not particularly influence the deviatoric (thus inelastic) behaviour of material. For this reason, it was chosen a representative sea depth of 100 meters, which corresponds to **1 MPa**. In Abaqus is very simple Such implementation is reported below.

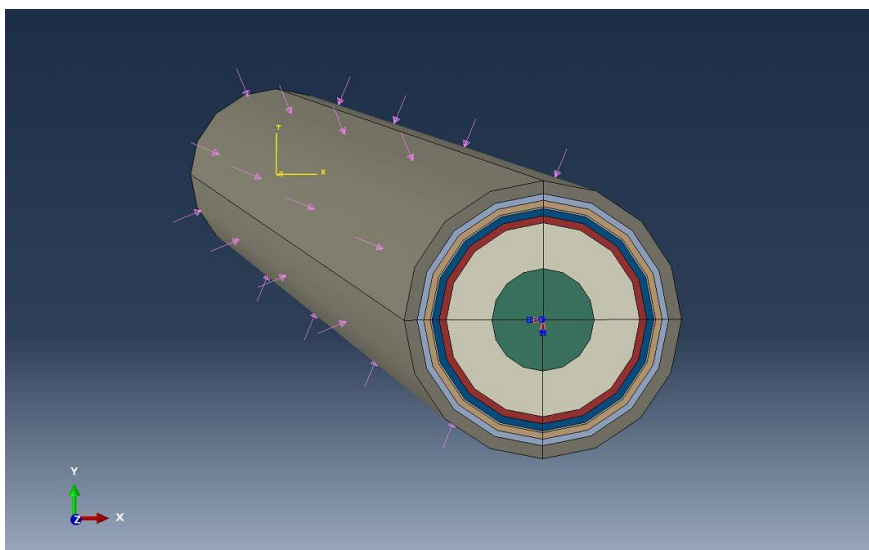


Figure 41 Static water pressure load

12.2.2 Static thermal expansion of insulation

Thermal load induced by the expansion of insulation system was modelled. His variation with time, due to the variation of power demand, is not modelled for the lack of reliable data and to simplify the analysis. Because a linear thermal expansion is considered, the impregnation level was considered by multiplying his value directly for the thermal expansion coefficient.

Because only the oil inside the insulation system expands significantly, the temperature field was assigned only to the insulation. In Abaqus, through the 'Predefined Field' it's possible to set the temperature field to the desired part.

Initially, as shown in the figure below, the temperature of the insulation was set to 30 °C.

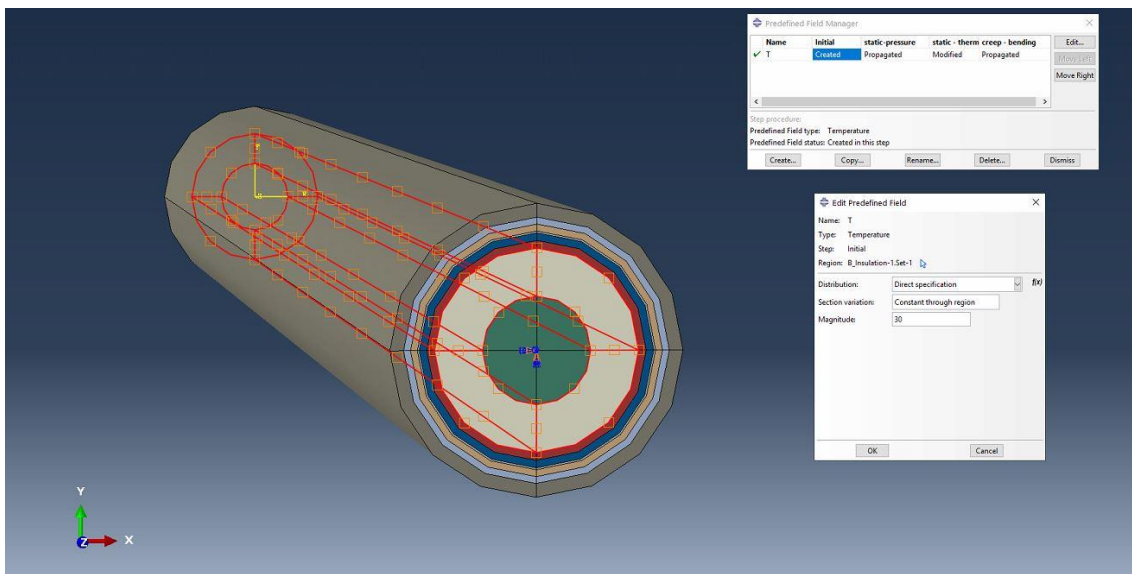


Figure 42 Initial thermal field of insulation system

When the thermal load must be active, the temperature of the insulation system reaches, linearly with time, 50 °C.

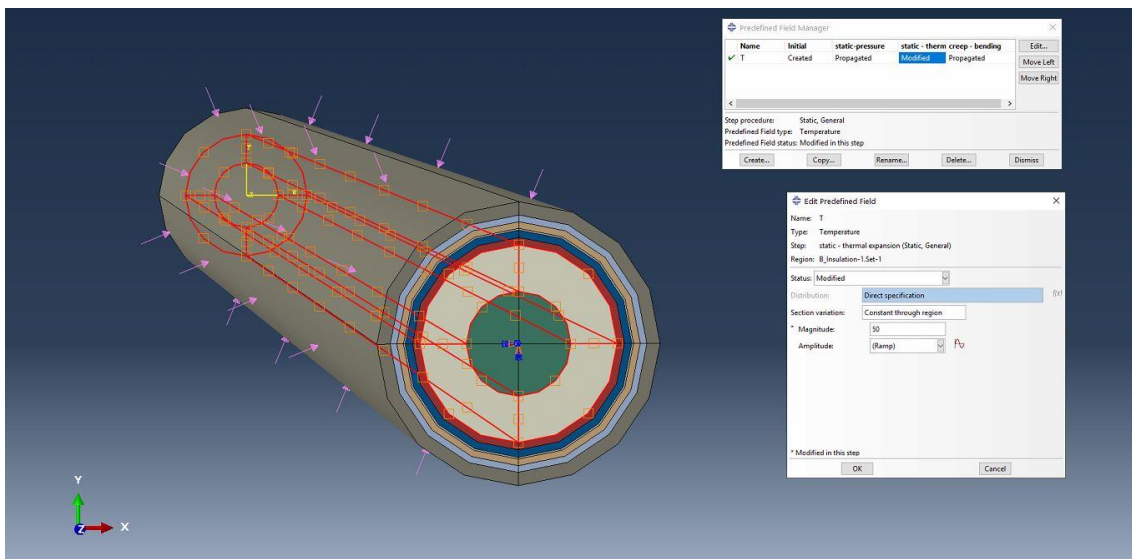


Figure 43 Final thermal field of insulation system

12.2.3 Cyclic bending

Cyclic bending due to the tide motion was implemented as a cyclic pure bending. Thus, the extreme sections of cable were rigidly rotated with time, in order to have always an equal curvature along the cable.

A whole cycle load was simulated, with a period of 12 hours, that's equal to the tide period. The wave form was chosen as sinusoidal. The higher difficulty was the decision of amplitude value. In absence of data, it was decided to choose the amplitude used in fatigue tests for testing the lead sheath, that corresponds at $1e-3$ of maximum longitudinal strain. Hence, through the beam theory was calculated the curvature value that corresponds to have $1e-3$ of maximum longitudinal strain on the lead sheath. The calculation of curvature Γ was computed as follows.

$$\Gamma = \frac{\varepsilon_{long}}{r_{ext}} = 1,25 \text{ } ^\circ/m \quad (94)$$

Where ε_{long} and r_{ext} are the maximum longitudinal total strains of the lead sheath.

The implementation of this condition of load was done through the kinematic coupling constraint as previously anticipated. For such application is enough to insert the rotation value (in radians) at the reference node defined. This is reported below.

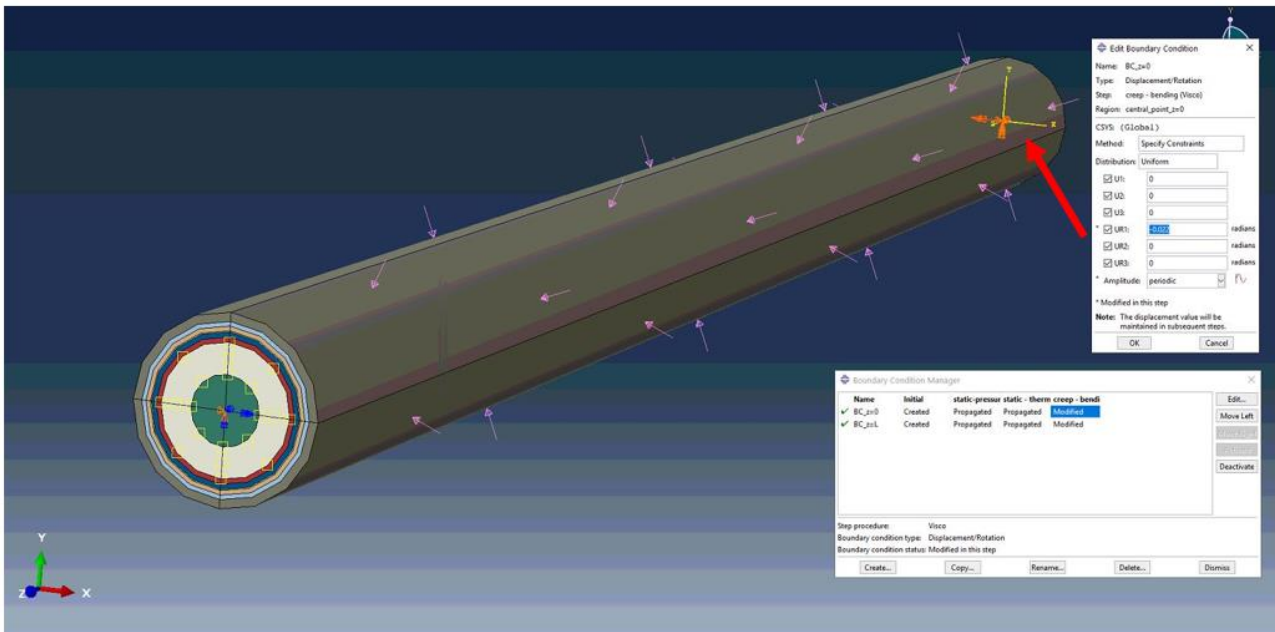


Figure 44 Rigid rotation of the fully constrained extreme section

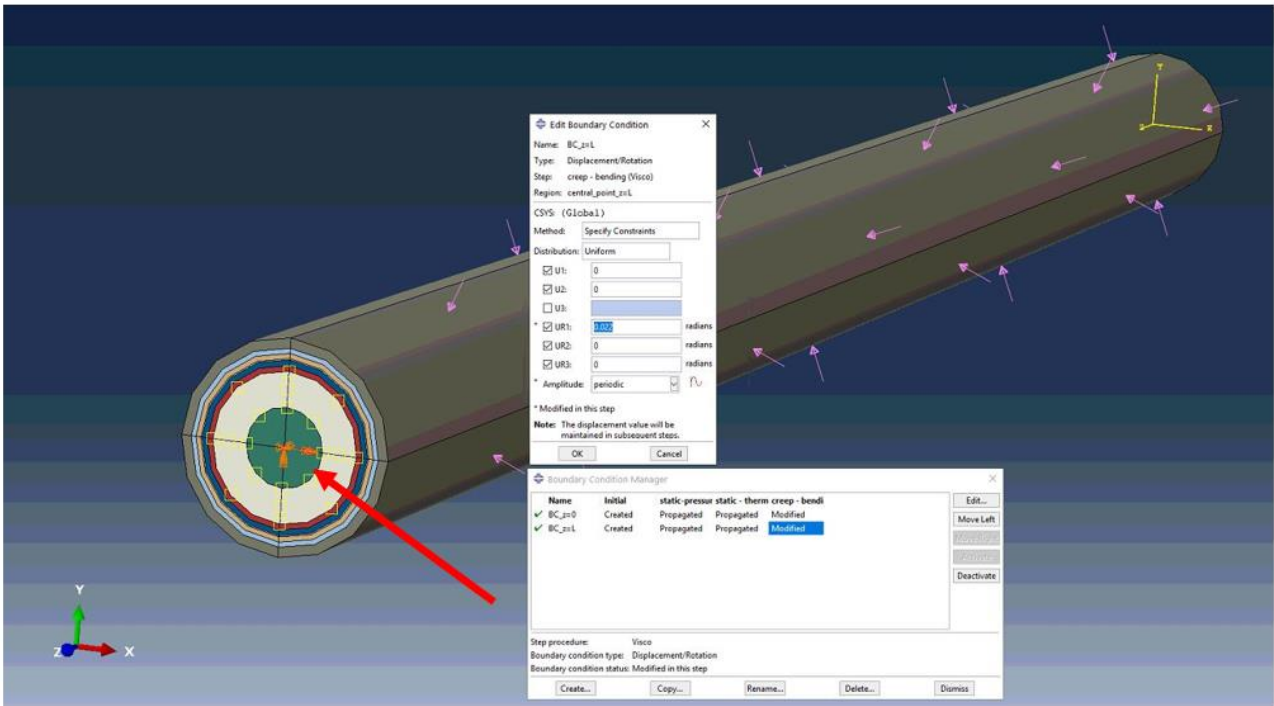


Figure 45 Rigid rotation of the axially free extreme section

Such implemented section rotations must be not linear with time, because the tide motion not act linearly over time on the cable. In first approximation, it can be represented by a **sinusoidal wave** implementable in Abaqus\CAE by using **Amplitude command** directly on the boundary condition definition. This command imposes the rotation of the section by following the input implemented.

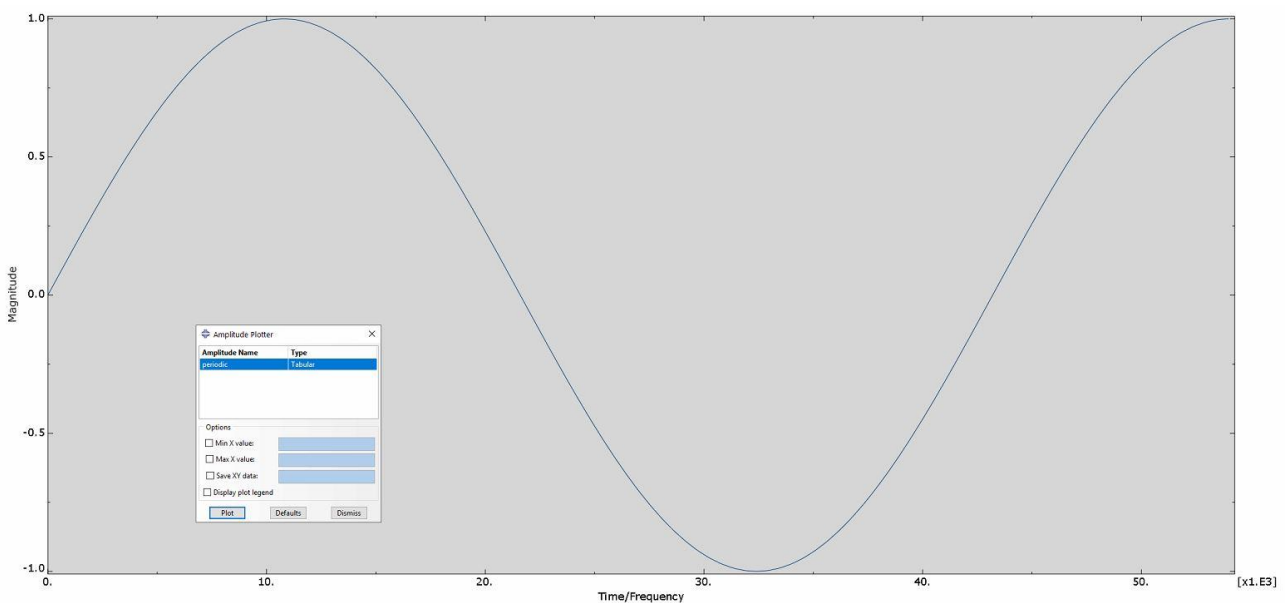


Figure 46 Temporal trend of bending load

The trend of section rotation shows the wave period of 12 hours (43200 s) and the simulated duration of 15 hours (54000 s).

12.3 CONSIDERATIONS ON BOUNDARY CONDITIONS

The amplitude of longitudinal load should change with time both for tides motion and for electric load changing. The latter involves also a changing in the amplitude of radial load. Surely, the frequency of electric load and of tides load is not the same. In order to execute a numerical simulation some assumptions must be done. Tides motion was assumed with a sinusoidal wave and period of 12 hours, while the electric load was modelled as constant. These assumptions are necessary to simplify the analysis.

Moreover, the steel tapes of reinforcement are applied with an unknown pre-tensioning. The effect of this pre-tensioning on the underlying lead sheath is to generate a radial pressure. Because no data exist to model this condition, and the radial load induced by the thermal expansion was modelled with representative data, it was assumed that the effect of the pressure of reinforcement is incorporated inside the effect of the pressure induced by the thermal load. This assumption should not affect the considerations found about the mechanical behaviour of lead sheath.

13 DESIGN CHANGES SIMULATED

The winding angle of steel tape was modified to verify if this design change can affect directly the mechanical behaviour of lead sheath through a changing of triaxiality factor.

Moreover, the viscous behaviour of lead sheath was discriminated by the time-independent behaviour, in order to investigate if the changing of triaxiality factor happens in both situations. For each kind of behaviour, three different winding angles of steel tapes were simulated.

All simulations start with a static loading that correspond respectively to the static water pressure and the static thermal expansion of insulation system. This choice was taken in order to consider the regime situation by neglecting the switching on period where the temperature rise. After an initial static loading, it follows a cyclic loading of the 15 hours duration. Thus, a 1 and $\frac{1}{4}$ cycle is simulated.

In summary, **six simulations** were executed, and they are characterized as follows.

- **60 degrees** for the winding angle of reinforcement, initial static loading and **time-independent cyclic behaviour** of the lead sheath.
- **60 degrees** for the winding angle of reinforcement, initial static loading and **time-dependent cyclic behaviour** of the lead sheath.
- **70 degrees** for the winding angle of reinforcement, initial static loading and **time-independent cyclic behaviour** of the lead sheath.
- **70 degrees** for the winding angle of reinforcement, initial static loading and **time-dependent cyclic behaviour** of the lead sheath.
- **80 degrees** for the winding angle of reinforcement, initial static loading and **time-independent cyclic behaviour** of the lead sheath.
- **80 degrees** for the winding angle of reinforcement, initial static loading and **time-dependent** cyclic behaviour of the lead sheath.

From a modelling viewpoint, changing of the winding angle was implemented by editing axis orientation of cylindrical system used for orthotropic properties.

Static water pressure step was executed by calculating only **2 points**, because hydrostatic pressure not deform irreversibly the material behaviour and, thus, remains linear.

Instead, **static thermal expansion** of insulation system was executed by calculating **10 points** in order to catch eventual non-linear behaviour of material.

Cyclic loading with **time-independent behaviour** was calculated by using **30 points** in order to appreciate the wave form.

Cyclic loading with **time-dependent behaviour** was computed with a not specified number of points because an **automatic time incrementation** was used and, thus, is not preventively assessable the number of increments needs to achieve the end of solution. This choice was done to ensure that increments in stress are calculated accurately. In fact, when automatic time incrementation is used, Abaqus compare the incrementation time with an error tolerance defined by the user. On the ground of the comparison results, time increment can be increased or decreased automatically in order to satisfy, as quickly as possible, the subsequent checks. The error tolerance can be chosen with a simplified approach. In fact, it's possible to choose the error tolerance in order to satisfy the following relation:

$$errtol \ll \frac{\Delta\sigma}{E} \quad (95)$$

In other terms, by choosing an acceptable stress error tolerance and dividing this by a typical elastic modulus is obtainable a value for *errtol*. It is important to recognize that this approach is very conservative, and often are acceptable higher values [6]. For this reason, it was considered the inverse of the elastic modulus of the E-alloy used for the sheathing. Moreover, when creep and plasticity occur simultaneously, both behaviours could interact, and a coupled system of constitutive equations needs to be solved. Implicit integration, when creep and plasticity are isotropic, can solve this system. For this reason, implicit integration was selected.

The setting of parameters is shown in the following.

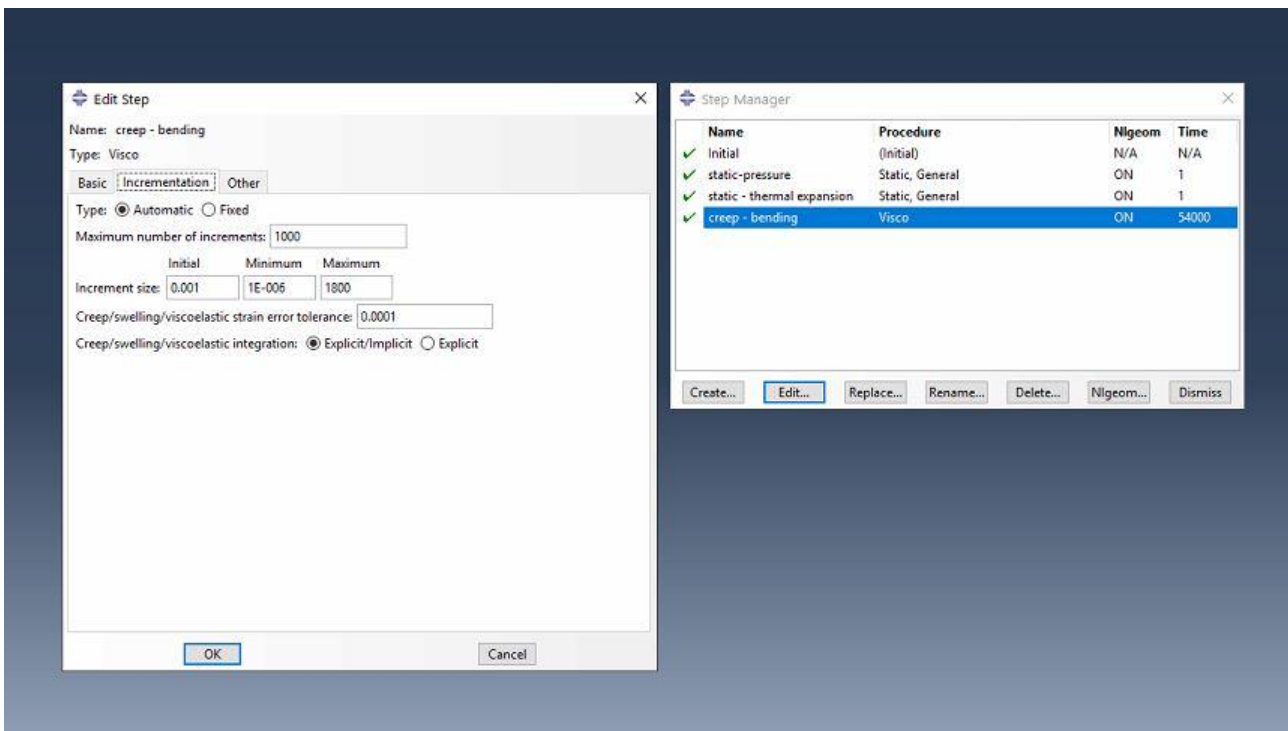


Figure 47 Setting parameters for creep analysis

All load cases were computed by using direct equation solver with the full Newton solution technique as reported in *Figure 48*.

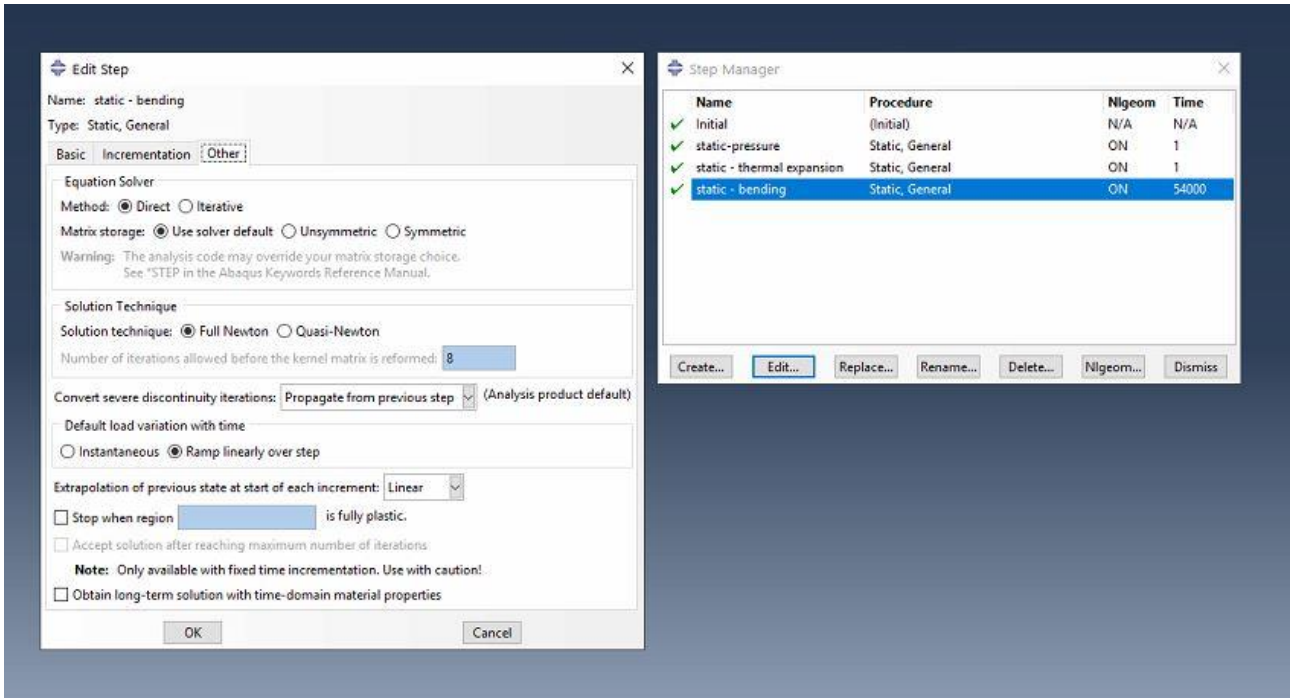


Figure 48 Setting parameters for numerical solution

PART IV

RESULT ANALYSIS

Although all parts of cable were simulated, it, obviously, only the behaviour of lead sheath was analysed, that's the critical part of cable under mechanical aspect.

The first part of analysis wants to catch the deformed of cable, eventual gradient in the stress-strain field, and the critical point of cable where, subsequently, focus the attention with a temporal analysis. In fact, the second part of analysis, is focused on the temporal trends of most important characteristic of the stress and strain field, assessed in the critical point.

14 GLOBAL ANALYSIS OF THE STRESS-STRAIN FIELD

14.1 DEFORMED

The first graphical output presented is a section of a portion of deformed cable first and after the application of thermal load. It should be noted that, for a best illustration of the radial strain, the deformed was enlarged of 100 times.

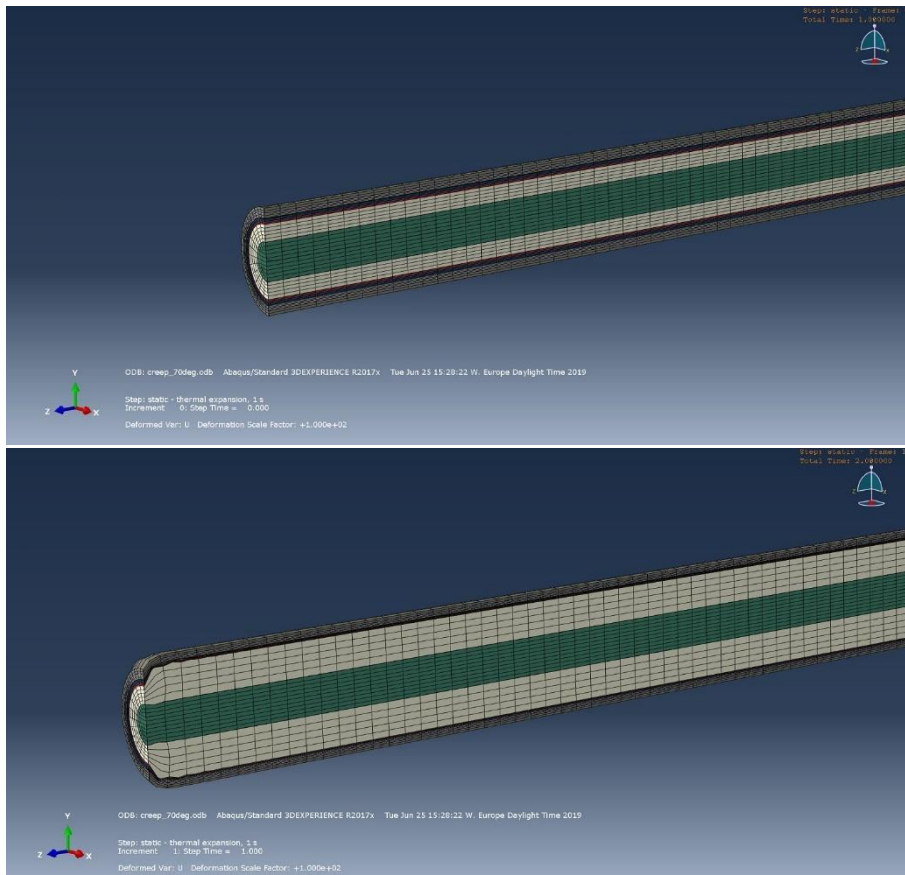


Figure 49 Deformed after water pressure and thermal load

It's possible to observe the action of the insulation system expansion on the lead sheath and how superior layers must contribute to limit the radial deformation.

Instead, in following are represented three critical configurations (the maximum curvatures) of the whole cable during the application of the cyclic bending together with the constant loads. Again, it should be noted that, for a best illustration of the curvature, the deformed was enlarged of 10 times.

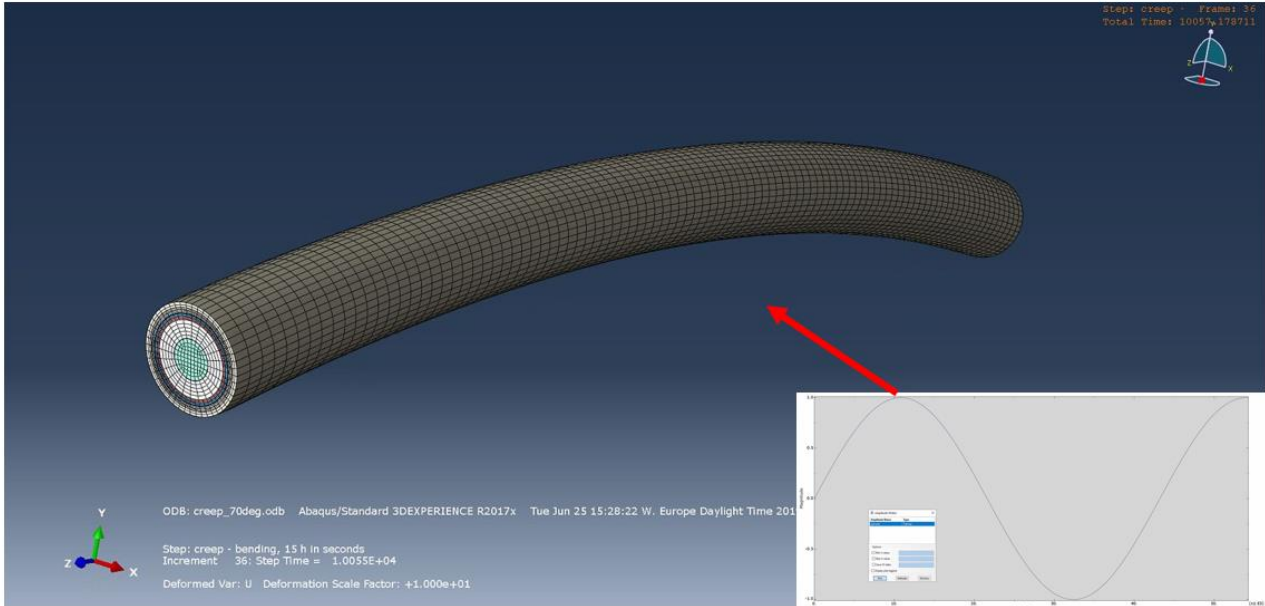


Figure 50 Deformed of cable after water pressure, thermal load and 0.25 bending cycle

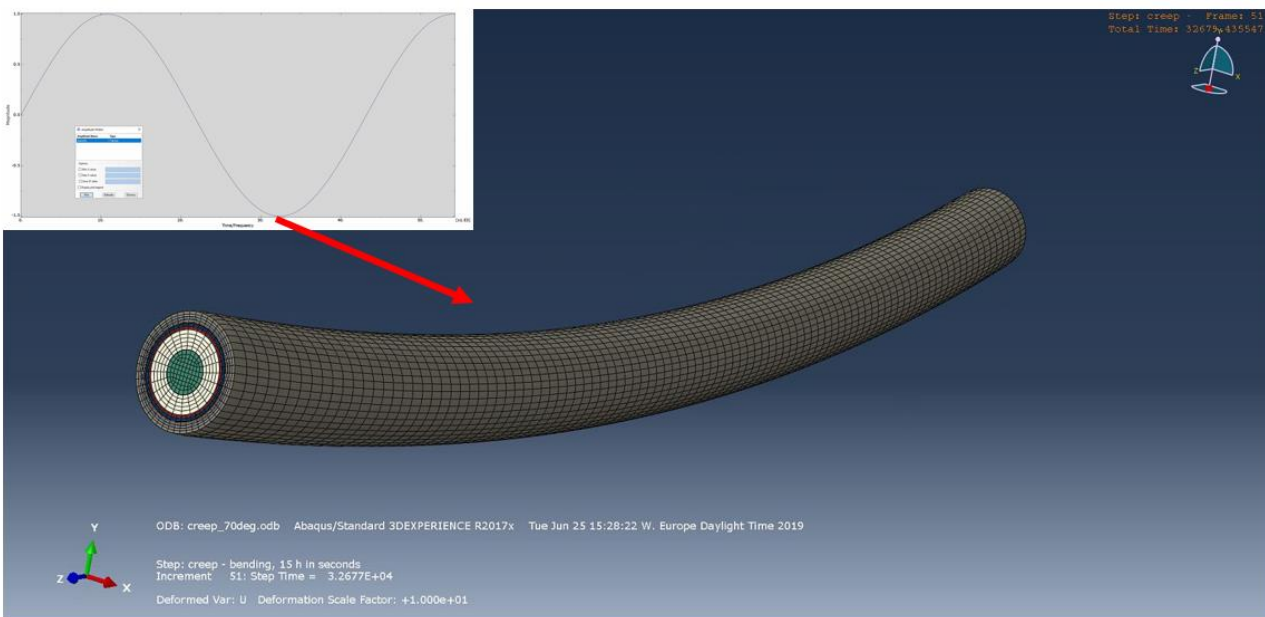


Figure 51 Deformed of cable after water pressure, thermal load and 0.75 bending cycle

PART IV RESULT ANALYSIS

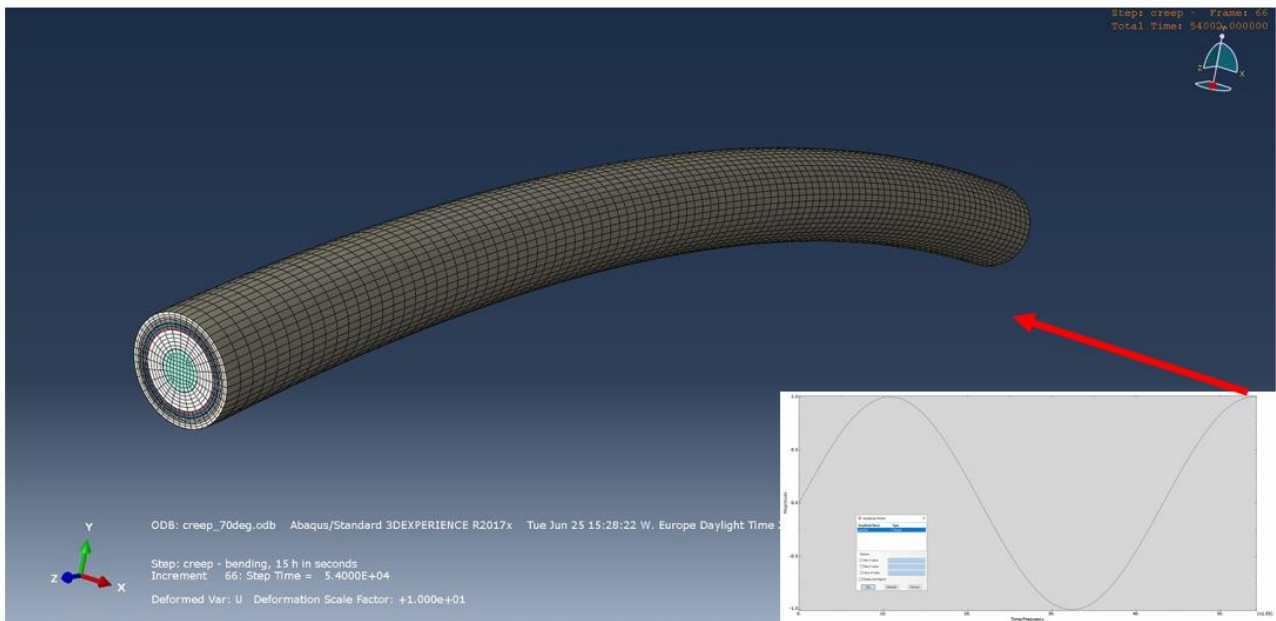


Figure 52 Deformed of cable at the end of simulation (1.25 bending cycle)

14.2 MAIN CONTOUR PLOTS

Output requests are computed in the integration points. From such points, then, are extrapolated numerical values to the other parts of element. This kind of output is called **element solution**. Instead, another type of output is so-called **nodal solution** where numerical value at node is obtained by the average of element values that share such node. This kind of solution, being averaged, appears smoother than the element solution. In Abaqus, “Average element output at nodes” are the element solutions. Through the “scalars before averaging” it’s possible to manage the average grade. 0% corresponds to the element solutions. Typically, nodal solution with 75% of average grade is used on default.

Now it follows the presentation of the principal contour plots obtained for lead sheath at the end of simulated duration of 15 hours (54000 seconds). Output selected are radial stress, circumferential stress, longitudinal stress, Von Mises equivalent stress and equivalent pressure. For each kind of stress is presented two different visualization for a better investigation about the eventual gradient of the stress field.

14.2.1 Radial stress

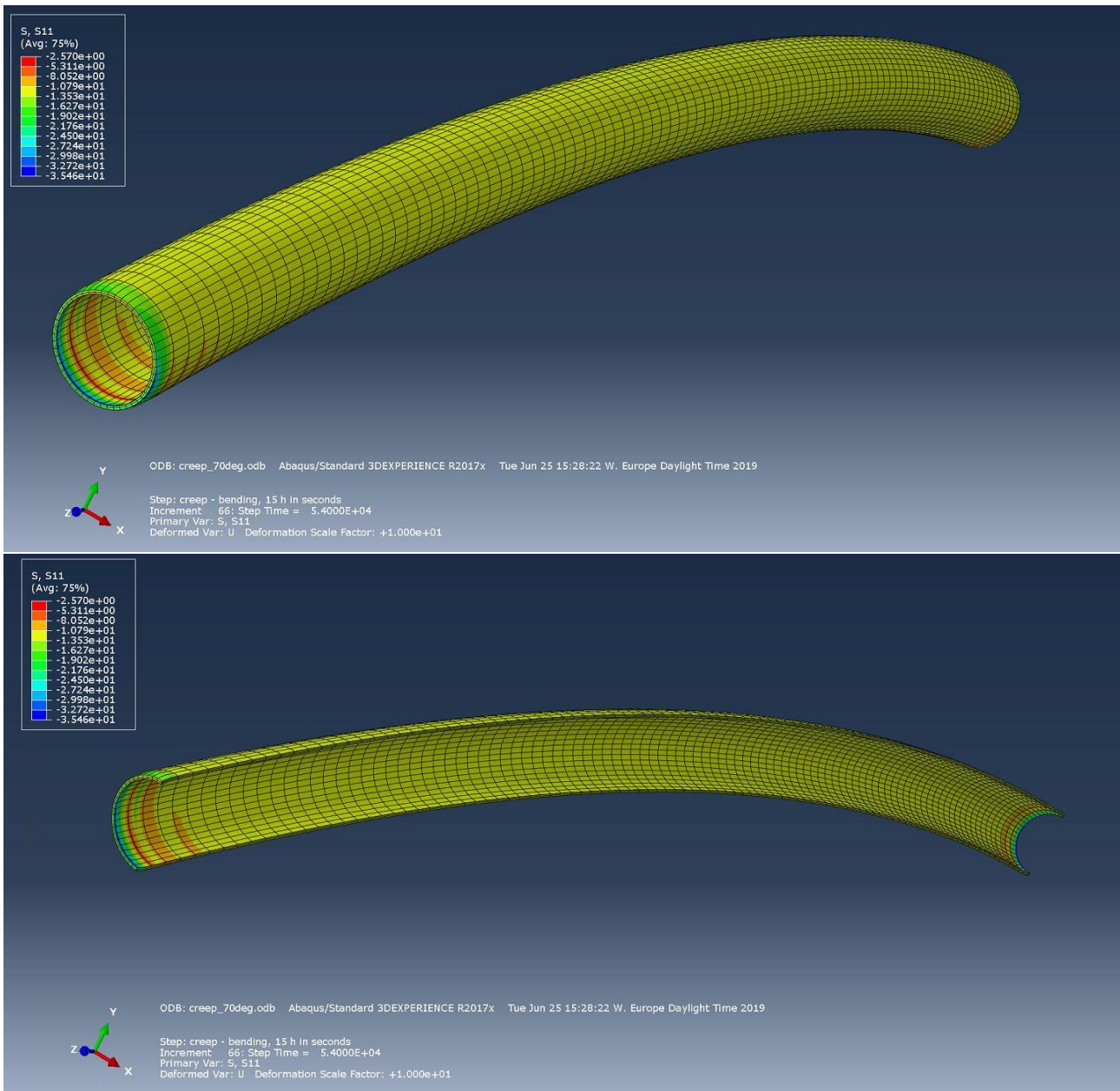


Figure 53 Contour plot of radial stress in lead sheathing

As it's possible to observe, the radial stress, at the end of simulation, has a very smooth aspect, without abrupt changing.

14.2.2 Circumferential stress

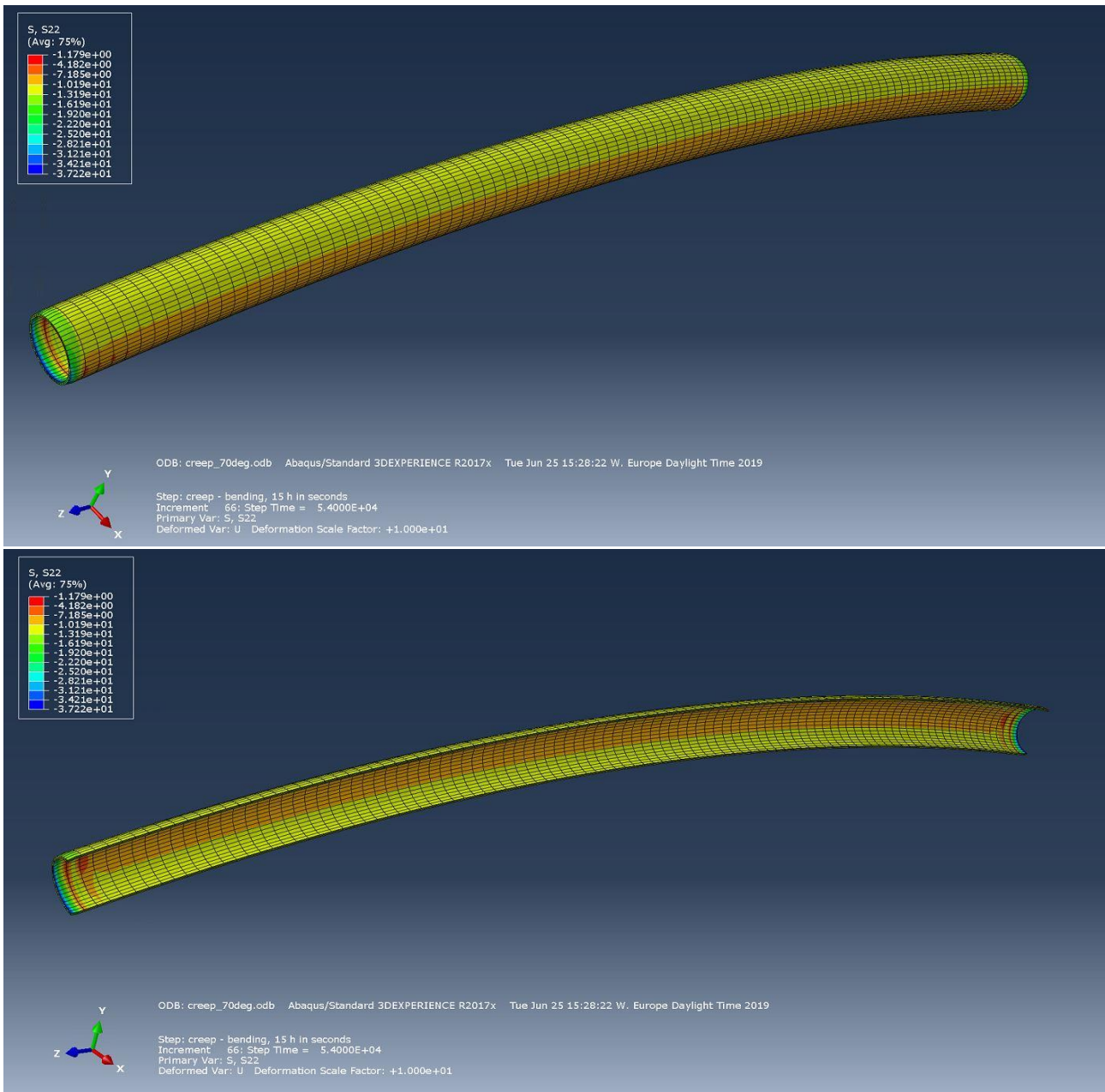


Figure 54 Contour plot of circumferential stress in lead sheathing

Circumferential component of stress not show critical gradients along the sheath.

14.2.3 Longitudinal stress

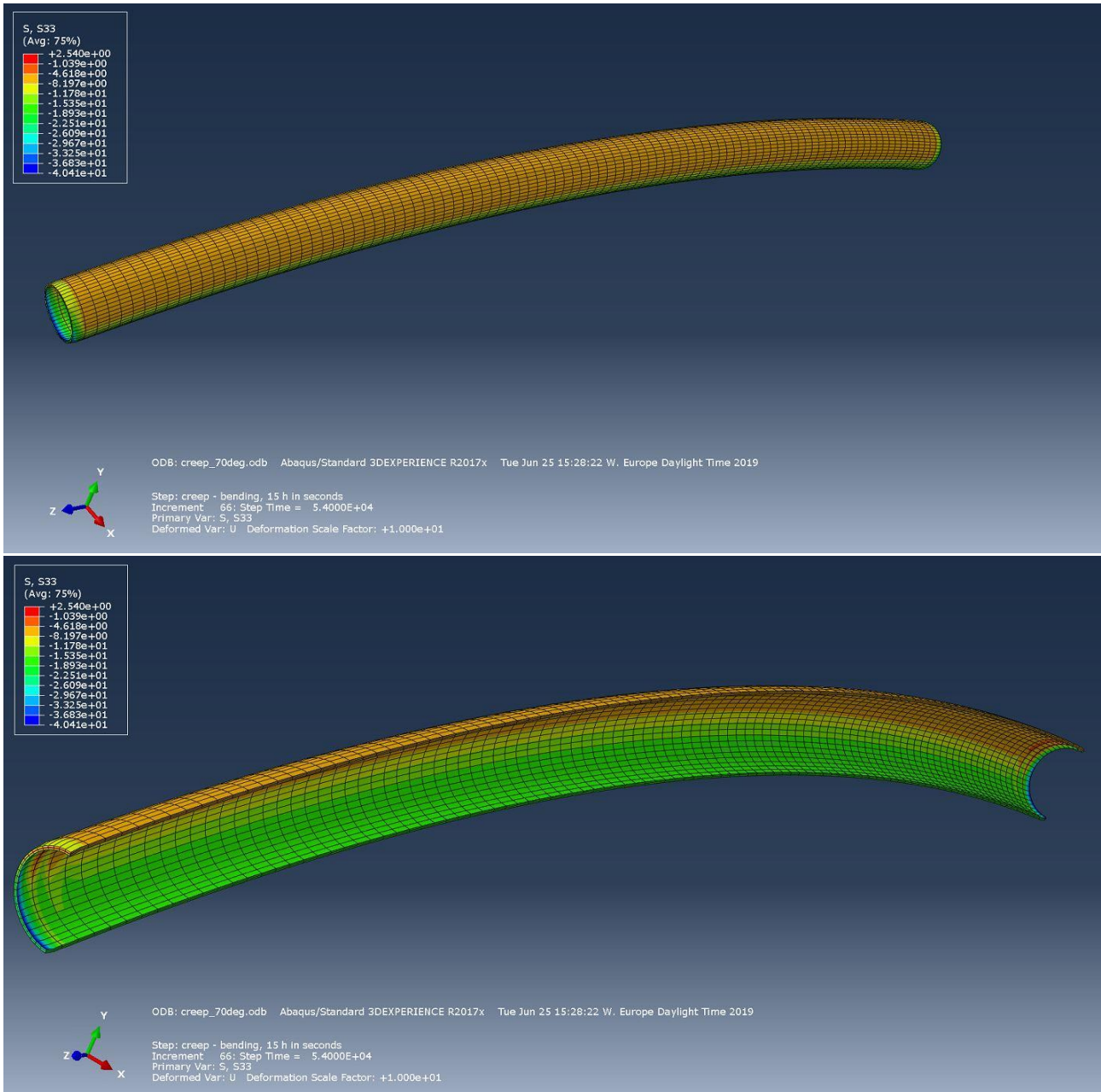


Figure 55 Contour plot of longitudinal stress in lead sheathing

Longitudinal stress has the typical trend of bending load and, along the upper generatrix, no gradient exists. Considering this component of stress, the most stressed points are in the upper extreme regions.

14.2.4 Von Mises equivalent stress

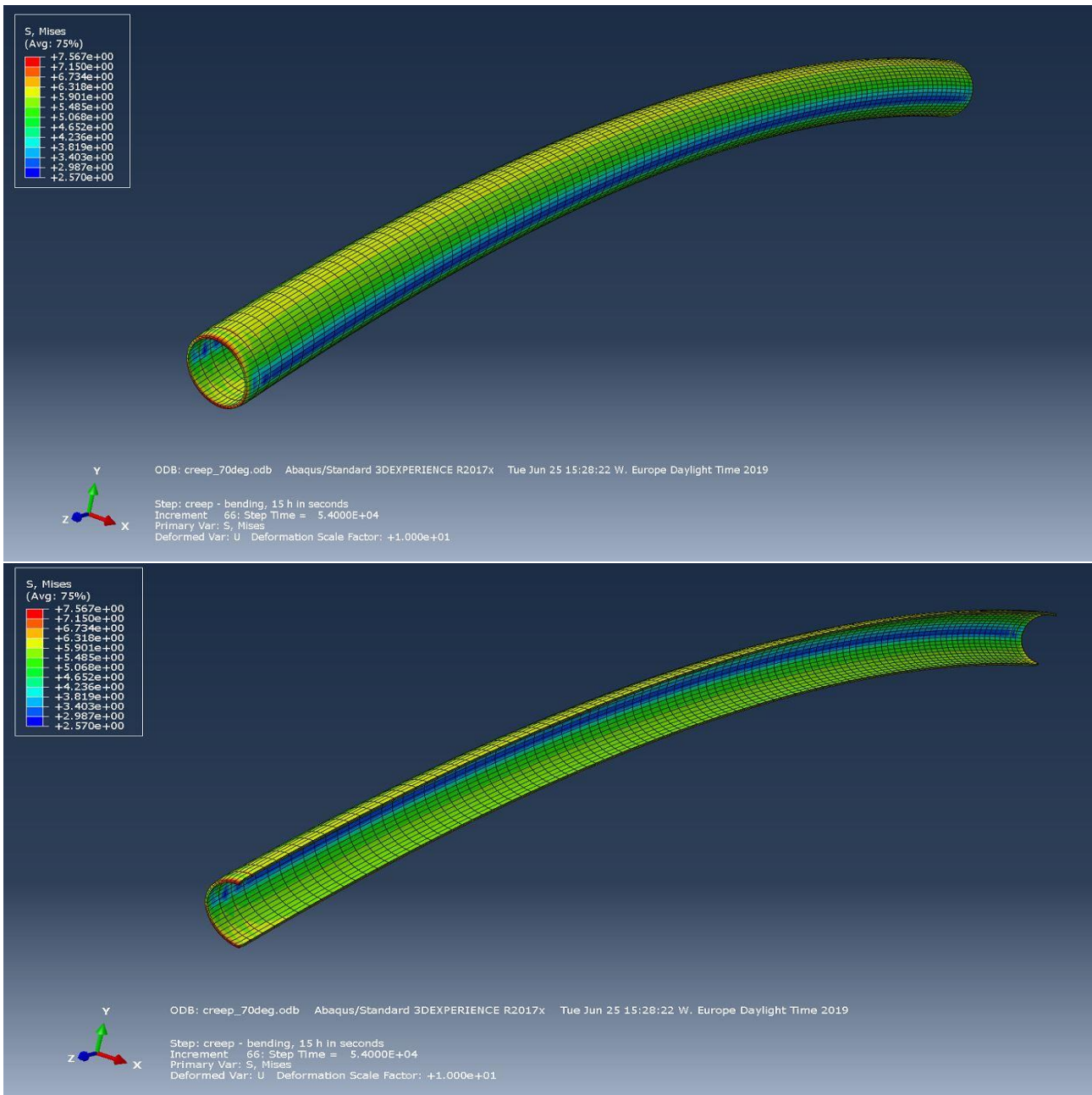


Figure 56 Contour plot of Von Mises equivalent stress in lead sheathing

Von Mises equivalent stress has more changing, along the cable, respect to the previous stress components. However, with reference to this type of stress, the most stressed points remain in the upper extreme regions.

14.2.5 Equivalent pressure

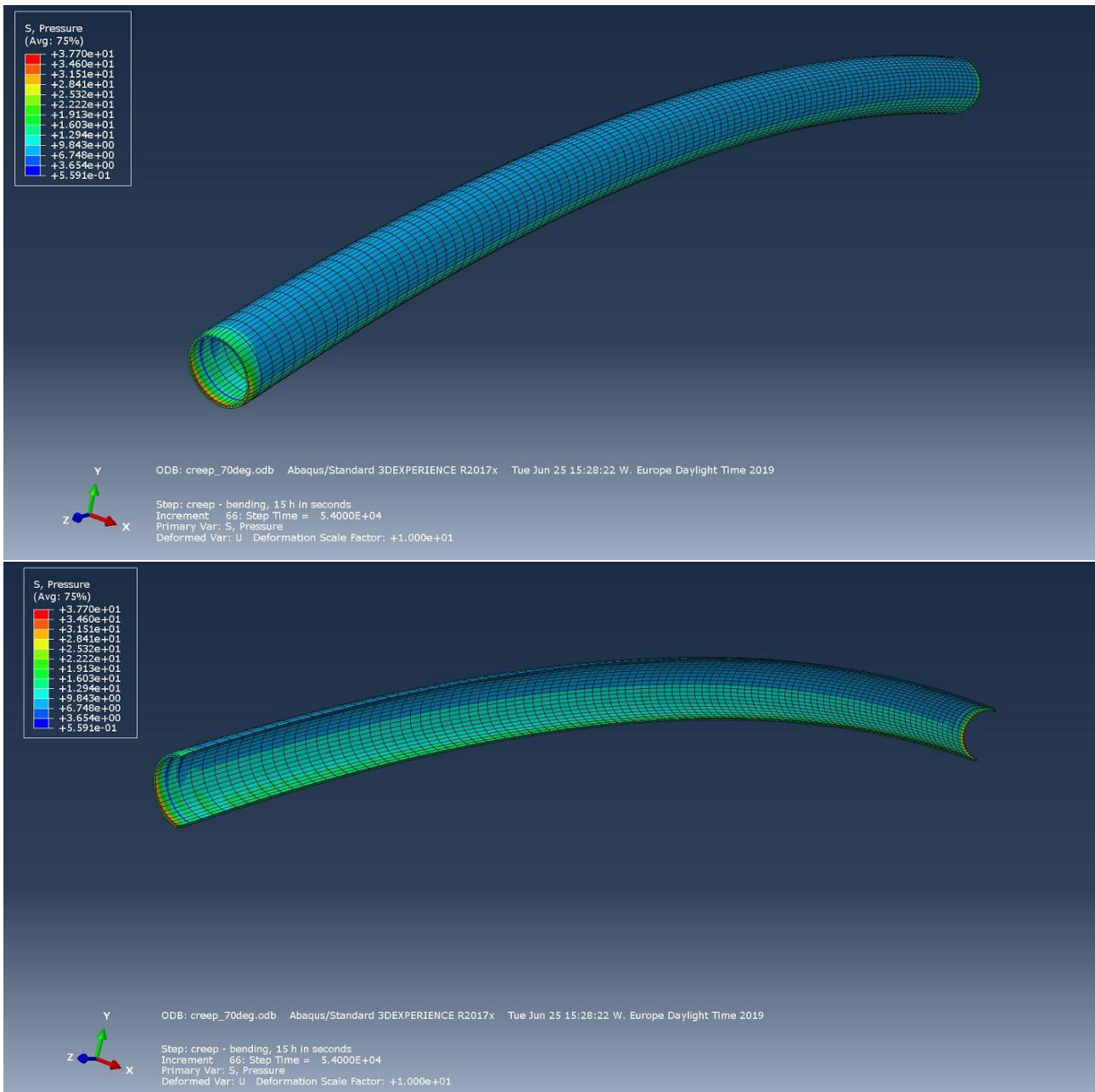


Figure 57 Contour plot of equivalent pressure in lead sheathing

The equivalent pressure has two recognizable zones of values: the lower region, with a highest equivalent pressure, and the upper region. This latter is more dangerous from a structural point of view because acts a weaker compressive state.

14.3 IDENTIFICATION OF THE CRITICAL POINT

Previous qualitative analysis of the main stress components carried to take as critical point, the lead sheathing's outer point of the middle section of cable, identified as RP-1 in the picture.

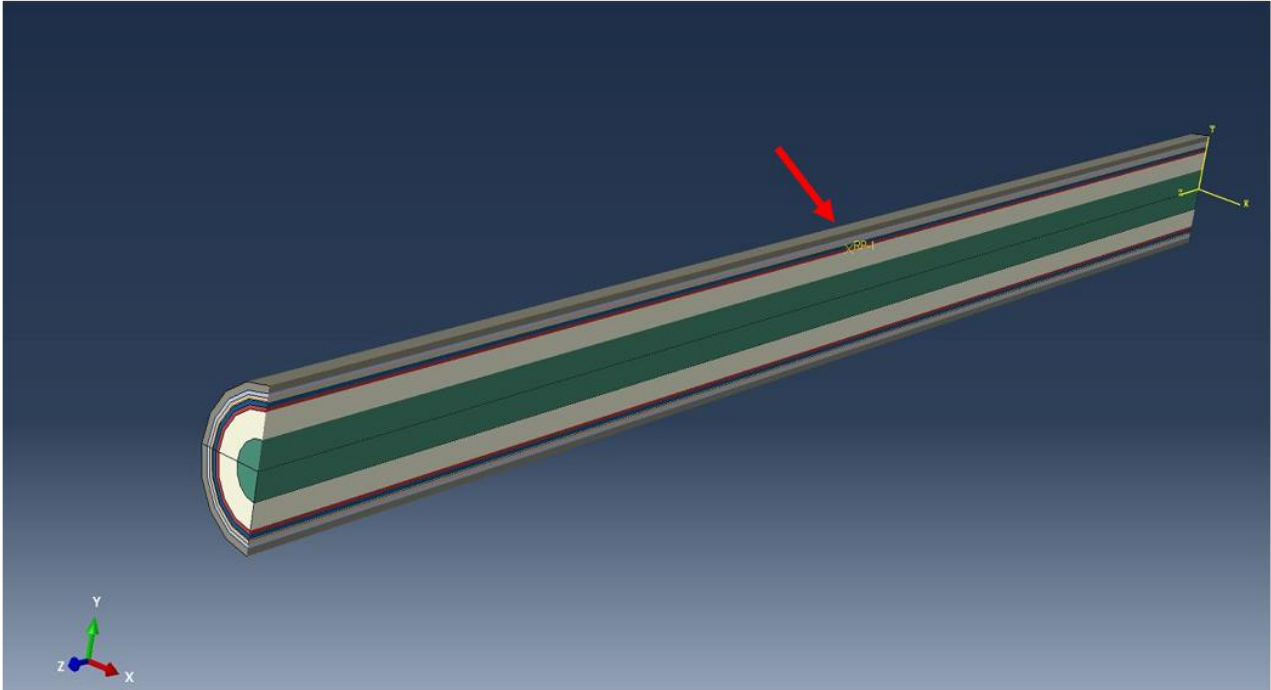


Figure 58 Critical point of cable

15 TEMPORAL ANALYSIS OF THE STRESS-STRAIN FIELD

Once that critical point of lead sheath was identified, the values of stress and strain was monitored for a simulated duration of 15 hours. Temporal trends are extracted in the first integration point of the element that include such critical point.

In the next chapters are illustrated trends of the main components of stress and strain field.

15.1 CHARACTERIZATION OF STATIC BEHAVIOUR

The main charts, representative of the static behaviour of lead sheath during the initial loading, are presented below.

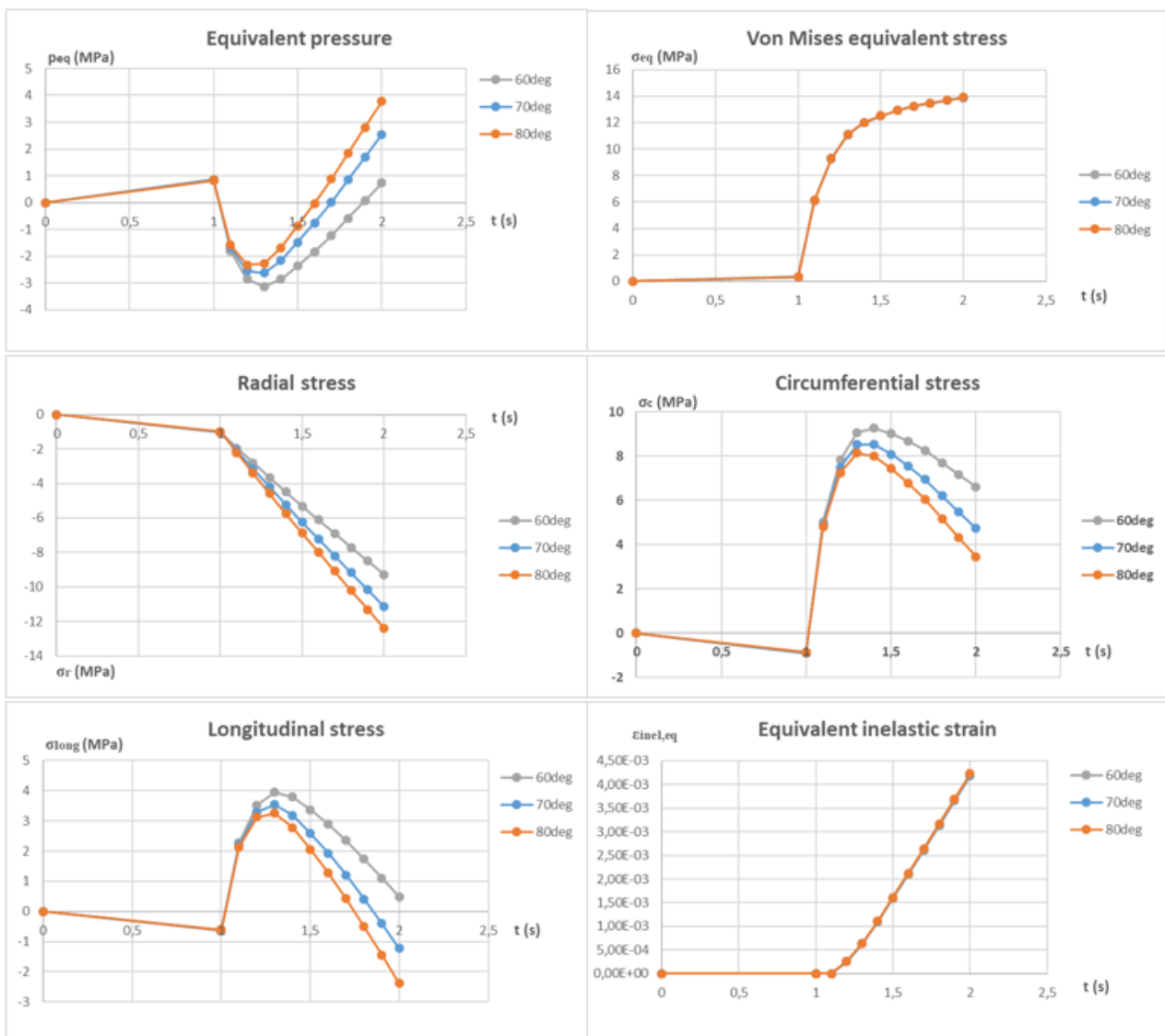


Figure 59 Characterization of static behaviour

External water pressure induces a hydrostatic stress on lead sheath. A small torsion exists, generated by the armouring, but it's a negligible contribute. For this reason, the equivalent pressure is not perfectly 1, and Von Mises equivalent stress is not perfectly 0. Material, during this loading, remains in the elastic field. This is also observable both by the linear trend of stress components and by the 0 value of equivalent plastic stress.

Thermal expansion of the insulation system creates an internal pressure on lead sheath. The material deforms irreversibly and, thus, equivalent plastic strain is not more 0. For what concerns the stress components the following features arise:

- Radial stress must increase, in a linear way, with the thermal load.
- Tangential and longitudinal stresses, until material remains in the elastic field, increase due to the interaction with thermal expansion of the insulation.
- When material starts to show plastic strains, tangential stress and longitudinal stress must necessarily decrease, in order to keep always the same difference between each other, as predicted by the Von Mises' criterion.

15.2 CHARACTERIZATION OF TIME-INDEPENDENT CYCLIC BEHAVIOUR

Main charts about cyclic behaviour are presented in the following.

During this step, there is the imposition of a constant radial load (external water pressure and insulation thermal expansion) and a variable longitudinal load (due to the tides motion). It's interesting analyse what happens along these two directions. The third direction, the circumferential direction, must have a response in order to ensure equilibrium and compatibility.

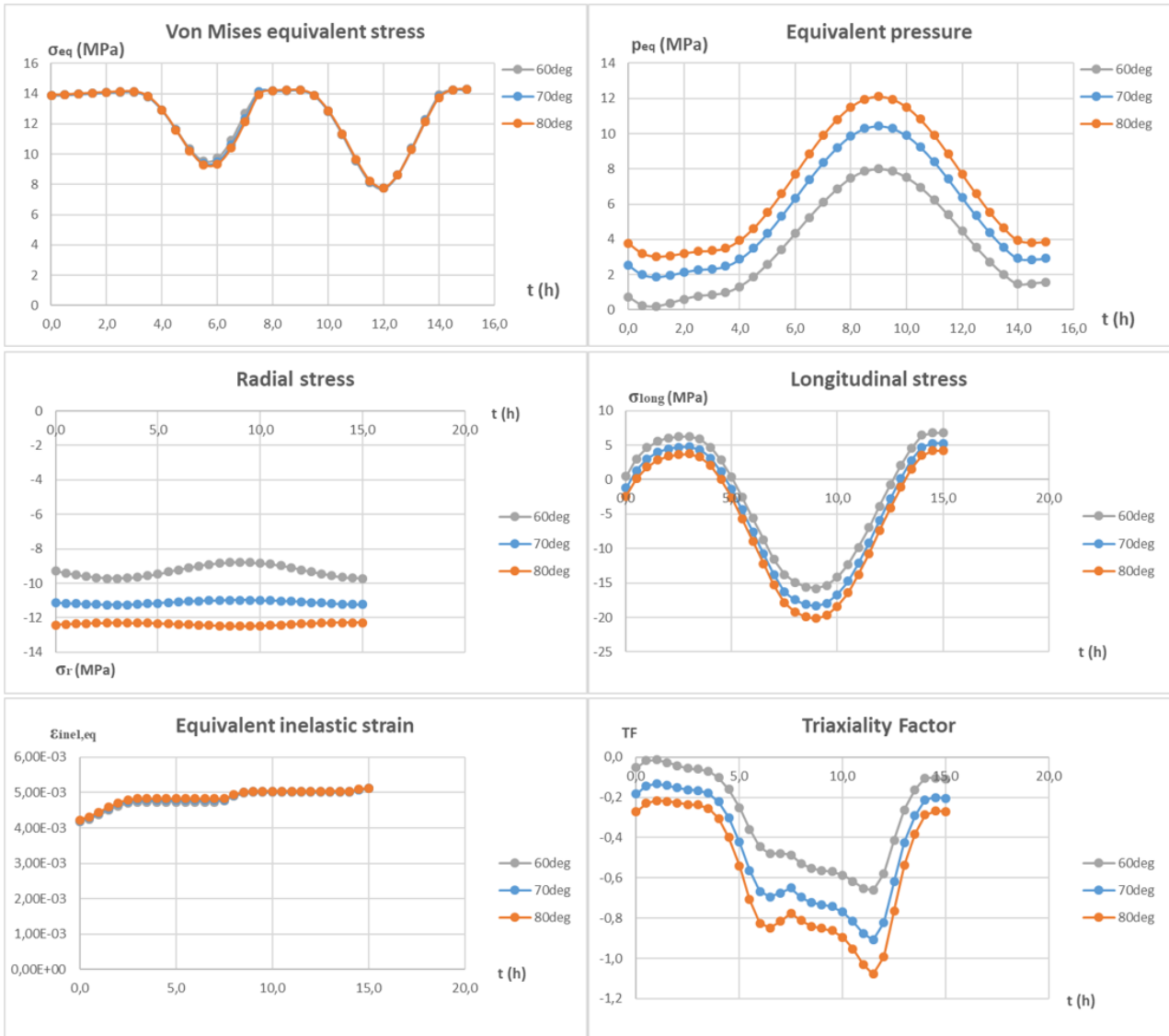


Figure 60 Characterization of time-independent cyclic behaviour

The more interesting features that stand out by analysing the charts are reported.

- Changing of the winding angle has no effect on Von Mises equivalent stress and equivalent plastic strain.
- Equivalent pressure is influenced by the value of winding angle of steel tapes.
- The Triaxiality Factor, the ratio between equivalent pressure and Von Mises equivalent stress (with a minus sign), is thus influenced by the winding angle of reinforcement.

15.3 CHARACTERIZATION OF TIME-DEPENDENT CYCLIC BEHAVIOUR

Now it follows the more significative diagrams for simulations computed with the creep behaviour of lead sheath.

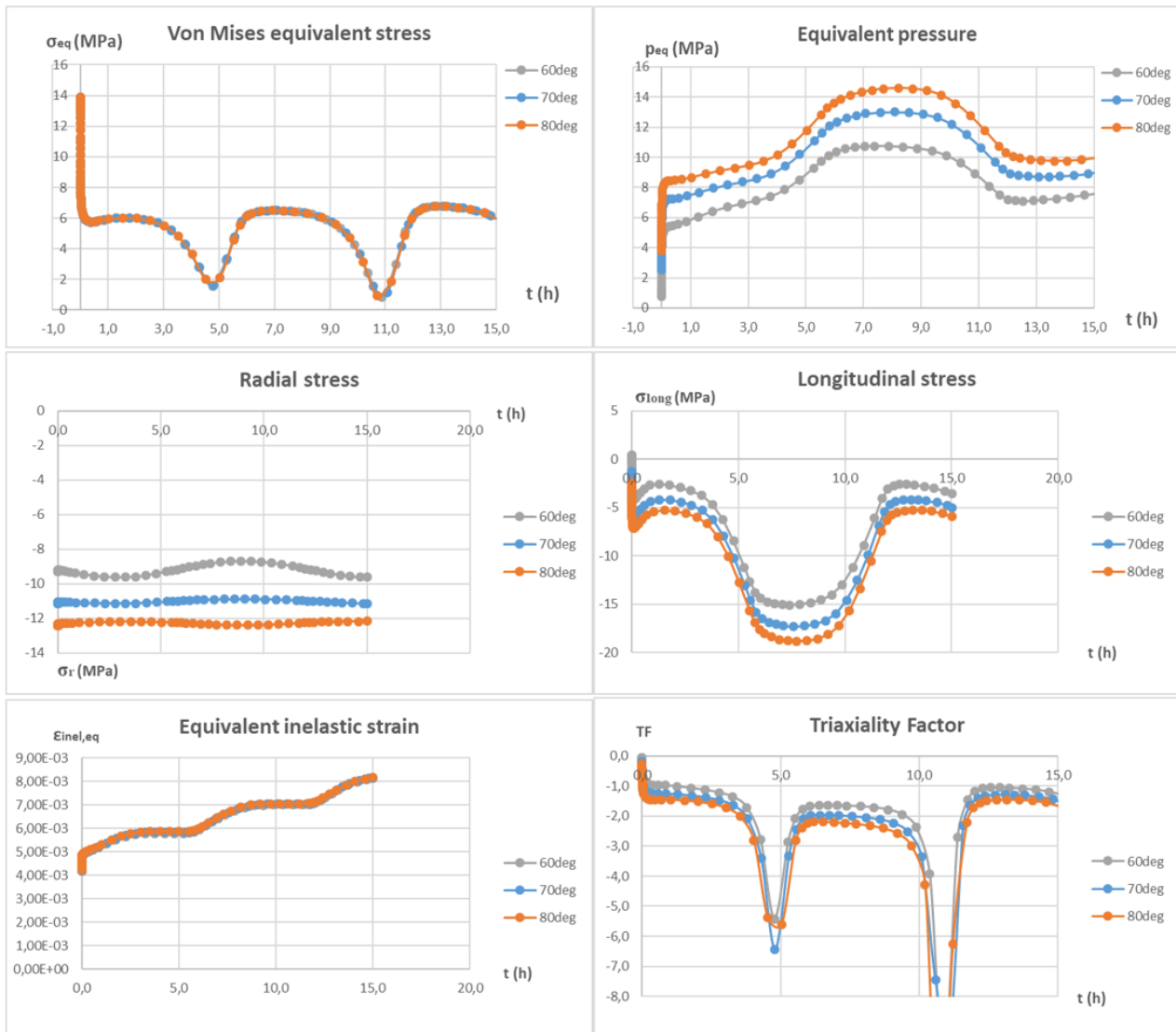


Figure 61 Characterization of time-dependent cyclic behaviour

The creep behaviour dominates the problem, because the frequency of bending load is very low. The relaxation of material is very appreciable because all the stress components, expect for radial stress that's imposed, decrease significantly.

The graph of TF is inferiorly truncated because when Von Mises equivalent stress tend to 0, the absolute value of TF increase a lot, but this isolated information is not relevant and not suitable from a graphical aspect.

16 FINAL CONSIDERATIONS

After a presentation of the main results obtained in the analysis, here are reported the two most important considerations.

16.1 INFLUENCE OF CREEP

As it anticipated before, the creep behaviour dominates the problem. It affects significantly the strain accumulation as shown in *Figure 62*.

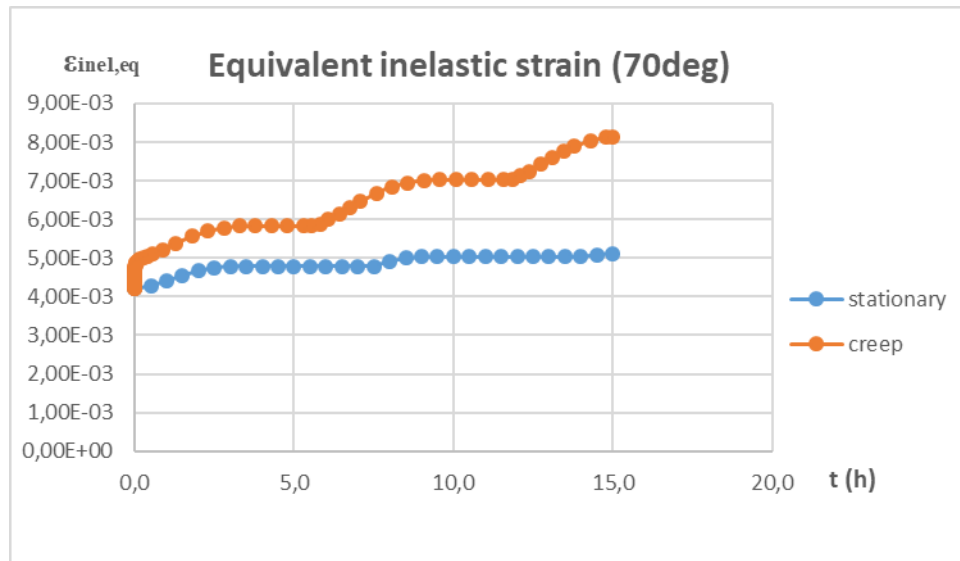


Figure 62 Comparison between viscous and stationary behaviour in terms of equivalent inelastic strain

This means that equivalent inelastic strain amplitude is higher in the case of creep, and, therefore, also the damage accumulated for cycle is higher.

16.2 INFLUENCE OF THE STEEL TAPES' WINDING ANGLE

Both time-independent and time-dependent analysis point out that **the winding angle of steel tapes** influence appreciably the stress state of lead sheath. As the winding angle increases, the equivalent pressure increases, while the Von Mises equivalent stress remains unchanged. This involves that **Triaxiality Factor on lead sheath** depends by the value of the winding angle of steel tapes as shown in *Figure 60* and in *Figure 61*.

It has been shown in the part dedicated to the theoretical study of problem, that Triaxiality Factor influence the creep-fatigue life of material. In fact, with reference to the **Strain-Range Partitioning method under multi-axial conditions**, that is the criterion more suitable for practical applications that involve creep-fatigue problems with multi-axial stress state, a more negative value of TF significates a minor damage accumulated for cycle, and, hence, a major life.

Moreover, the TF intervenes also in other multiaxial fatigue models that not necessarily involve time-dependent behaviour of material as it happens for the **total equivalent strain range theory modified by multiaxiality factor**.

17 CONCLUSIONS

Although the analysis executed is only qualitative, it clearly arises the effect of winding angle of steel tapes on stress-state of lead sheath.

All the inelastic behaviour explored, time-independent and time-dependent, show, without doubts, the obtainable **enhancing on fatigue performance or creep-fatigue performance of lead sheath by increasing the tape's winding angle.**

For what concerns multiaxial fatigue performance, the total equivalent strain range method modified by Multiaxiality Factor evidence as a more negative value of MF increases the fatigue life.

Instead, for what regards multiaxial creep-fatigue performance, the SRP method under multiaxial conditions show always that as MF decreases, creep-fatigue damage decreases.

As more times cited, MF is a direct function of the Triaxiality Factor, hence, the same considerations done on MF are valid for the TF.

Because TF is the ratio between equivalent pressure and Von Mises equivalent stress (with a minus sign), the trends of these characteristics are again presented with tables attached that exhibit such achieved results.

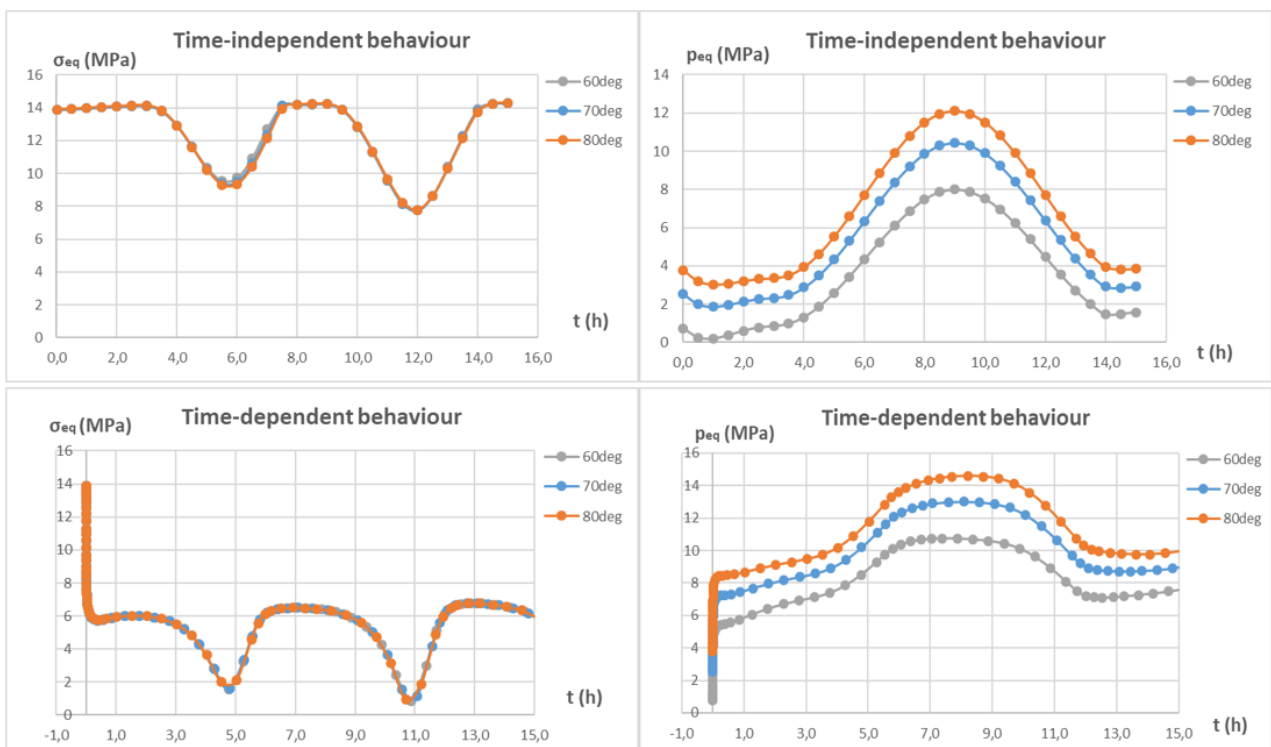


Figure 63 Winding angle effect of steel tapes for stationary and viscous behaviour

Table 16 Triaxiality Factor for different winding angle values of steel tapes

STATIONARY SIMULATION		VISCOUS SIMULATION	
<i>Winding angle of tape</i>	<i>Cyclic mean TF (3-15h)</i>	<i>Winding angle of tape</i>	<i>Cyclic mean TF (3-15h)</i>
60 degrees	-0,37	60 degrees	-2,11
70 degrees	-0,54	70 degrees	-2,52
80 degrees	-0,66	80 degrees	-2,89

Triaxiality Factor on lead sheath always decreases when tape's winding angle increases.

The improvements gained should be independent by specific numerical values of boundary conditions implemented, thus the Nexans company should obtain a practice enhancing, without any further experimental work, with exception only for the future experiments necessary to validate the model.

Moreover, the model created can be used for future simulations when more data will be available or new conditions will have to be investigated.

REFERENCES

- [1]: T. Worzyk, '*Submarine Power Cables: Design, Installation, Repair, Environmental Aspects*', Springer, 2009.
- [2]: www.Nexans.com
- [3]: J. Roesler, H. Harders, M. Baeker, '*Mechanical Behaviour of Engineering Materials*', Springer, 2010.
- [4]: S.S. Manson, G.R. Halford, '*Fatigue and Durability of Metals at High Temperatures*', ASM International, 2009.
- [5]: R.K. Penny, D.L. Marriott, '*Design for Creep*', Springer, 1995.
- [6]: Abaqus Analysis User's Guide, '*Rate dependent plasticity*', SIMULIA, 2016.
- [7]: E.H. Wong, W.D. van Driel, A. Dasgupta, M. Pecht, '*Creep fatigue models of solder joints: A critical review*', Microelectronics Reliability ELSEVIER, 2016.
- [8]: S.S. Manson, G.R. Halford, '*Treatment of multiaxial creep-fatigue by strainrange partitioning*', NASA Technical Memorandum, 1976.
- [9]: M.H. Hirschberg, G.R. Halford, '*Use of strainrange partitioning to predict high-temperature low-cycle fatigue life*', NASA Technical Note, 1976.
- [10]: P.J. Bonacuse, S. Kalluri, '*Elevated Temperature Axial and Torsional Fatigue Behaviour of Haynes 188*', NASA Technical Memorandum, 1992.
- [11]: L. Viespoli, J. Audun, A. Alvaro, N. Bård, A. Sommacal, F. Berto, '*Tensile characterization of a lead alloy: creep induced strain rate sensitivity*', Materials Science & Engineering: A. vol. 744, 2018.
- [12]: Z.Y. Huang, J.A. Pilgrim, P.L. Lewin, S.G. Swingler, G. Tzemis, '*Numerical thermo-mechanical stress analysis for HVDC Cables*', Electrical Insulation Conference, 2014.
- [13]: E. Ildstad, R. Hegerberg, '*Cavity Formation in Mass-Impregnated HVDC Subsea Cables-Mechanisms and Critical Parameters*', IEEE Electrical Insulation Magazine, 2014.
- [14]: Abaqus Theory Guide, '*Elements*', SIMULIA, 2016.
- [15]: Nam-Ho Kim, '*Finite Element Analysis of Contact Problem*', www.mae.ufl.edu
- [16]: Abaqus Analysis User's Guide, '*Mesh tie constraints*', SIMULIA, 2016.
- [17]: P.P. Milella, '*Fatigue and Corrosion in Metals*', Springer, 2013.